



NTNU – Trondheim
Norwegian University of
Science and Technology

An Experimental Investigation on Bio-Fouling Induced Drag

Arne Kristian Sæther

Marine Technology

Submission date: Januar 2015

Supervisor: Marilena Greco, IMT

Co-supervisor: Lars Gansel, SINTEF Fisheries and Aquaculture

Norwegian University of Science and Technology
Department of Marine Technology



MASTER THESIS IN MARINE TECHNOLOGY

FALL 2014

FOR

Arne Kristian Sæther

An experimental investigation on bio-fouling induced drag

(En eksperimentell undersøkelse av drag induisert av begroing)

Marine fish farming represents an important resource for Norwegian economy and is in rapid development. However several hydrodynamic challenges exist depending on the specific features of the aquaculture system and its working location. When nets are adopted, among the others a relevant issue is represented by bio fouling. This occludes the net, blocking the passage of water, and causes extra weight, leading to lower buoyancy of the cages, increase of the drag force, and deformation of the cage. The project thesis focused on the literature study on different types of bio fouling, on the experimental, theoretical and numerical studies carried out and their outcomes. It also concerned the identification of a suitable experimental set-up to examine the relevance of some parameters on the bio fouling induced loads. Present master thesis will focus on the increase of the drag forces due to bio fouling. This might be relevant for a proper structural design but a reliable method for its estimate is not available yet. An experimental campaign will be attempted as a logical continuation of a physical study carried out by SINTEF Fisheries and Aquaculture on hydroid fouling, which seems to be the most dangerous type of bio fouling. In that study short pieces of fishing line were fixed between two thin steel rods, to mimic hydroids growing on twines, and drag tests were performed using single twines, two parallel twines with different distances, and single and double twine crosses.

Objective

The aim for this thesis is to continue the physical study by SINTEF Fisheries and Aquaculture. The plan is to try several different twine spacing, and also more than two parallel twines, to investigate the effect of the number of twines, and get closer to a realistic net configuration. Measurements of the drag forces and flow visualizations will be used for the physical investigation.

The work should be carried out in steps as follows:

1. Summarize major findings/outcomes from the project thesis that are relevant for the present master work. Identify the tank where performing the tests and examine the experimental set-up in terms of frame to be used to keep in place the twines, twines configurations, current speeds, models of hydroids. Identify also the load cells and the visualization technique to be used for the tests.
2. Calibrate the cell loads; measure the drag acting on the frame without twines and at all selected current speeds; check the reliability of the load measurements performing a preliminary test with geometry and conditions consistent with available drag experiments; perform preliminary flow-visualizations with two parallel twines at different distances and in different current speeds.
3. Perform drag tests with two parallel twines at few spacing identified as the most interesting from the flow visualizations in step 2, and then increase the number of twines keeping the same spacing.



4. Perform drag tests with twines crossing each other; in particular, examine a single cross, the cross of two pairs of parallel strings, and the cross of three and four parallel strings.
5. For at least one of the test conditions examined in the previous steps perform a repeatability test and in general examine possible error sources in the experiments.
6. Perform the physical investigation based on the measurements and flow visualizations and verify possible usefulness for the case of a realistic net.

The work may show to be more extensive than anticipated. Some topics may therefore be left out after discussion with the supervisor without any negative influence on the grading.

The candidate should in his report give a personal contribution to the solution of the problem formulated in this text. All assumptions and conclusions must be supported by mathematical models and/or references to physical effects in a logical manner.

The candidate should apply all available sources to find relevant literature and information on the actual problem.

The thesis should be organised in a rational manner to give a clear presentation of the work in terms of exposition of results, assessments, and conclusions. It is important that the text is well written and that tables and figures are used to support the verbal presentation. The thesis should be complete, but still as short as possible. In particular, the text should be brief and to the point, with a clear language. Telegraphic language should be avoided.

The thesis must contain the following elements: the text defining the scope (i.e. this text), preface (outlining project-work steps and acknowledgements), abstract (providing the summary), table of contents, main body of thesis, conclusions with recommendations for further work, list of symbols and acronyms, references and (optional) appendices. All figures, tables and equations shall be numerated.

The supervisor may require that the candidate, in an early stage of the work, present a written plan for the completion of the work. The plan should include budget for the use of computer and laboratory resources that will be charged to the department. Overruns shall be reported to the supervisor.

From the thesis it should be possible to identify the work carried out by the candidate and what has been found in the available literature. It is important to give references to the original source for theories and experimental results.

Supervisor :Marilena Greco
Co-supervisor:Lars Gansel
Submitted :20 August 2014
Deadline :13 January 2015

Marilena Greco
Supervisor

Preface

This report is my final master thesis of my MSc in Marine Technology. My specialisation is in Marine Hydrodynamics, and the topic of this thesis is the influence bio fouling has on the hydrodynamic forces on fish farm net pens. The work is a experimental study using models with artificial hydroids to investigate the drag increase due to bio fouling. A similar study have been done by Pål Lader and others at SINTEF Fisheries & Aquaculture, and my work is meant to be a continuation of their work. The project was done in two main parts, first an experimental campaign in a towing tank, and then a period when I analysed the results, and also wrote this report. For the first part I had about two weeks to make the models and do all the preparations, and then I had two weeks in the small towing tank at Tyholt. Ideally I should have had more time for the preparations, but the other available time slot in the tank was much later, which would have given short time for the analysis in the end. In the second part I tried to start writing the report early, and write the different parts along the way, to avoid a stressful write up in the end.

Overall the work went well, and the experiments were mostly successful, although the short preparation time caused some deviations from the initial plan. The equipment for the flow visualisation could not prepared before I started, so it had to be made between the tests. This slowed down the work a bit, and considering that most of the videos did not give much useful results, I wonder if it had been better to focus on doing more other tests. Towards the end of the work I realised that there was a significant difference between my results and the results from the previous study, but I din not have much time to investigate this more. I guess that is a disadvantage of writing parts of the report early, and hence doing parts of the analysis later, since it gives less time to clarify possible issues with the results. But, I still feel starting the writing early was a good choice.

I would like to thank Lars Gansel, who was my contact person at SINTEF, and Pål Lader; for their advise on possible topics for the thesis; information from previous studies; and help with the work, in particular with the planning of the experiments. I would also like to thank the lab technicians, Terje Rosten and Torgeir Wahl, for assisting with the set up, calibration and use of the equipment in the lab. And of course I want to thank my supervisor, Professor Marilena Greco, for good and regular follow up through the semester, and help when I have needed it.

Trondheim, 13.01.2015

A handwritten signature in black ink, reading "Arne Kristian Sæther". The signature is written in a cursive style and is positioned above a horizontal dotted line.

Arne Kristian Sæther

Abstract

Marine fish farming is an important and growing industry. Fouling organisms that grow on the net cages and other structural components of the fish farms are a substantial problem for the industry. The overall aim of this study is to increase the understanding of how the bio fouling influence the hydrodynamic forces on the nets. More specifically the focus is on hydroid growth, and the use of models of net twine with artificial hydroid fouling.

The models that were used are made of two 1.5 mm steel rods that are twisted together, with short pieces of 0.32 mm multifilament fishing line fixed between them, similar to a test tube brush. The twisted steel rods were replicating a 3 mm twine, with the fishing lines acting as evenly distributed hydroid growth. Previously drag tests had been done with one and two of these models, with two parallel twines with varying distance, and also a cross configuration. In the present study the goal was to investigate possible interaction effects between twines, by using various configurations with a higher number of twines; and also make small net sections and estimate the drag increase due to bio fouling. 16 twine models were made, and tests were done with a single twine; and 2, 4, 6 and 8 parallel twines; and also crossing twines, with the same numbers of twines in each direction. In total 18 different configurations were tested, with twine spacings of 12 mm and 24 mm.

The experiments were done in a towing tank, with the twine models fixed in a frame, orthogonally to the direction of travel. The drag force was measured on the frame, and the contribution from the frame itself was subtracted from the total force to find the drag on the twine models. Then the drag coefficients were calculated and plotted in various diagrams to visualise any trends. All the configurations were tested at a range of velocities from 0.05 m/s to 1.4 m/s. Most of the results were consistent, except for the two lowest velocities (0.05 m/s and 0.1 m/s) where the precision error was significant.

It was found that the drag coefficient for the fouled twine models were decreasing with increasing current velocity. At 0.1 m/s ($Re = 300$) the drag coefficients were between 3.5 and 4.0, while for 1.4 m/s ($Re = 4200$) they were approximately 3.0. This is probably either because of deflection of the hydroids at higher velocities, or because the hydroids themselves have a smaller diameter, and hence are in a lower Reynolds number range (from $Re = 32$ to $Re = 448$), where the drag coefficient is dependent on the velocity. The variations in drag coefficients between the different model configurations were small, there were some consistent trends, but the magnitude were insignificant. This means that the interaction effects between the twines are relatively small, and it is likely that data from tests with few twines can be extrapolated to net panel applications. The drag coefficients for the net sections in the middle of the cruciform configurations were calculated. For the net sections with 12 mm spacing the results were inconclusive, while for 24 mm spacing the net drag coefficient varied between 0.66 and 0.59 for different velocities. This is twice as high as empirical data for a similar clean net.

Several possibilities for further work were identified during the work with

the thesis. One is to do more similar experiments, both with equivalent models to verify the results, and with either more or less hydroids, to study the influence of the amount of fouling. Another is to try to quantify the bending stiffness of real hydroids compared to the stiffness of the hydroid models (fishing line). The mechanical properties of real hydroids and the hydroid replicas have only been compared qualitatively in previous studies, so quantifying these would be useful both for validation of the models, and for improving them. Further investigations of the drag coefficient of the hydroid stems independently, with regards to the Reynolds number dependency of the drag coefficients of the whole models, would also be interesting.

Sammendrag

Oppdrett av fisk er ein viktig veksande industri. Organismar som veks på nøter og andre delar av merdane på oppdrettsanlegga er eit betydeleg problem for denne industrien. Det overordna målet for dette studiet er å forbetre forståinga av korleis groen påverkar dei hydrodynamiske kreftene på nøtene. Meir bestemt er fokuset på hydroidar, og bruk av modellar av tråd med kunstig hydroid groe.

Modellane som vart brukte er laga av to 1.5 mm ståltrådar som er tvinna, med korte stubbar av 0.32 mm multifilament fiskesnøre festa mellom seg, på same måten som ein piperensar. Dei tvinna ståltrådane tilsvarer ein 3 mm tråd, medan fiskesnøret vert som jamnt fordelt hydroid groe. Tidlegare har det vore gjort testar med ein eller to slike modellar, med to parallele trådar med ulike avstandar, og også ein kryss-konfigurasjon. I dette studiet er målet å undersøkje moglege interaksjonseffektar mellom trådar, ved å bruke ulike konfigurasjonar med fleire trådar; og også å lage små nett og estimere auka i drag på grunn av groe. 16 trådmodellar vart laga, og testar vart gjort med ein einskild tråd; 2, 4, 6 og 8 parallele trådar; og kryssande trådar med det same antalet trådar i kvar retning. Totalt vart 18 ulike konfigurasjonar testa, med trådavstand på 12 mm og 24 mm.

Experimenta vart gjorde i ein slepetank, med trådmodellane festa i ei ramme, vinkelrett på fartsretninga. Drag kreftene vart målte på ramma, og bidraget frå ramma vart trekt frå totalkrafta for å finne krafta på trådane. Deretter vart dragkoeffisientane rekna ut, og plotta i ulike diagram for å synleggjere eventuelle trendar. Alle konfigurasjonane var testa med fleire hastigheiter, med eit spenn frå 0.05 m/s til 1,4 m/s. Dei fleste resultatata var konsekvente, med unntak av for dei to lågaste hasigheitene (0.05 m/s og 0.1 m/s) der usikkerheita var betydeleg.

Det vart funne ut at dragkoeffisienten for trådmodellane med groe minka for aukande straumhastigheit. Ved 0.1 m/s ($Re = 300$) var dragkoeffisientane mellom 3.5 og 4.0, medan for 1.4 m/s ($Re = 4200$) var dei om lag 3.0. Dette skuldast sannsynlegvis enten det at hydroidane vert bøygde ved høgare hastigheiter, eller det at hydroidane har ein mindre diameter enn trådmodellen, og derfor er i eit lågare Reynoldstall område (frå $Re = 32$ til $Re = 448$), der dragkoeffisienten varierer med hastigheten. Variasjonane i dragkoeffisientane mellom dei ulike konfigurasjonane var små, der var nokre konsekvente trendar, men storleiksorden på desse var ubetydeleg. Dette betyr at interaksjonseffektane mellom trådane er relativt små, og det er sannsynleg at data frå testar med få trådar kan ekstrapolerast til bruk på nøter. Dragkoeffisienten på nettseksjonane i midten av kryss-konfigurasjonane vart rekna ut. For netta med 12 mm trådavstand var resultatata usikre, medan for netta med 24 mm trådavstand varierte dragkoeffisienten mellom 0.66 og 0.59, avhenig av hastigheit. Dette er dobbelt så høgt som erfaringsdata frå tilsvarande reine nett.

Fleire moglegheiter for vidare arbeid vart funne gjennom arbeidet med denne oppgåva. Ei moglegheit er å gjere fleire liknande eksperiment, både med tilsvarande modellar for å verifisere resultatata, og med enten meir eller

mindre hydroidar, for å undersøkje kva verknad mengda med groe har. Ei anna moglegheit er å prøve å tallfeste bøyestivheita til ekte hydroidar samanlikna med hydroidmodellane (fiskesnøre). Dei mekaniske eigenskapane til ekte hydroidar og hydroid-substitutta har berre vorte samanlikna kvalitativt i tidlegare studie, så det å tallfeste desse ville vere nyttig både for kvalitetssikring av modellane, og for å forbetre dei. Vidare undersøkingar av dragkoeffisienten til hydroidstilkane isolert sett, med tanke på korleis dragkoeffisientane til heile trådmodellane varierer med Reynoldstallet, ville også vere interessant.

Contents

1	Introduction	1
2	Methods	4
3	Theory	5
3.1	Results From Pre-Project	5
3.1.1	Empirical models for forces on clean nets	6
3.1.2	Experimental studies on fouled nets	7
3.2	Additional Theory	9
4	Experiments and Observations	13
4.1	Models	13
4.2	Equipment and Set Up	15
4.3	Calibration	19
4.4	Experiments	21
4.5	Calculation of Drag Forces	27
4.6	Drag on Net Section	30
4.7	Accuracy and Reliability	31
4.7.1	Precision Error	31
4.7.2	Bias Error	33
4.8	Decay Tests	34
4.9	Projected Area and PNO	36
5	Results	40
5.1	Drag Forces	40
5.2	Drag Coefficients	42
5.3	Drag on Frame	45
5.4	Accuracy and Reliability	45
6	Discussion	48
6.1	Velocity Dependency	48
6.2	Comparison of Configurations	49
6.3	Drag on Net Section	51
6.4	Comparison with Similar Experiments	54
6.5	Some Limitations	55
7	Conclusions	56
7.1	Recommendations for Further Work	57
	References	58
A	Drawings of Frame	59
B	Drag Forces and Coefficients for Each Test Series	64
C	Plots of Drag Coefficients vs. Number of Twines	70

D Overview of MatLab Scripts	76
E List of Digital Attachments	79

List of Figures

1	Sketch of net pens with morings (figure taken from pre-project).	5
2	Drag coefficients from the experiments by Gansel et al. (2013)	8
3	Drag coefficients with 16 mm hydroids	11
4	Drag coefficients for different single twines	12
5	All the finished models in a protective case	13
6	The shaft that the fishing lined was spooled onto with scale marking the distance between each tread	14
7	The small towing tank at MarinTek, Tyholt	15
8	Detail of the clamps that held the models in place	16
9	The complete frame rig mounted on the towing carriage	17
10	MGCplus data acquisition system	18
11	Examples of good and bad visualisations	19
12	Drawing of the set up used for calibration	20
13	Calibration: Force plotted as a function of voltage, including equation for linear curve fit.	21
14	Illustration of how the distance between the twines is measured	22
15	Example plots of drag force, velocity and voltages	28
16	Example plots of drag force, velocity and voltages	29
17	Estimation of drag on net section.	31
18	Time series for decay test of the frame	35
19	Frequency spectra from the decay test of the frame	36
20	Example of image conversion for projected area	37
21	Illustration of PNO.	39
22	Drag force per twine for parallel twines with 24 mm spacing .	40
23	Drag force per twine for parallel twines with 12 mm spacing .	41
24	Drag force per twine for crossing twines with 24 mm spacing .	41
25	Drag force per twine for crossing twines with 12 mm spacing .	42
26	Drag coefficients for parallel twines with 24 mm spacing	43
27	Drag coefficients for parallel twines with 12 mm spacing	43
28	Drag coefficients for crossing twines with 24 mm spacing	44
29	Drag coefficients for crossing twines with 12 mm spacing	44
30	Drag force on the frame without any models	45
31	Drag on one twine, with precision error	46
32	Drag coefficients with precision error	47
33	Deflection of hydroid models at different velocities	48
34	Drag coefficient vs. number of twines, 0.3 m/s	49
35	Drag coefficient vs. number of twines, 0.8 m/s	50
36	Drag coefficient vs. number of twines, 1.2 m/s	50
39	Comparison with results from Lader et al.	54

List of Tables

1	Results from experiments by Swift et al. (2006)	8
2	Overview of all the configurations	23
3	Total drag, mean drag and standard deviation for the repeated tests	32
4	Precision limit and uncertainty for repeated tests	33
5	Projected area of twine and fouling for all configurations . . .	38

1 Introduction

Marine fish farming is a growing industry, and it is an important contributor to the Norwegian economy. Because the world's population is growing, it is also expected that a larger proportion of the world's food demand will have to be covered by seafood in the future. Therefore, the aquaculture industry is considered to have a large potential, and research and continued development of the technology related to this industry is important.

An important branch of the Norwegian aquaculture industry is rearing of fish; salmon in particular, but also other species. Normally the fish is kept in large net cages (often called net pens) in the ocean. Fouling organisms that grow on these net cages and their supporting structures are a substantial problem in the aquaculture industry (Fitridge et al. 2012). The problems caused by such bio fouling can be divided into three categories: firstly, it restricts the water exchange, and thereby causes lower oxygen levels in the water; secondly, it increases the risk of diseases, because bacteria and viruses can settle on the fouling organisms; and thirdly, it gives larger loads and deformations on the structure, because the bio fouling increases the drag forces and the mass of both the net and other structural components. This study is focused on the third of these points, and the overall goal is to increase the understanding of how the bio fouling influence the hydrodynamic forces on the net.

Before the work on this master thesis commenced, a pre-project containing a review of recent research related to bio fouling on net pens, and some suggested topics for this thesis, was written. In that project it was found that the current models relating the amount of bio fouling to the increase in hydrodynamic forces have many limitations, and are still under development. Therefore, the suggested studies aimed at either validating one of these models, or try to gather more data on how bio fouling is affecting lift and drag forces on net panels. Because the limitations of the existing models would have made it difficult to make a realistic test case for a validations study, it was decided to focus this master thesis on gathering more data, which then can be used in the further development of such models. The relationship between the inflow angle, and the drag- and lift-forces for a fouled net has not yet been investigated, so the preferred plan for the master thesis was to do an experimental study where the lift- and drag forces on a fouled net panel were measured for a range of inflow angles. However, when this was planned more in detail, it was found to be too costly, so another study requiring a simpler set up was proposed.

This newly proposed topic for this master thesis is a continuation of a recent experimental study done by P. Lader et al. (2014). Experiments with live bio fouling from the sea are difficult to do in a controlled environment in a tank, because most tanks can only be used with freshwater. Therefore, P. Lader et al. (2014) studied the growth rates and structural properties of hydroids on net panels, and made physical models of twines with artificial hydroid fouling that had similar properties. These models can be used in freshwater tanks as well as seawater, and preliminary drag tests with a single

twine, two parallel twines, and single and double crosses were done by P. Lader et al. (2014). The aim for the current study is to expand on this work by using the same type of models, and do more drag tests with different configurations. The plan is to try several different spacings between the parallel twines, and also investigate the effect of the number of twines, by varying the number of parallel twines between two and eight. Hopefully, the higher number of twines get closer to representing a real net for the configurations with crosses.

The more detailed plan for the work can be roughly divided into six steps. The first step (i) is to summarise the most important points from the pre-project; then identify which tank facilities to use for the experiment, and design and build the experimental set up; and also examine which configurations and velocities that should be tested. The second step (ii) is to calibrate the load cells, and then measure the drag force on the frame for all towing velocities, so that the drag contribution from the frame can be subtracted from the later tests. The calibration should be validated by doing preliminary tests with models where the drag coefficient is known. To try to identify which twine spacings are most interesting, a few preliminary tests with flow visualisation and two parallel twines at different distances, should also be done in this step. These first two steps are mainly preparations for the following experiments.

The next three steps are the main part of the experiments. Step three (iii) consists of performing drag tests for a single twine; and two, four, six and eight parallel twines; for the twine spacings identified in step two. This should be done for a range of current velocities. The fourth step (iv) is drag tests with twines crossing each other. The twine spacing and number of parallel twines will be the same as in step three, but there will be both horizontal and vertical twines. That gives a single cross, and two-by-two, four-by-four, six-by-six and eight-by-eight crossing twines. Step five (v) is to do repeated tests for at least one of the tests conditions, and calculate the uncertainty for the tests. A general discussion of possible error sources should also be made.

The last step (vi) is to analyse the results from the experiments, both drag forces and flow visualisations, and see if any useful conclusions can be drawn. Topics of particular interest are whether the results can be representative for a realistic net, and how the drag forces are influenced by the presence of hydroid bio fouling.

Most of the work was done according to the plan above, but one significant change was made in step two (ii). The time from when the reservation of the towing tank was confirmed, and the practical preparations could start, to the actual start of the experiments, was very short; and because of that, it was impossible to get the flow visualisation set up ready for the first part of the experiments. This meant that the preliminary tests with two parallel twines could not be done, and the different twine spacings for the experiments had to be chosen without knowing at which spacings possible changes in the flow structure occurred. To make it easier to compare the results to the results

found by P. Lader et al. (2014), and in that way validate the results for the similar configurations, it was decided to use the same twine spacings, of respectively four and eight twine diameters (12 mm and 24 mm). Since the equipment for the visualisation had to be prepared and mounted during the experiments, the progress was also slightly slower than expected, and the number of velocities for each configuration had to be reduced for the last half of the experiments.

2 Methods

The intention of this study is to continue the work done by P. Lader et al. (2014), and hence the methods used were similar. Bio-fouling induced drag forces were studied using twine models with artificial hydroid fouling. These twine models were 50 cm long, and they were made of two twisted 1.5 mm steel rods with short pieces of multi filament fishing line acting as hydroids. The artificial hydroids were evenly distributed with 15 hydroids per centimeter, and they had uniform length and thickness of respectively 16 mm and 0.32 mm. A detailed description of the models and how they were produced can be found in chapter 4.1.

The experiments were done in the small towing tank (tank II) at MARINTEK/ NTNU in Trondheim, Norway. This towing tank is 25 m long, 2.8 m wide and 1 m deep (Marine Technology 2014). The models were mounted in a frame that was attached to the towing carriage with two force transducers, such that the total drag forces on the frame and the models could be measured. The drag force and the velocity of the towing carriage were recorded, and then the average drag and the standard deviation of the time series were calculated using MatLab. To find the drag on just the twines, the drag on the frame without any twine models was measured for all the different velocities, and then subtracted from the total drag. More details about the set up and the calculation methods can be found in chapter 4.2.

Approximately 300 different runs were done, with configurations ranging from 1 single twine, to eight by eight parallel twines crossing each other, forming a small net patch. The different configurations were tested at velocities from 0.05 m/s to 1.4 m/s, and since the tank length is fixed, the length of the recordings varied from around 10 seconds at 1.4 m/s to a couple of minutes at 0.05 m/s.

Simple flow visualisation was also attempted for some of the configurations to try to understand the flow around the twines better. This was done by adding a solution of fluorescein (green colour) in front of the models during the runs, and take a video recording of the models and the wake behind the models.

There are several advantages of doing the experiments in a towing tank, using models with artificial bio-fouling. One is that it is laboratory conditions, so it is easy to control the environment, and there are few unknown factors. Another is that it is easy to reproduce, because the models are all the same, with given dimensions. This also makes it comparable to the previous study by P. Lader et al. (2014).

The weakness of this method is that it is not an exact representation of the real scenario at a fish farm. In reality hydroids and other fouling organisms will be more randomly distributed, often in colonies, and they will have varying size (P. Lader et al. 2014; Guenther, Misimi, and Sunde 2010). These tests are also done with few parallel twines and small net patches, and might not be very representative for larger net panels and full size net pens.

3 Theory

The pre-project that was written prior to this thesis included a thorough literature study of the state of the art in research on the effect of bio fouling on fish farm nets. This study addressed recent experimental studies of the increased drag caused by fouling, the conditions for growth of marine bio fouling, and also the most used modelling techniques for forces and deformations on clean nets. In the following paragraphs the relevant topics that were covered in the previous project will only be summarised briefly, while relevant research that was not mentioned is investigated more in depth.

3.1 Results From Pre-Project

In the pre-project it was found that the fish farming net pens which this study is oriented towards normally are shaped like vertical cylinders. They are kept afloat by a floater ring on the sea surface, and the net is kept in shape with a heavily ballasted bottom ring. The floater ring is moored either with direct anchor lines to the seabed or land, or via buoys that are anchored to the seabed (Fig. 1). Bio fouling can be a problem for this type of net pens in several ways: it restricts the water exchange, increasing the risk of too low oxygen levels; it provides a settling place for bacteria and viruses, causing increased disease risk; and it increases the hydrodynamic forces, giving larger deformations and structural fatigue (Fitridge et al. 2012). In the Norwegian fish farming industry the most common way to cope with the bio fouling is to use copper-based coatings on the nets to decrease the growth rate, and then either wash or dry the nets when it is required (Guenther, Misimi, and Sunde 2010)

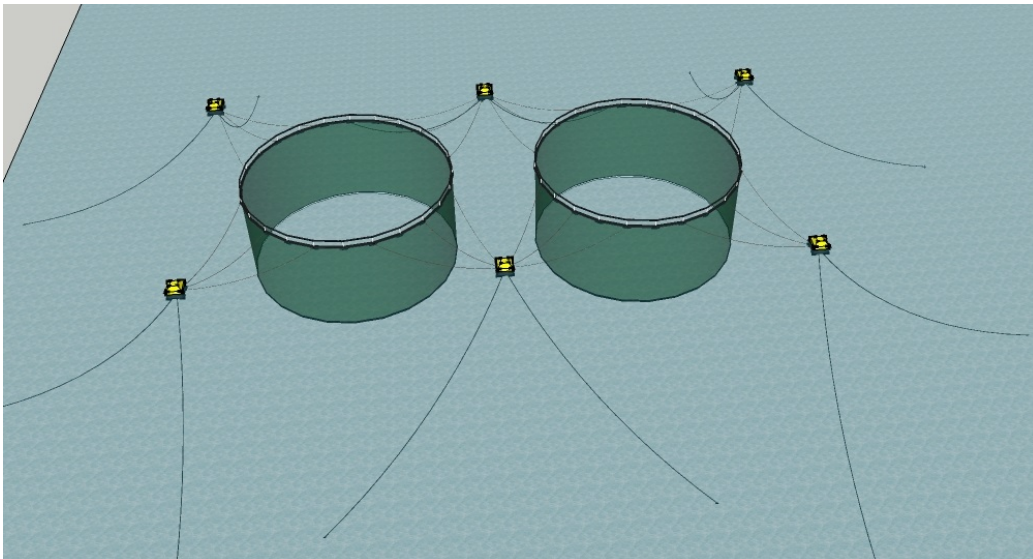


Figure 1: Sketch of net pens with morings (figure taken from pre-preoject).

The general term bio fouling covers a variety of marine organisms; the most common species in the context of fish farming are hydroids, algae, mus-

sels, sea-squirts and skeleton shrimps (also known as ghost shrimps, *caprellidae*). In particular the hydroid *Ectopleura Larynx* is dominating in South-West- and Mid-Norway (Guenther, Misimi, and Sunde 2010). The settling and growth rate of different organisms depends on many factors, including temperature, water depth, light conditions, surface structure and materials, in addition to the natural randomness. Therefore, it is very unlikely to have a uniform distribution of fouling organisms, and it is impossible to model the bio fouling exactly.

Several different finite element models for simulating net forces and deformations were studied in the pre-project. These models can be divided into two main groups, based on how the hydrodynamic forces are modelled (Kristiansen and Faltinsen 2012). One group is Morison models, where the hydrodynamic forces on the net elements are calculated by using Morison's equation. A weakness with this type of models is that the interaction effects between the twines are neglected. The other group is screen models, where the net is represented by net panels, and the drag and lift forces on a panel are estimated by empirical equations. Some of these empirical equations are presented below (Ch. 3.1.1). For screen models the forces can also be calculated using CFD, but this requires very much computational power, and is therefore not efficient (P. F. Lader and Fredheim 2006).

3.1.1 Empirical Models for Forces on Clean Nets

In the pre project several empirical formulas for the forces on a net panel were identified. Most of these formulas use the solidity ratio (S_d) to describe the net properties. The solidity ratio is defined as the ratio between the projected area of the twine, and the outline area of the net panel (Balash et al. 2009).

Milne (1979) found two equations for the drag coefficient of nets, one for knotted nets (eq. 1) and one for knotless nets (eq. 2).

$$C_d = 1 + 1.89S_d + 2.34S_d^2, \text{ knotted} \quad (1)$$

$$C_d = 1 + 1.37S_d + 0.78S_d^2, \text{ knotless} \quad (2)$$

Løland (1991) gives formulas for the drag and lift when the angle between the inflow current and the net panel is α (eq. 3 and 4).

$$C_d = 0.04 + (-0.04 + 0.33S_d + 6.54S_d^2 - 4.88S_d^3) \cos(\alpha) \quad (3)$$

$$C_L = (-0.05S_d + 2.3S_d^2 - 1.76S_d^3) \sin(2\alpha) \quad (4)$$

Balash et al. (2009) found the following analytical equation (eq. 5) which is expressed by the drag coefficients for a cylinder ($C_{D|cyl|}$) and a sphere ($C_{D|sp|}$), representing respectively the twine and the knots.

$$C_{d|net|}^{out} = \frac{(C_{D|cyl|} + C_{D|sp|} \frac{\pi}{8\alpha\beta})}{(1 + \frac{\pi}{8\alpha\beta})} \cdot \frac{S_d}{(1 - S_d)^2} \quad (5)$$

where $\alpha = \frac{D}{l}$ and $\beta = \frac{D}{d}$. D is the diameter of the knot (assumed to be spherical), d is the twine diameter and l is the mesh length (centre-centre distance between two knots).

Experiments showed that the drag coefficients from the analytical equation are too high for high solidity nets and too low for low solidity nets. Based on the experimental results Balash et al. (2009) suggested the corrected equation below (eq. 6).

$$C_{d|net|}^{out} = \frac{(C_{D|cyl|} + C_{D|sp|\frac{\pi}{8\alpha\beta}})}{(1 + \frac{\pi}{8\alpha\beta})} [8.03S_d^2 - 0.74S_d + 0.12] \quad (6)$$

For a knotless net equations 5 and 6 can be simplified (eq. 7 and 8 respectively).

$$C_{d|net|}^{out} = C_{D|cyl|} \frac{S_d}{(1 - S_d)^2} \quad (7)$$

$$C_{d|net|}^{out} = C_{D|cyl|} [8.03S_d^2 - 0.74S_d + 0.12] \quad (8)$$

3.1.2 Experimental Studies on Fouled Nets

The pre-project also included a review of two experimental studies done with real bio fouling. Some results from these studies are presented in this thesis because they are useful for comparison of results.

The first of these studies was a series of towing tests done by Swift et al. (2006). In this study the drag on nine square net panels were measured when the nets were clean, and then again after five months of immersion. The bio fouling on the net panels consisted mainly of Skeleton Shrimp (*Caprella sp.*), but also some colonial hydroids (*Tubularia sp.*) and small blue mussels. The amount of fouling on the nets was measured both by weight and volume, and the solidity was found from photos of the nets. Several different towing velocities was used, and the drag coefficient was found by least mean square curve fitting, assuming that the drag increased with the velocity-squared. A possible error source in the experiments was that the clean net towing tests were done in a towing tank, while the bio fouled panels were towed alongside a boat in seawater. Some of the results from the experiments can be found in table 1 below.

Table 1: Results from experiments by Swift et al. (2006). Only drag coefficients based on the outline area are included.

Net number	Clean net C_d	Mass of growth [kg]	Solidity	Biofouled C_d	Increase [%]
1	0.176	5.3	0.566	0.599	240
2	0.195	3.48	0.743	0.513	163
3	0.195	2.7	0.671	0.353	81
4	0.195	2.58	0.813	0.464	138
5	0.195	5.64	0.771	0.576	195
6	0.195	4.28	0.629	0.531	172
7	0.175	4.96	0.502	0.318	82
8	0.175	2.01	0.572	0.185	6
9	0.176	3.26	0.547	0.26	48

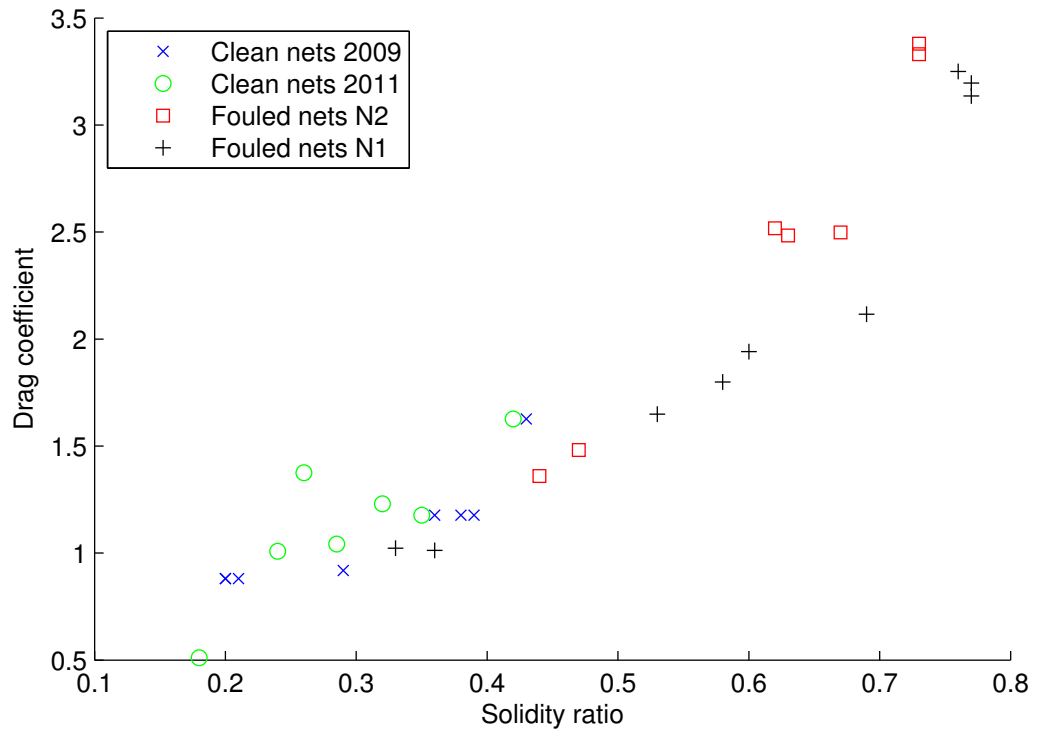


Figure 2: Drag coefficients from the experiments by Gansel et al. (2013)

The other experimental study was done by Gansel et al. (2013). It focused on identifying the relationship between solidity and drag coefficient both for clean nets, and nets with hydroid bio fouling. The experiments were done in a flume tank, with current velocities of 0.05 m/s and 0.1 m/s. For the tests with bio fouling two different net types, with solidities of 0.2 and 0.29 were used. They were deployed in the sea for either two, six or ten weeks, giving a solidity range from approximately 0.3 to 0.8 (including bio fouling and net).

The study was focused on hydroids, so only nets with a significant majority of the hydroid *Ectopleura Larynx* were used. Eight different clean nets, with a solidity range from 0.2 to 0.43, was also tested. A problem in this study was that the tests were done in a freshwater tank, and the freshwater changes the properties of the hydroids. The drag coefficients for different solidities, both for clean and fouled nets, are displayed in figure 2.

3.2 Additional Theory

The present study is based on an experimental study done by P. Lader et al. (2014) at SINTEF Fisheries & Aquaculture. Their study consisted of two main parts: in the first part they studied the growth of the hydroid *Ectopleura larynx*, and in the second part they measured the drag on twine models with artificial hydroid fouling. The aim of their study was to achieve a better understanding of how the forces on a net change because of hydroid fouling. This is desirable because it can lead to better and more efficient fish farm designs in the future.

Previous experimental studies with live bio fouling have shown several difficulties. Drag measurements at sea might be inaccurate because it is hard to control the environment (Swift et al. 2006), while tests in hydrodynamic laboratories is difficult because most laboratories are fresh water based, and the hydriods die quickly when put in freshwater (Gansel et al. 2013). Because of these difficulties P. Lader et al. (2014) wanted to develop models of twines with artificial hydroids.

The hydroid *Ectopleura larynx* consist of three main parts: a root system, called hydrorhiza; a stem, called hydrocaulus; and the head, called the hydranth. The hydrocaulus and hydranth together are often referred to as the polyp. To study the growth characteristics of the hydroids six nets were left submerged in the sea for three weeks, and six nets for six weeks, and then the hydroids in a sampling area on each net were counted and measured. It was found that the length of the stems was approximately Rayleigh distributed, with an average length of 6.4 mm and 11.2 mm, after respectively three and six weeks. The thickness of the stems appeared to be Gaussian distributed with an average of 0.29 mm, and it was independent of the immersion time. The enumber of hydroids was approximately 1.4 hydroids/mm of twine for the shortest interval, and just slightly lower for the longest interval. The size of the heads was approximately 0.7-0.8 mm for all the nets, but after the longest immersion time very few hydroids had heads (P. Lader et al. 2014).

Based on the measurements from the first part P. Lader et al. (2014) made models of single twines with artificial hydroids. The models was made of a pair of thin (1.45 mm) steel rods which was twisted together forming a twine, and short pieces of multi filament nylon fishing line acting as hydroids. Since the models were similar to the ones used on the present study, more details on how they were made can be found in chapter 4.1. To make the production of the models possible some simplifications were made: It was assumed that all hydroids on one model had the same dimensions (stem length and diameter, and head size), and that all models had a constant

hydroid density (hydroids/mm).

Four types of models with different amounts of artificial fouling were tested. Three of them had a hydroid density of 15 hydroids/mm, and stem lengths of 9 mm, 16 mm and 20 mm respectively (later abbreviated to 9N, 16N and 20N). The last had a much higher hydroid density of 70 hydroids/mm, with a stem length of 16 mm (16H). P. Lader et al. (2014) states that a model with shorter stem lengths would have matched the field measurement better, but it was practically difficult to make models with shorter stem length than 9 mm. Two models without fouling was also used, one with two (TW) and one with three (TW3) twisted steel rods (P. Lader et al. 2014).

How well the models represented a thread with real bio fouling, particularly with regards to the stiffness of the hydroids, was only assessed by visual comparison of the deformation and motions of the hydroids, when models with real and artificial hydroids was dragged side by side in a tank (P. Lader et al. 2014). Even though the hydroids seemed to behave similarly, it would be useful to find a way to measure and compare the stiffness of the hydroids and the nylon line.

P. Lader et al. (2014) did drag tests of single twines, two parallel twines with distances of both four and eight diameters, and a cross, for all the model types. For the 20N model they also tested double crosses (a cross with two parallel twines in each direction). The tests were done at velocities from 0.1 m/s to 1/4 m/s, with 0.1 m/s increments. Some of the results from these tests are included in figures 3 and 4. As expected the drag increases with increasing amounts of fouling. In contrast to the drag on a smooth circular cylinder, the drag coefficient seems to be Reynolds number dependent. For all the models with the normal hydroid density there is a drop in C_D above Re 2600. This drop is believed to be caused by the geometry of the twisted core, because it is significant for the twisted rods without fouling (TW), and less visible with larger amounts of fouling. For the models with fouling the drag coefficient is also generally decreasing for increasing velocity. This is probably because the hydroids deform and become more streamlined at higher velocity (P. Lader et al. 2014).

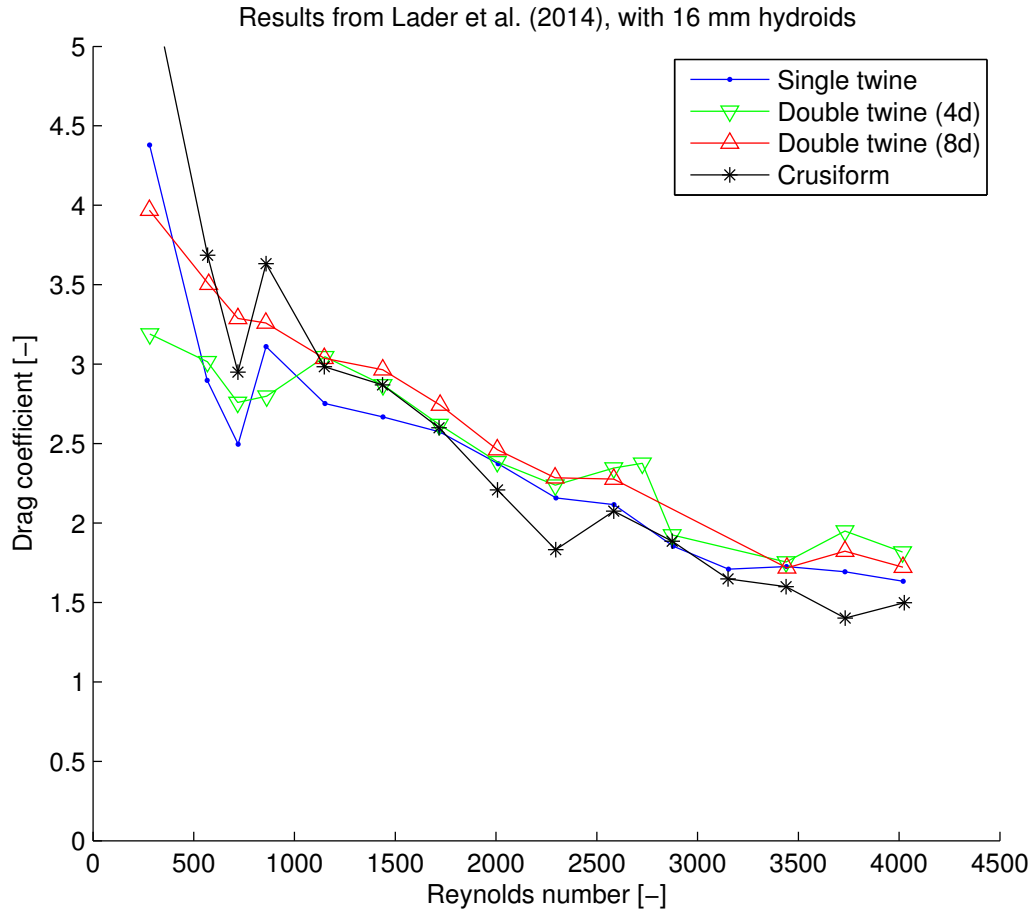


Figure 3: Drag coefficient for the different configurations with 16 mm hydroids. Results from P. Lader et al. (2014).

Results from Lader et al. (2014)

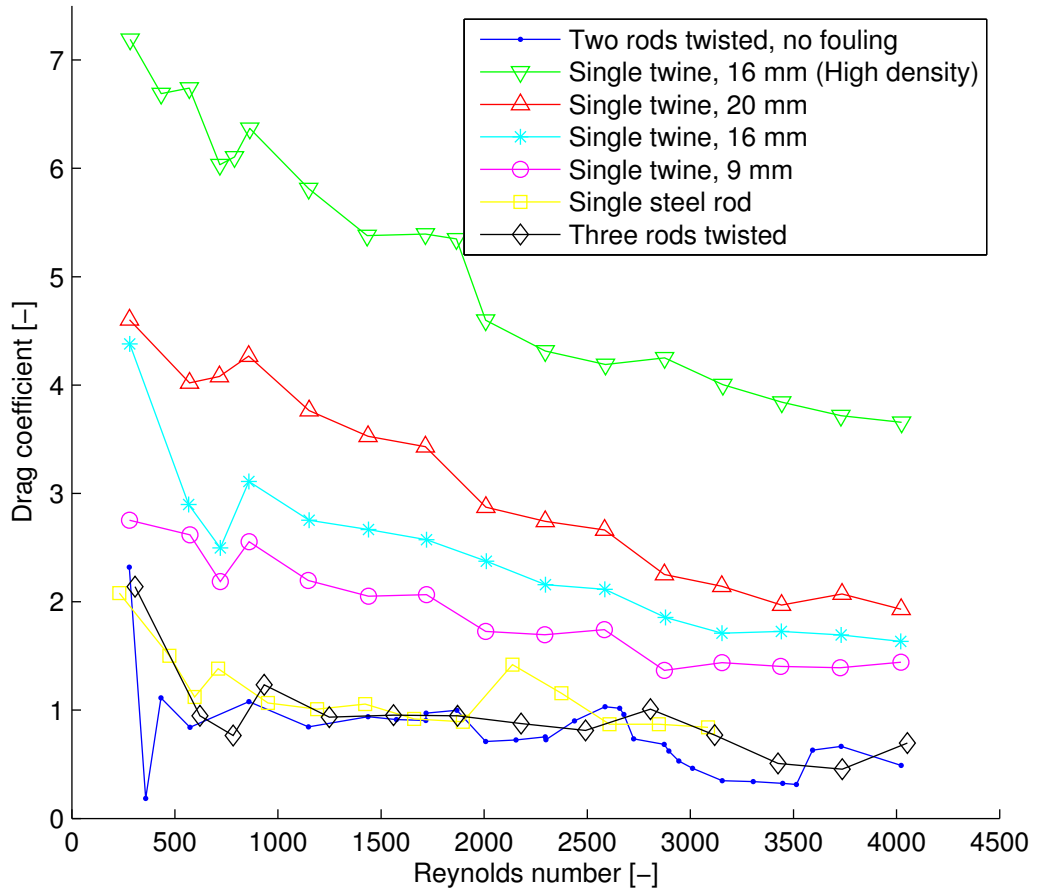


Figure 4: Drag coefficients for single twines. Different hydroids lengths, and cores without fouling. Results from P. Lader et al. (2014).

4 Experiments and Observations

4.1 Models

P. Lader et al. (2014) used twine models with different hydroid lengths and densities. This study is only focused on the version with 15 hydroids per cm, and a hydroid length of 16 mm, so the models used were intended to be equivalent to those models in all aspects except for the length. In present experiments the mounting frame were 50 by 50 cm, so the models had a 50 cm long test section with artificial hydroids, plus 2 cm of clean twine at each end for mounting, giving a total length of 54 cm. To allow for many different configurations, and small net patches, 16 twine models were made. Figure 5 shows the finished models fixed in a purpose built transport case.



Figure 5: All the finished models in a protective case

The models consist of two 1.5 mm diameter steel rods which were twisted together to form a 3 mm twine. The artificial hydroid fouling was made of short pieces of multifilament spectra fishing line with a diameter of 0.32 mm. These pieces of fishing line, which were 32 mm long, were placed between the steel rods, and when the steel rods were twisted they got clamped between the rods. In this way each thread is fixed in the middle, and makes two 16 mm hydroid models. The ends of the hydroid models were melted using hot air, to create a small head.

When the steel rods are twisted, they will contract such that the finished model is shorter. It was found that this contraction was 6% when the models were twisted one turn per 12 mm (41.67 turns on 50 cm). This means that the 50 cm long section with artificial hydroids must be 53.2 cm before twisting.

To get 15 hydroids per centimeter for the finished model, one needs 7.5 pieces of fishing line per cm, or 375 pieces for the 50 cm finished model. Since the fishing line were attached to the rods before they were twisted, the 375 pieces were distributed evenly on 53,2 cm, giving a 1.419 mm distance between each thread.

To make the production easy a wooden shaft with a slot for one of the steel rods were made. This shaft was coupled to a slowly rotation engine, such that the fishing line could be spooled onto the shaft before it was cut. The circumference of the shaft, with one steel rod fixed to it, was approximately 35 mm, adjusted such that one turn would give a thread piece with 32 mm length when the ends were melted. To get the threads evenly distributed with the right distance a scale with markers with 1.419 mm spacing was printed and glued to the shaft (Fig. 6). The distance could then be made consistent by making sure that the line was spooled on with one revolution per marker along the shaft. After the line was spooled on some glue was applied to the thread and the steel rod, to keep the thread pieces in place temporary. Then the line was cut into pieces of appropriate length and the ends melted to form heads. This was done in one operation using a heat gun to melt off the lines on the back side of the wooden shaft, opposite of the steel rod. To get an accurate cut, a thin piece of plywood with a 3 mm wide slot was used to shield the threads, such that only a 3 mm section was exposed to the heat. When the lines were cut, the second steel rod was placed on top of the first one, before they were removed from the wooden shaft and twisted using an electric drill. A small piece of tape was attached to the chuck of the drill, so the number of turns could be counted manually.



Figure 6: The shaft that the fishing lined was spooled onto with scale marking the distance between each tread

Since the models were made manually, some inaccuracies were inevitable. However, this was never more than three or four misplaced threads per model, and hence insignificant compared to the total number of hydroid models on each model.

4.2 Equipment and Set Up

As mentioned earlier, the experiments were done in the small towing tank at Tyholt (Fig. 7). To simulate current, and find the drag coefficient, the models were towed at several different velocities, and the drag forces measured. The models should always be kept orthogonal to the current direction, so they had to be mounted in a frame. This frame was then attached to the towing carriage with two force transducers measuring the horizontal sheer force, which is equal to the total drag on the frame and the models mounted to the frame. The frame was made with a 50 by 50 cm square test section where the models could be mounted both vertically and horizontally. When the frame was in the water the upper side of the test section was approximately 15 cm below the surface. The dimensions were chosen based on the width and depth of the tank, to avoid too much interaction with the free water surface, and the bottom and side walls.



Figure 7: The small towing tank at MarinTek, Tyholt

It is preferable that the drag force on the frame is as low as possible, to make it less significant compared to the drag on the models. Therefore, the parts that were submerged during the test were made of streamlined aluminium profiles. The profiles had an elliptical cross section which were 30 mm by 12 mm. These parts were welded together and ground, to keep them smooth. At the middle of each of the sides of the lower square a 30 cm long

cutout were made by splitting the profile longitudinally. The loose piece that was cut out was attached to the frame by two screws, such that it formed a clamp where the ends of the models fastened. Both sides of the clamps were covered by flexible rubber to get a better grip (Fig.8). This clamp design was chosen because the shape, and hence also the drag, would be independent of how many models were attached.

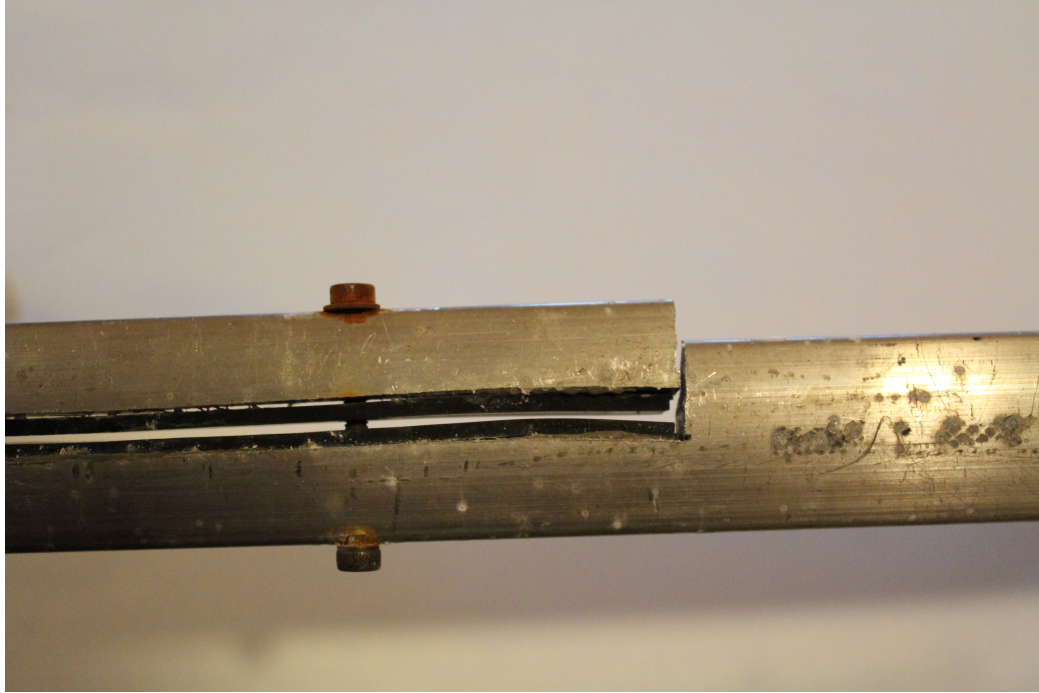


Figure 8: Detail of the clamps that held the models in place

The parts that were above the water, where the drag does not matter, were made by simpler 30 mm by 30 mm square aluminium profiles. These were easier to handle, and they could be mounted together by using angle brackets and M6 bolts. Detailed drawings of the frame are included in appendix A. Figure 9 shows the frame rig mounted on the towing carriage.

Two HBM SP4M load cells with 18 kg maximum capacity were used to measure the drag force. These load cells were chosen because they had the most suitable measuring range for this experiment among the ones that were available at MARINTEK. The highest force per model measured by P. Lader et al. (2014) was right below 3 N at 1.4 m/s. Since the models used in this experiment are 50 cm long, compared to 30.5 cm in the previous experiments, the expected maximum drag force on one model was 5 N. This gave an estimated maximum force of 80 N or approximately 8 kg with 16 models. Initially the plan was to use two 3 kg load cells, but the preliminary estimates showed that those were too small. Although one 18 kg load cell would be sufficient to take the drag forces, it was decided to use two load cells to get a higher stiffness. This was done to avoid vibrations, in particular sideways motions and rotation about the vertical axis. The load cells have built in compensation for off-centre loads, so the point of attack for the

forces does not influence the output. This simplified the design of the frame rig significantly, since the average resultant force normally would act 40 - 50 cm below the load cells.



Figure 9: The complete frame rig mounted on the towing carriage

The load cells were connected to an MGCplus data acquisition system (DAQ) which was placed on the towing carriage (Figure 10). The DAQ has

built in amplifiers and filters, and was connected to a computer where the data was recorded. In addition to the voltages from the load cells; the time, the velocity and position of the carriage, and the total force, were recorded. The drag force was calculated by adding the voltages, and then multiplying the sum with a calibration factor. A 200 Hz sampling frequency was used for all the tests. This is a relatively high sampling rate, and it should be sufficient to measure dynamic behaviour like for instance vibrations. Because it was mainly the steady state condition with constant velocity that was relevant for this study, 200 Hz might have been much more than necessary. However, since there were only six data channels the size of the data files would not be too large, so it was decided to keep the frequency high in case of any vibrations. According to normal practise (Steen 2014) a low pass filter with cut off at 1/10 of the sampling frequency (20 Hz) was applied. This is to avoid folding and non-physical effects if there are any high frequency vibrations or noise close to the sampling frequency.

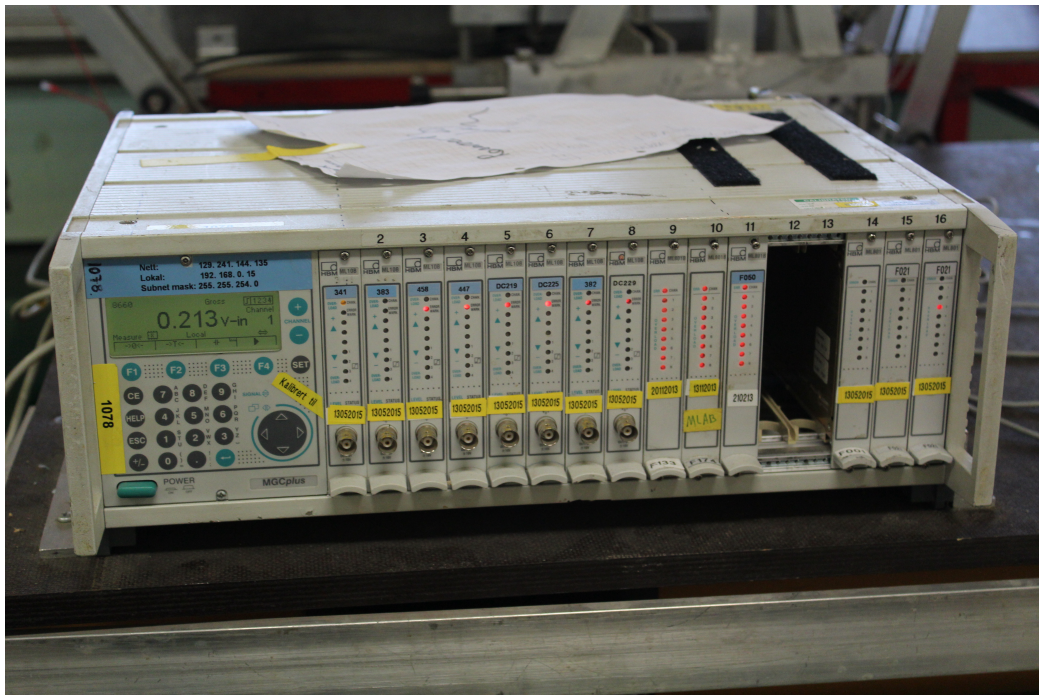


Figure 10: MGCplus data acquisition system

In the last part of the experiment period a simple system for flow visualisation was also implemented. This consisted of a thin brass pipe adding dye in front (upstream) of the models, and a GoPro video camera filming the models and the wake behind the models. A solution of fluorescein was used as dye. The solution was kept in a reservoir on the towing carriage, and then led through a silicon hose down to the 3 mm brass pipe which was mounted in front of the frame. The flow rate was controlled with an adjustable clamp squeezing the hose. The camera, a GoPro Hero3, was mounted right behind the frame, viewing straight down on the wake from above. This caused the camera to be close to the surface, and hence it created relatively large waves

at higher velocities, but it was assumed that it would not influence the results much, since it was behind the frame and the models.

Figure 11 shows two example images taken from the visualisation videos. At 0.6 m/s (Fig. 11b) the dye only forms a cloud behind the models, and it is impossible to see any flow structures. This was the case for all the tests at medium and high velocities. For the lowest velocity (11a) some flow structures were visible, but it was still difficult to see enough to draw any conclusions about the flow pattern. Because of the limited quality of the visualisation videos, they were not used much later in the analysis, and the emphasis was on the drag forces.

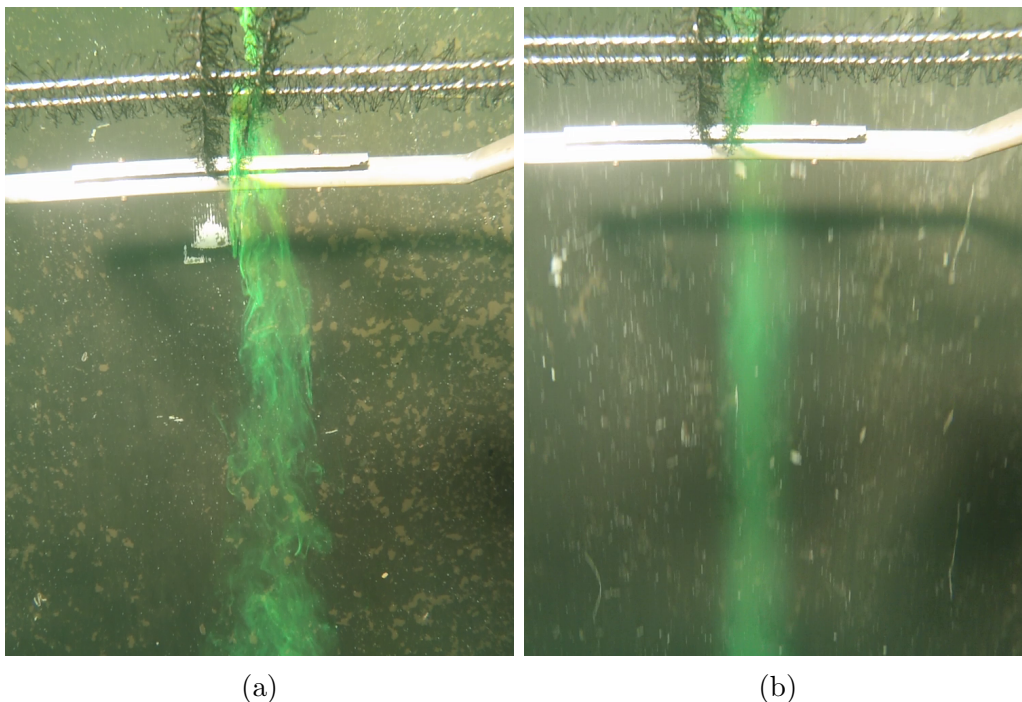


Figure 11: Examples of relatively good and bad visualisations. 11a is from a 0.05 m/s run where some flow structures are visible, while 11b is from a run at 0.6 m/s where the dye only forms a cloud.

4.3 Calibration

As described earlier, the output voltages from the load cells were first added together, and then multiplied with the calibration factor. The two load cells were calibrated as one unit like this because it is difficult to know how the force is distributed between them when both are fixed to the same structural members. Another option would have been to calibrate the load cells individually before they were mounted, but uncertainty about whether the properties could change when the two load cells were fixed in place, weighted for the first option.

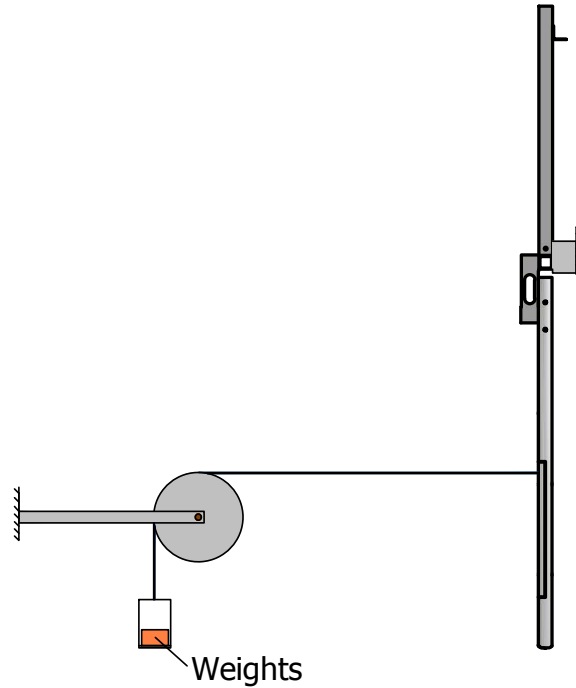


Figure 12: Drawing of the set up used for calibration

The actual calibration was done by mounting the frame to a rigid bench, and then apply known forces ranging from 0.5 kg to 10 kg. The forces were applied horizontally approximately in the middle of the measurement section, using a simple line and pulley arrangement (Fig. 12). A set of standard weights was used to get an accurate and steady pulling force. The weights applied were 0.5 kg, 1 kg, 2 kg, 5 kg, 7 kg and 10 kg. These forces were chosen based on the estimate of the expected maximum force done earlier. Using the calibration module in the recording software, the mean voltage from each of the load cells was extracted from the timeseries, and exported to an excel sheet. Then, the voltages were added together and the known force, given in Newton, was plotted as a function of the voltage (Fig. 13). The calibration factor, which is the relation between voltage and force, was found by making a linear curve fit with the built in function in excel. This gave a calibration factor of 16.273 N/V. A separate force-channel which calculated the force in real time was set up in the recording software, to make it easier to interpret the results immediately.

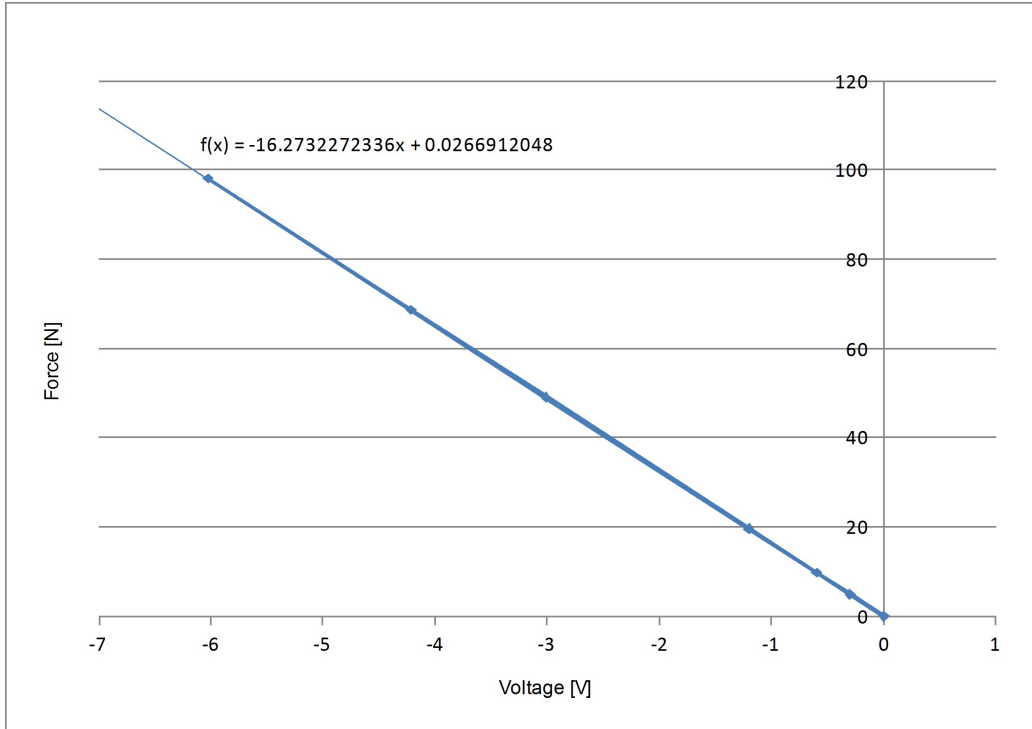


Figure 13: Calibration: Force plotted as a function of voltage, including equation for linear curve fit.

To eliminate any large errors, the calibration was tested manually two times. Once right after the calibration was finished, and then another time at the end of the experiment period, right before the equipment was dismantled. This was done by pulling the frame with a portable dynamometer, and compare the force on the dynamometer with the recorded force. Since it is difficult to apply a steady force by hand this was not a very accurate test, but it confirmed that the calibration was not far off. This simple test was also done applying the force at the upper and lower parts of the frame, to make sure that the bending moment did not influence the measured force.

4.4 Experiments

This study focuses mainly on how the configuration of twine models influence the drag on the twine, and if the trends with the fouled twine models are similar to the trends for clean twines or cylinders. Therefore, systematic tests of 18 different configurations were done. The first two configurations were done on single twines. One with two twines placed parallel to each other, but so far apart that they would not interact, such that the drag would be two times the drag on one single twine. The other had two single twines crossing each other, creating one cruciform. The remaining 16 configurations were different combinations of parallel twines, and cruciform structures with several parallel twines in each direction. Tests were done with 2, 4, 6 and 8 parallel twines, and crosses with the same numbers of twines in each direction. All these tests were done with both 24 mm and 12 mm distance between the

twines. 24 mm distance equals approximately 8 diameters, and 12 mm equals 4 diameters. The spacing measured is the gap between the twines, and not centre-centre distance (Fig. 14).

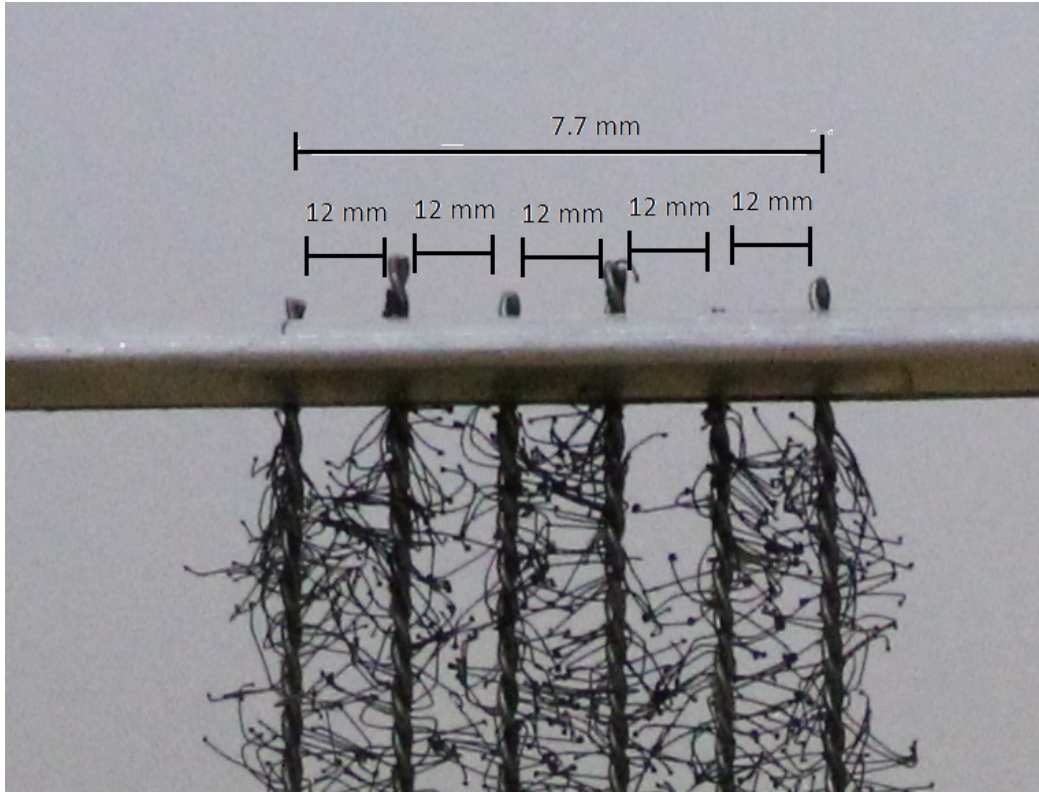


Figure 14: Illustration of how the distance between the twines is measured

Through the first half of the experiments, that was the two configurations with single twines and the ones with 24 mm spacing, the drag was measured for 15 different velocities, from 0.1 m/s to 1.4 m/s, with 0.1 m/s increments. When the visualisation equipment was in place, at the last of the tests with 24 mm spacing, a run at 0.05 m/s was also done, in an attempt to see the flow pattern clearer. After the first test with 12 mm spacing, some of the velocities were left out to save time. Based on the results from the first test with 12 mm spacing, the following velocities were chosen to be most interesting for the rest of the configurations: 0.05 m/s, 0.1 m/s, 0.3 m/s, 0.5 m/s, 0.6 m/s, 0.7 m/s, 0.8 m/s, 1.0 m/s, 1.2 m/s and 1.4 m/s. The two lowest velocities were included only for the visualisation, because the drag measurements for these velocities were inaccurate. All the configurations that were tested are presented in a structural manner in table 2

Table 2: Overview of all the configurations that were tested, with an image of the models in the frame and the specifications

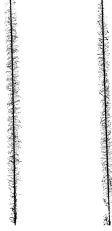
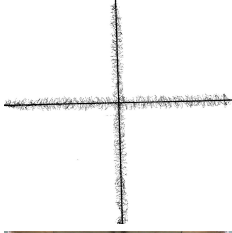


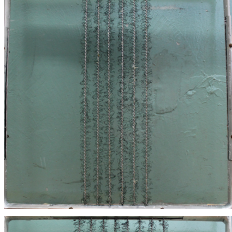

Image	Name	Parallel /Cross	Nr. of Twines	Spacing	Velocities	Visualisation
	singletwine	Par	2	-	0.1 to 1.4	No
	singlecross	Cross	2x1	-	0.1 to 1.4	No
	2par8dd	Par	2	24mm	0.1 to 1.4	No
	4par8dd	Par	4	24mm	0.1 to 1.4	No
	6par8dd	Par	6	24mm	0.1 to 1.4	No
	8par8dd	Par	8	24mm	0.1 to 1.4	No

Table continues on next page

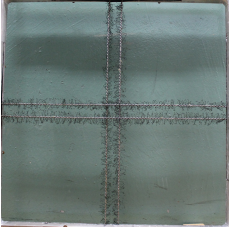
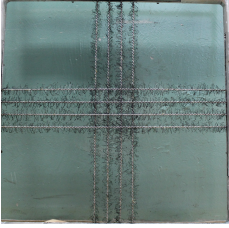
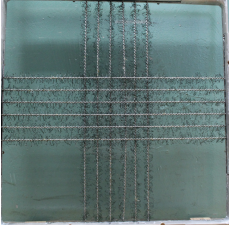
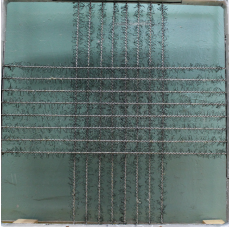
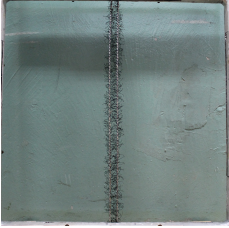
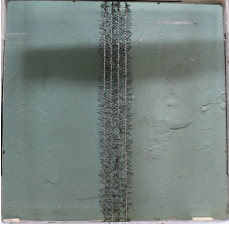
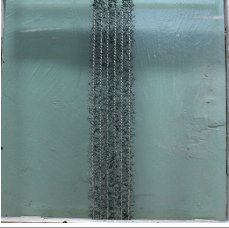
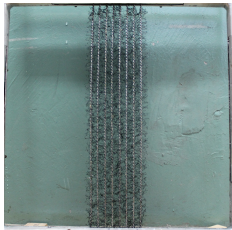
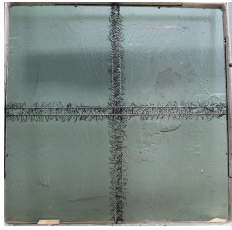
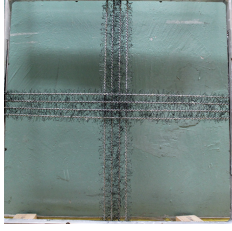
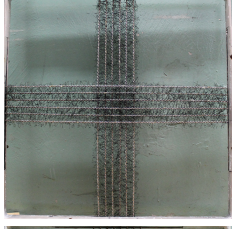
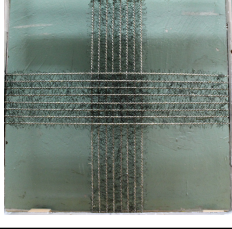
Image	Name	Parallel /Cross	Nr. of Twines	Spacing	Velocities	Visualisation
	2cross8dd	Cross	2x2	24mm	0.1 to 1.4 and 0.05	Yes
	4cross8dd	Cross	2x4	24mm	0.1 to 1.4	Yes
	6cross8dd	Cross	2x6	24mm	0.1 to 1.4	No
	8cross8dd	Cross	2x8	24mm	0.1 to 1.4	No
	2par4dd	Par	2	12mm	0.05, 0.1, 0.3, 0.5, 0.6, 0.7, 0.8, 1.0, 1.2 and 1.4	Yes
	4par4dd	Par	4	12mm	0.05, 0.1, 0.3, 0.5, 0.6, 0.7, 0.8, 1.0, 1.2 and 1.4	Yes
	6par4dd	Par	6	12mm	0.05, 0.1, 0.3, 0.5, 0.6, 0.7, 0.8, 1.0, 1.2 and 1.4	Yes

Table continues on next page

Image	Name	Parallel /Cross	Nr. of Twines	Spacing	Velocities	Visualisation
	8par4dd	Par	8	12mm	0.05, 0.1, 0.3, 0.5, 0.6, 0.7, 0.8, 1.0, 1.2 and 1.4	Yes
	2cross4dd	Cross	2x2	12mm	0.1 to 1.4 and 0.05	Yes
	4cross4dd	Cross	2x4	12mm	0.05, 0.1, 0.3, 0.5, 0.6, 0.7, 0.8, 1.0, 1.2 and 1.4	Yes
	6cross4dd	Cross	2x6	12mm	0.05, 0.1, 0.3, 0.5, 0.6, 0.7, 0.8, 1.0, 1.2 and 1.4	Yes
	8cross4dd	Cross	2x8	12mm	0.05, 0.1, 0.3, 0.5, 0.6, 0.7, 0.8, 1.0, 1.2 and 1.4	Yes

To be able to estimate the precision error of the experiments, five of the tests were repeated five times each. Ideally, this should have been done for all runs, but that would have been impossible within the limited time. The tests that were repeated, were selected such that they should represent the range of velocities and configurations as good a as possible. For the configurations with 2 parallel twines and 24 mm spacing, the runs at 0.1 m/s, 0.8 m/s and 1.4 m/s were repeated, this covered both low and high velocities for the configurations with few twines, and hence relatively small forces. The other two sets of repeats were done with the cruciform-configuration with 8 twines in each direction, and 24 mm spacing, which was one of the configurations

with the highest forces. The repeated velocities for this configuration was between the three first ones, at 0.4 m/s and 1.1 m/s.

It was necessary to measure the drag on the frame without any models to be able to subtract the contribution from the frame from the other measurements. Two series of runs were performed with only the frame, one at the first day of the experiment period and one at the end. The first one was done with velocities from 0.1 m/s to 1.5 m/s, while the second also included a run at 0.05 m/s. It was desirable to do these tests twice because the drag on the frame is included in all calculations, so an error here would influence all the results at that velocity. Another advantage of performing the same tests both at the start and the end, was that it could reveal if the sensors have drifted significantly through the two weeks. The second series was done with the camera housing and the pipe for the dye in place.

When the frame with models was towed through the water it created waves and currents. To avoid that these waves and currents caused noise or disturbances in the measurements, it was necessary to wait for the water to calm between each run. A waiting time of approximately 10 minutes between the start of each run seemed to be appropriate; judged by the waves, and some particles drifting on the surface. After the pipe for the dye was mounted, it was also possible to see the currents deeper below the surface by adding some dye. This showed that there were almost no current after only a few minutes, even when there still was waves on the surface, so 10 minutes was probably more than strictly necessary.

At speeds below 0.7 m/s the waves were small, and the wave pattern was dominated by divergent waves from the two vertical profiles that pierced the surface. From 0.8 m/s and upwards it seemed like the upper transverse part of the frame, and possibly the models, created a transverse wave propagating along the tank, with phase velocity equal to the towing speed. These waves were larger, and had a significantly longer wavelength, compared to the divergent waves. The wave pattern did not differ much between the different configurations, so it is believed that it was mainly caused by the frame, and hence the influence on the drag force on the twine models should not be significant.

The load cells were always zeroed before each run to avoid errors caused by drifting or small changes in the mounting. The frame had to be removed from the towing carriage every time the configuration was changed, and the history of the zero values showed small changes every time the frame rig had been detached from the towing carriage, while there were almost no changes between each run. This suggests that the mounting could influence the zero point of the load cells. The zero points were taken using the built in zero settings tool in the recording software, and they were based on at least 45 seconds long measurements in calm water, right before the run.

To make sure that everything was working, the measurements were always started before the towing carriage, and stopped after the carriage had stopped. This meant that the time series included both the acceleration and deceleration phases, and they had to be trimmed at both ends to only get

the relevant steady state section. For the runs with visualisation, the camera recording and the flow of dye also had to be started and stopped for each run, and since there was no way to remotely control the camera while it was submerged, this slowed down the experiments a bit. Leaving the camera on all the time was not a good option because of limited battery life and storage space on the camera.

4.5 Calculation of Drag Forces

All calculations and data analysis were done using MATLAB. This was because most of the calculations had to be repeated for every run, and then it was practical to automate the process. The binary files from the recording software in the lab could easily be imported into MATLAB using the `catman_read` function, and MATLAB had good built in functions for analysing the time series. The code that was used can be found in the digital attachments.

Firstly, the steady state time interval of the time series was identified, and the transient parts in both ends were removed. This was not entirely automatic, since the time interval was selected manually in the recording software, based on visual inspection of the velocity and force plots. In most cases steady state occurred shortly after the set speed was achieved, and continued as long as the speed was constant (Fig. 15). However, for some of the runs there were oscillations in the start, and hence a longer part of the time series had to be cut off (Fig. 16). The cut off times were exported from the recording software to MATLAB in an excel sheet, and the transient parts were trimmed off in MATLAB.

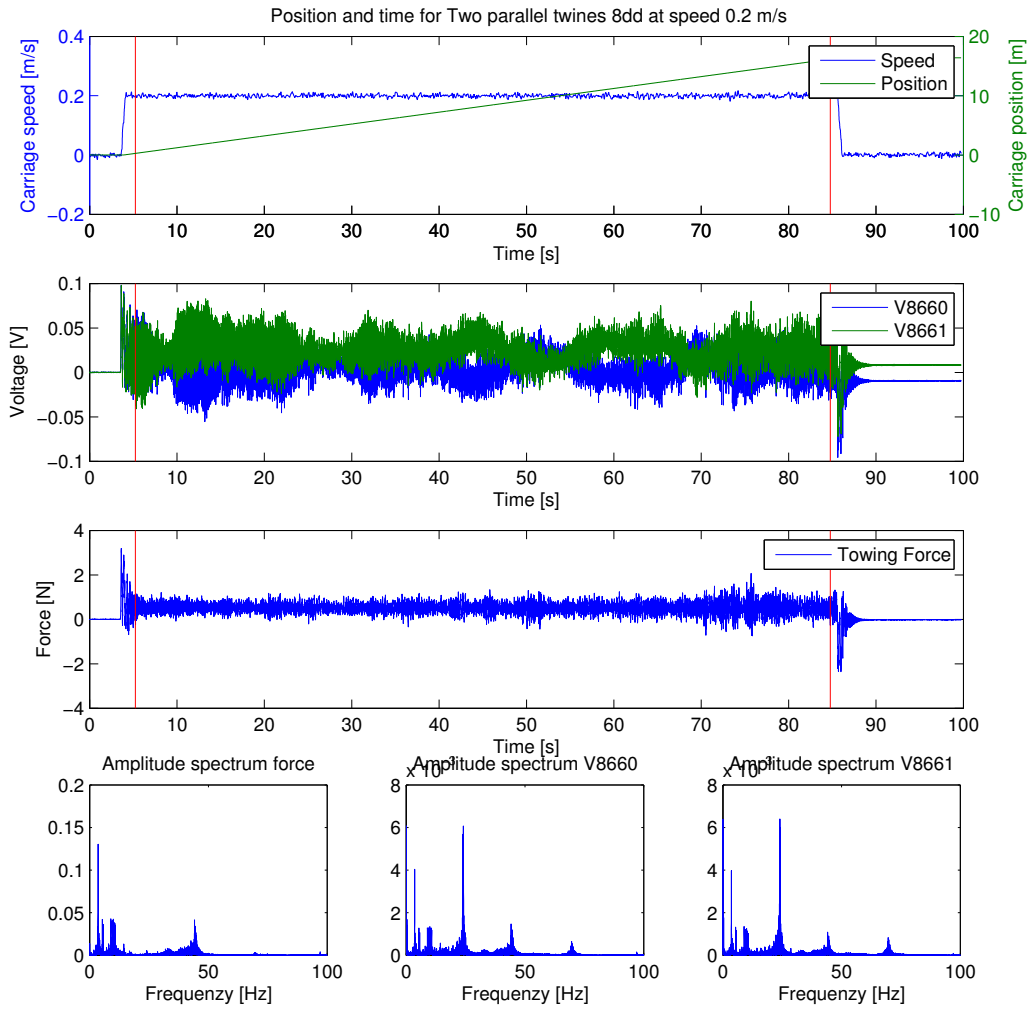


Figure 15: Example plots of drag force, velocity and voltages. The start and end cut-off times are marked. The runs were done at different velocities, so the length of the time series is different. The lower row shows the frequency spectra for the force, and the two load cell voltages.

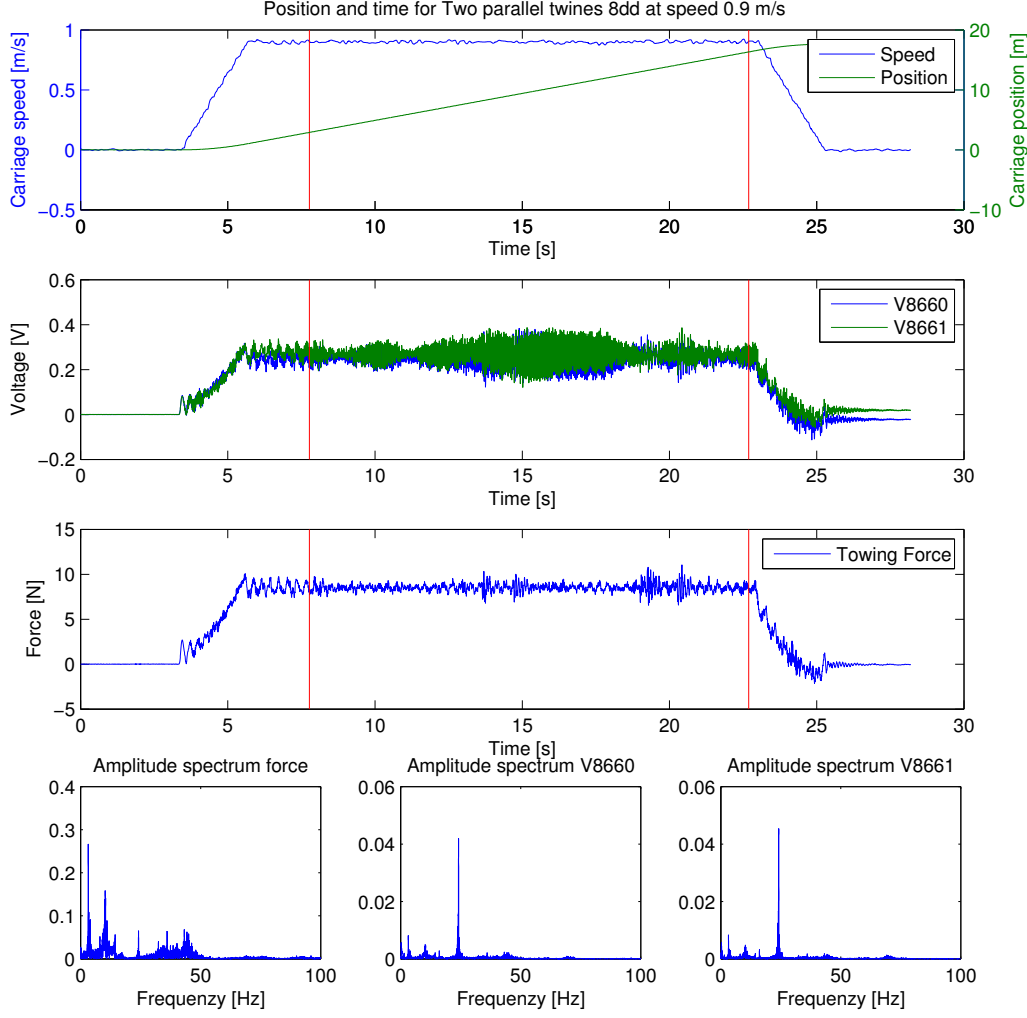


Figure 16: Example plots of drag force, velocity and voltages. The start and end cut-off times are marked. In this case there are more vibrations.

Secondly, the average drag forces were calculated using the mean-function in MATLAB. This was done for the runs with only the frame first, and then for the remaining tests. The drag force on the models was found by subtracting the frame drag for the respective velocity from the total drag. It was assumed that the drag on the frame itself was not significantly influenced by the presence of the models.

Thirdly, the drag on one twine model, and also the drag coefficient, were calculated. The drag per twine was calculated by simply dividing the drag on the models with the number of twines. For the drag coefficient the following definition was used (eq. 9):

$$C_D = \frac{2F_D}{\rho A_p U^2} \quad (9)$$

Where F_D is the drag force on one twine, ρ is the density of water, which was 1000 kg/m^3 , A_p is the projected area, and U is the average speed. To make it easier to compare the drag coefficient with data for clean twines and

nets, only the area of the twine core was included in the projected area. This means that the projected area was considered to be $A_p = 0.5m \cdot 0.003m = 0.0015m^2$.

It is useful to express the velocity with the dimensionless Reynold's number, which is defined (10):

$$Re = \frac{UL}{\nu} \quad (10)$$

Where L is the characteristic length or diameter, and ν is the kinematic viscosity. The diameter of the twine core, 3 mm, was used for the characteristic diameter. Assuming that the water temperature is approximately equal to the room temperature in the tank, 20°C, the kinematic viscosity was $\nu = 1 \cdot 10^{-6}$ (Faltinsen 1993, p.175).

To quantify the noise in the measurements the standard deviation of the time series was calculated. This was done with the std-function in MATLAB. The std function use the following textbook definition of the standard deviation (eq. 11):

$$s = \sqrt{\frac{1}{n-1} \sum_{i=1}^n (x_i - \bar{x})^2} \quad (11)$$

The standard deviations of the total force for all the runs are plotted as errorbars in the figures in appendix B

4.6 Drag on Net Section

Because most of the available empirical data from other experiments are drag coefficients for net panels, normalised to the outline area of the net, the drag coefficients for the net section in the middle of the configurations with crosses was estimated. This estimate would be quite rough, but it could still be useful for comparing the results with other experiments. The drag coefficient for the net section in the middle was calculated by subtracting the drag force on the sections with only parallel twines (outside of the net in the middle) from the total drag force on the configuration with crosses. This was based on the assumption that the drag force per length of twine on the sections with only parallel twines was equal to the force on the corresponding parallel twine configurations.

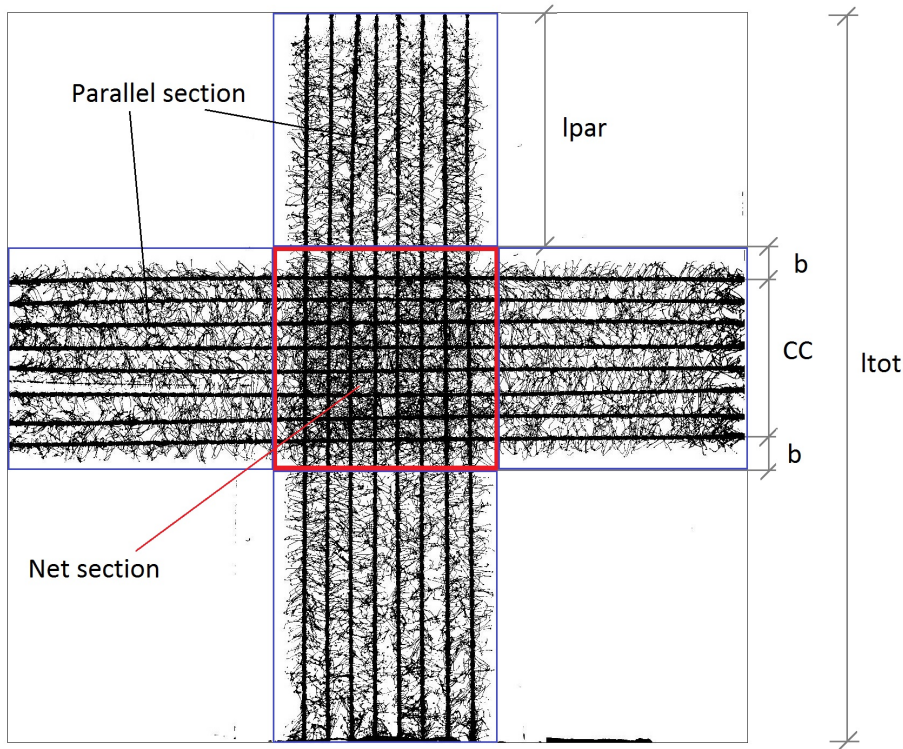


Figure 17: Estimation of drag on net section.

Figure 17 illustrates how the net section in the middle (red square), and the parallel sections (blue squares) was defined. The side length of the square was the centre-centre distance between the outer twines (CC), plus a boundary (b) that was set to 16 mm on each side (similar to the twine length). The drag force on the net section (F_{net}) can be calculated based on the dimensions (shown in figure 17), the total drag force on the cross configuration ($F_{Tot,C}$) and the total drag force on the corresponding parallel twines configuration ($F_{Tot,P}$), with the following equation (eq. 12):

$$F_{net} = F_{Tot,C} - 4 \cdot F_{Tot,P} \cdot \frac{lpar}{ltot} \quad (12)$$

The same calculation method was used to estimate the projected areas of the net sections, based on the projected areas of the corresponding parallel and cruciform configurations (Ch. 4.9). These were then used to calculate the solidity of the net sections with fouling.

4.7 Accuracy and Reliability

4.7.1 Precision Error

Based on the tests that were repeated several times, the precision error can be estimated. The precision limit and uncertainty were calculated using the student t-distribution, as described in the lecture notes by Prof Steen (2014).

First, the total drag is calculated in the same way as above (Ch. 4.5) for all the runs. Then the mean and standard deviation for the five runs were calculated using the respective MATLAB functions (Eq. 11). The total drag for all the runs, and the means and the standard deviations are presented in table 3 below.

Table 3: Total drag, mean drag and standard deviation for the repeated tests

Config- uration	Speed [m/s]	Total drag [N]					Average [N]	Std. dev.
		Run 1	Run 2	Run 3	Run 4	Run 5		
2par8dd	0.1	0.132	0.13	0.132	0.135	0.138	0.133	0.00316
2par8dd	0.8	6.75	6.66	6.79	6.76	6.76	6.74	0.0493
2par8dd	1.4	19.5	19.5	19.4	19.4	19.4	19.4	0.0633
8cross8dd	0.4	7.12	7.26	7.29	7.32	7.33	7.26	0.0841
8cross8dd	1.1	49.9	50.3	50.3	50.2	50.4	50.2	0.203

The method for estimating the uncertainty is based on the assumption that the measured values is Gaussian distributed around a mean. For this distribution the confidence interval is given by:

$$Prob(X_j - t\sigma \leq \mu \leq X_j + t\sigma) = \gamma \quad (13)$$

Where γ is the confidence interval, in this case $\gamma = 0.95$. When the number of samples is finite, σ and t are unknown, and the equation can be written as:

$$Prob(-t \leq \frac{X_j - \mu}{S_X} \leq t) = \gamma \quad (14)$$

Where $\frac{X_j - \mu}{S_X}$ follows the student t-distribution with $N - 1$ degrees of freedom. t can be found from the inverse of the cumulative density function for the t-distribution, $F^{-1}()$. Here $N = 5$, so t is then:

$$t = F^{-1}\left(\frac{1}{2}(1 + \mu)\right) = F^{-1}(0.975) = 2.776 \quad (15)$$

The precision limit is found from

$$P_X = tS_X \quad (16)$$

And the uncertainty given in percent is then calculated by:

$$\frac{P_X}{\bar{X}} 100\% = \text{uncertainty}[\%] \quad (17)$$

The standard deviation for the mean of N samples is given by:

$$S_{\bar{X}} = \frac{S_X}{\sqrt{N}} \quad (18)$$

The precision limit and uncertainty for the mean can be calculated using $S_{\bar{X}}$ in equations 16 and 17. Table 4 presents the precision limits and uncertainties for the different tests.

Table 4: Precision limit and uncertainty for repeated tests

Config- uration	Speed [m/s]	Signle run			Mean		
		S_X	P_X	Uncert. [%]	$S_{\bar{X}}$	$P_{\bar{X}}$	Uncert. [%]
2par8dd	0.1	0.00316	0.00878	6.57	0.00141	0.00392	2.94
2par8dd	0.8	0.0493	0.137	2.03	0.022	0.0612	0.907
2par8dd	1.4	0.0633	0.176	0.905	0.0283	0.0786	0.405
8cross8dd	0.4	0.0841	0.233	3.21	0.0376	0.104	1.44
8cross8dd	1.1	0.203	0.565	1.12	0.091	0.253	0.503

The uncertainty is largest for the lowest velocity, and smaller for the higher velocities. This is probably because the forces are much smaller at the low velocity, and then the noise becomes more significant compared to the total force. However, an uncertainty of 6.57 % in the worst case is relatively good. Table 4 gives both the uncertainty for a single test, and the uncertainty for the mean of the repeated tests. Since most of the tests were done only once, it is the values for a single run that are most relevant for those tests.

In table 4 the uncertainties are given for the total force. The uncertainty for a quantity $f(x, y, \dots)$ that is calculated based on measurements of the values x, y, \dots with uncertainties $\Delta x, \Delta y, \dots$ can be calculated by the equation:

$$\Delta f = \left(\left(\frac{\delta f}{\delta x} \Delta x \right)^2 + \left(\frac{\delta f}{\delta y} \Delta y \right)^2 + \dots \right)^{1/2} \quad (19)$$

In this case we only have the uncertainties for one of the variables, the total force, so equation 19 is equivalent to calculating the uncertainty from the standard deviation of the calculated variables. Ignoring the uncertainty of the other variables in the calculation might lead to a slight underestimate of the uncertainty, but most of the other variables are constants where the precision error is negligible. The force per twine and the drag coefficients for the repeated runs are plotted together with the respective precision errors in the results section (Ch. 5.4). When the force contribution from the frame is subtracted, the precision error becomes larger compared to the force. For the run at 0.1 m/s, where the total force initially is small, this causes uncertainty to be scaled up significantly, suggesting that the results for the lowest velocities are inaccurate.

4.7.2 Bias Error

Although the precision error seem to be relatively small except for the lowest velocities, there might be bias errors. These are hard to identify, because they

give the same effect on all similar tests. The most obvious possible bias error is calibration error; if the calibration factor is wrong, all force measurements will be wrong. In this case the calibration was done carefully, and tested both before and after the experiments (Ch. 4.3), so the calibration error should not be significant. However, the results from the measurements of the drag on only the frame were slightly different (Fig. 30 in Ch. 5.3) between the two series. The first series (OnlyFrame) was done at the start of the experiment period, while the second (OnlyFrame2) was done at the end. This difference might indicate that the sensors have drifted slightly, but not so much that it was noticed in the manual testing of the calibration.

Another possible error source is the waves. At the highest velocities the frame generated waves with a relatively long wavelength (assuming linear wave theory; approximately 1.25 m at 1.4 m/s). These long waves are relatively deep, and can change the particle velocity locally. This could be an error source at the highest velocities, but the wave heights did not exceed 5 cm, so the influence should not be significant.

If the results shall be transferred to real net applications, the modelling accuracy is also an error source. As mentioned before the stiffness of real hydroids has not been measured and compared to the replicas quantitatively. A difference in the stiffness will give a significant error compared to a real life scenario. For the cruciform configuration there is also a difference in the net section in the middle; in a real net all twines are in the same plane, and crossing twines are joined in a knot; while in these experiments the twine models are stiff, so one has to be placed in front of the other in the "knots".

4.8 Decay Tests

In some of the initial runs without models, the lower part of the frame was vibrating back and forth with an amplitude of approximately 1-2 cm. It was believed that these vibrations followed the natural frequency of the frame rig, but to check if this was the case it was necessary to perform decay tests, and determine the natural frequency. Since the mass and added mass would be different for the different configurations, it was expected that the natural frequency also would vary, and hence a decay test was done for most of the configurations. At the end of the experiments, when the tank was drained, a decay test with the frame in air was done as well, just for comparison.

The decay tests were performed by hitting the frame with a small hammer while the carriage was stationary. For each configuration the frame was hit twice: First once at the centre of the upper transverse profile of the underwater square, giving a force straight backwards. Then once at the side, close to the end of the same profile, to make a twisting moment about the vertical axis. The latter was done to identify possible vibration modes different from the main back and forth vibration. Both the total force, and the voltages from the individual load cells, were recorded and analysed independently. A MATLAB script was used to do the calculations and make the plots efficiently. First, the two time intervals for the centre and side were selected manually from a plot of the full time series (Figure 18). Then, these inter-

vals was extracted, and the frequency spectra were calculated using the Fast Fourier Transform function (`fft`) in MATLAB. The output from the function was scaled such that the x-axis gives the frequency in Hz, and the y-axis the amplitude, using a method described in the MATLAB documentation (*Amplitude Estimation and Zero Padding* 2014). Since this was a decay test, where the amplitude is decreasing with time, the amplitude values are not exact, and they can only be used to compare the energy for the frequencies within one spectrum, and identify the frequency with largest motions, which will be the natural frequency for the given configuration. The plots from all the decay tests are included in the digital attachments.

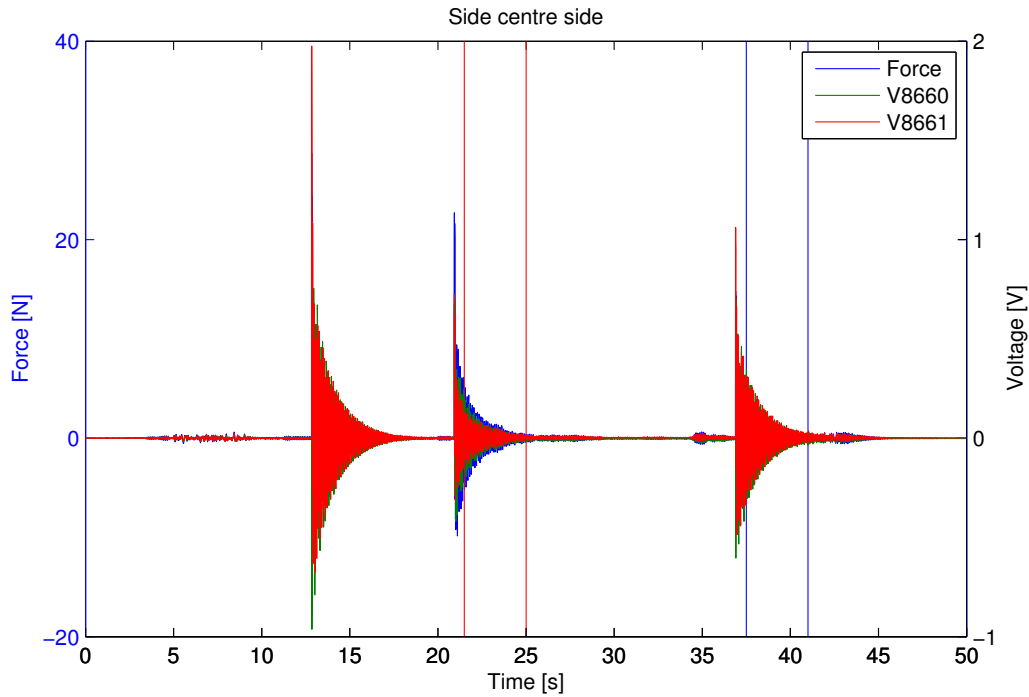


Figure 18: Time series for decay test on the frame. In this decay test the frame was first hit at the side, then the centre, and then the side again. The two red vertical lines marks the interval used for the centre, and the two blue lines marks the interval for the side.

Figure 19 shows the spectra from the time series in figure 18. In the spectra from when the side of the frame was hit, it is interesting to notice the peak at approximately 25 Hz, which is large for the voltages from the individual load cells, while it is barely visible in the force spectrum. The force is proportional to the sum of the two voltage inputs, so when the force amplitude is much smaller than the voltage amplitudes, this must mean that the signals from the load cells are similar, but in opposite phase, and therefore cancel each other out. It is likely that this is a vibration mode which is rotation about the vertical axis, with a natural frequency corresponding to the peaks in the voltage spectra. The same vibrations were also visible in the time series from some of the tests; there were clear vibrations in the voltages, and smaller vibrations in the towing force. This can for instance

be seen in figure 16, in the time range from 13 s to 18 s.

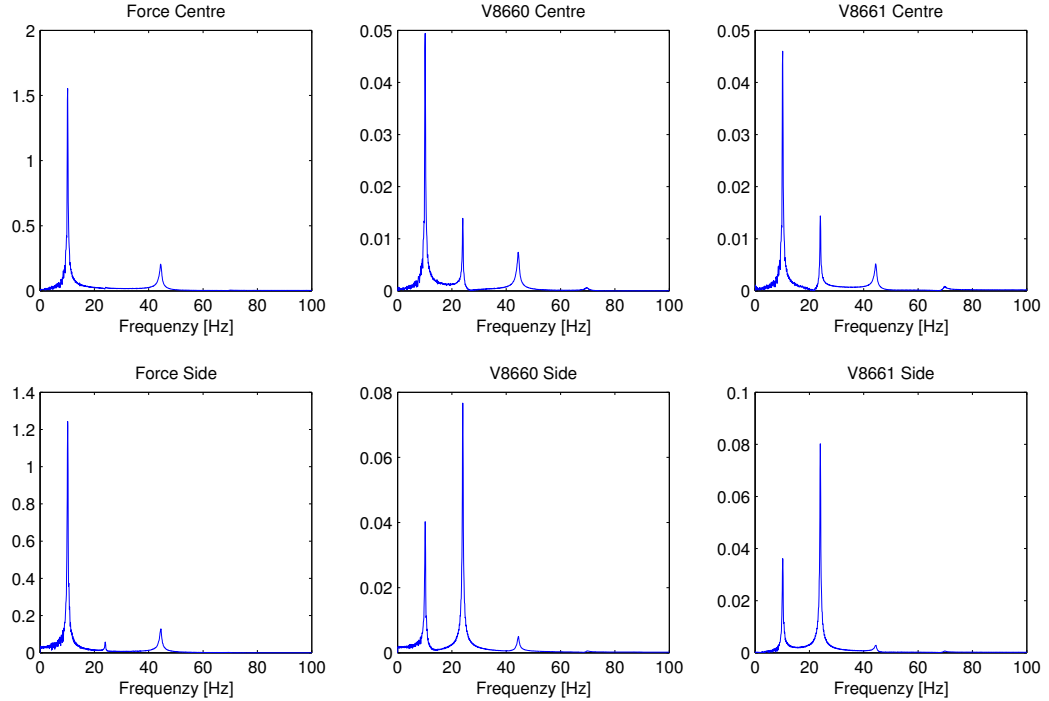


Figure 19: Frequency spectra from the decay test of the frame. The first row is for the centre hit, and the second is for the side hit. The left column is from the force, representing the sum of the voltages, while the centre and right columns are the voltages from the individual load cells.

4.9 Projected Area and PNO

To be able to calculate the drag coefficient with relation to the actual projected area of the models with fouling, all the configurations were photographed, and the projected area was calculated by image analysis in MATLAB. The analysis is based on converting the images into black and white by applying one or more thresholds on illumination or colour, in such a way that the models and the fouling becomes black, and the rest of the image (background) becomes white. The projected area is then calculated by counting the black pixels, and then multiply the number of black pixels with the area of one pixel, which is found by dividing the area of the test section ($0.5m \cdot 0.5m$) on the total number of pixels.

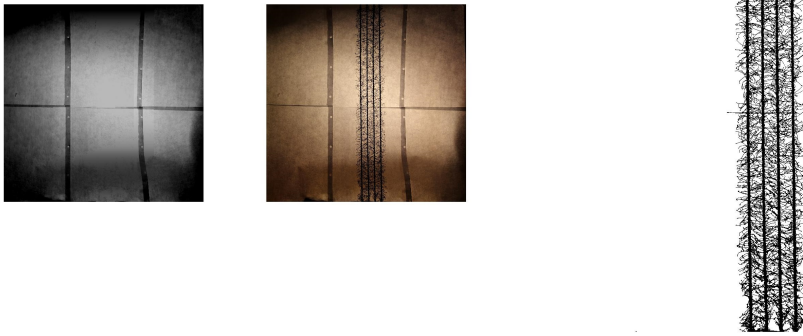


Figure 20: Example of image conversion for projected area. Left: The threshold image, which was the same for all the configurations. Middle and right: Original and converted image respectively. (The converted image is enlarged, to make the details more visible)

The first attempt of calculating the projected areas was done using images taken in the lab. However, the light conditions in the lab was not ideal, and hence the contrast between the fouling and the background was not good enough to get satisfactory results. Because of this a second attempt was made, setting up the different configurations in the frame again, and take new pictures. In this attempt the room was completely dark except from an illuminated white paper sheet that was used as a background. This created a better contrast between the dark models and the brighter background. Because the background was not evenly lit, the threshold for whether a pixel should be counted as model or background was created by merging the backgrounds from different configurations into one image that only showed the background, and then adjusting this image so that it became approximately 10% darker (to have a margin). All pixels that were darker than the corresponding pixel in the background threshold image were counted as model or fouling, and became black pixels in the converted image. It was sufficient to only use the red colour channel of the images, so the background threshold image which is shown in grayscale in figure 20 (left) consists only of the red channel from the images that were merged. Figure 20 also shows an example of an image before (middle) and after (right) conversion, for the configuration with 4 parallel twines with 12 mm spacing. The projected areas for the different configurations are presented in table 5.

Table 5: Projected area of twine and fouling for all configurations

Model configuration	Projected Area [m^2]
Single twine	0.006195
Single cross	0.00623
Two parallel twines, 24mm spacing	0.0062059
Four parallel twines, 24mm spacing	0.016247
Six parallel twines, 24mm spacing	0.022991
Eight parallel twines, 24mm spacing	0.030765
Two parallel twines, 12mm spacing	0.0079546
Four parallel twines, 12mm spacing	0.015421
Six parallel twines, 12mm spacing	0.021986
Eight parallel twines, 12mm spacing	0.028276
Two by two crosses, 24mm spacing	0.015255
Four by four crosses, 24mm spacing	0.029093
Six by six crosses, 24 mm spacing	0.03935
Eight by eight crosses, 24mm spacing	0.050881
Two by two crosses, 12mm spacing	0.015272
Four by four crosses, 12mm spacing	0.028448
Six by six crosses, 12 mm spacing	0.039863
Eight by eight crosses, 12mm spacing	0.05066

This method is similar to the one Guenther et al. (Guenther, Misimi, and Sunde 2010) used to calculate the percentage net aperture occlusion (PNO). The PNO is a parameter commonly used to quantify the amount of bio fouling on a net, so these results can also be useful when comparing the results with other experiments. The PNO is defined as the ratio between the area covered by bio fouling (excluding the net twine) and the area of the openings in the net (for a clean net). Based on the illustration in figure 21 below, the PNO would be given by (Eq. 20):

$$PNO = \frac{redpixels}{redpixels + whitepixels} \cdot 100\% \quad (20)$$

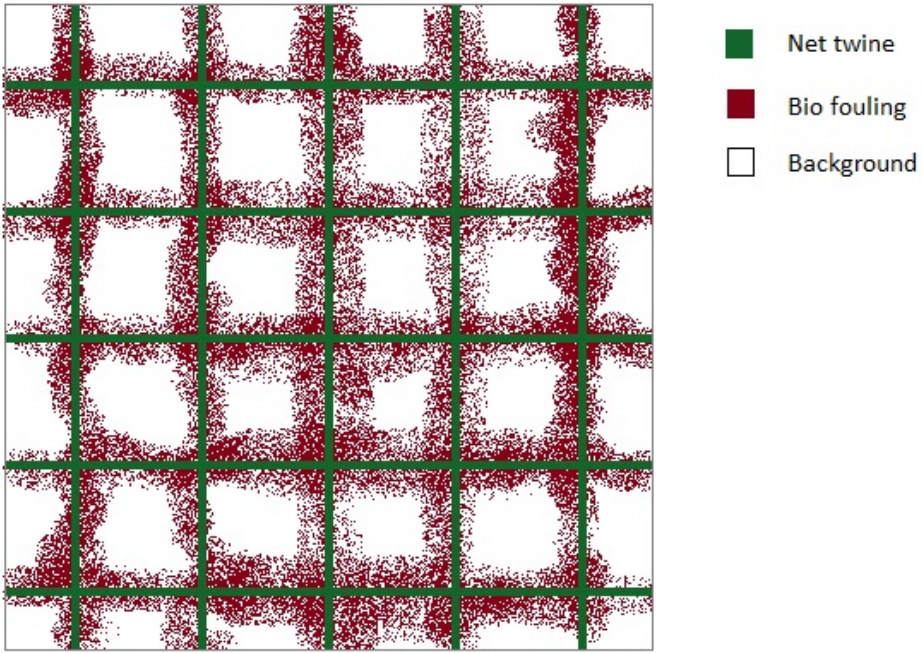


Figure 21: Illustration of PNO.

5 Results

Since almost 300 measurements were done, it is pointless to present time series and other detailed data from each run in this report. Therefore, only the important finished results are included here. For the same reason, some datasets are split into several figures, to avoid too many lines on top of each other, and improve readability. A more detailed discussion of the results follows in the discussion chapter (6).

5.1 Drag Forces

The following four figures displays the drag force acting on one twine as a function of towing velocity, for all the different configurations. Figures 22 and 23 includes the configurations with parallel twines, for respectively 24 mm spacing (8 diameters distance, 8dd) and 12 mm spacing (4 diameters distance, 4dd); while the configurations with crosses are in figures 24 and 25, for respectively 24 mm spacing and 12 mm spacing. The single twine and single cross configurations are included in all the figures, to give a common reference point when comparing configurations in different figures.

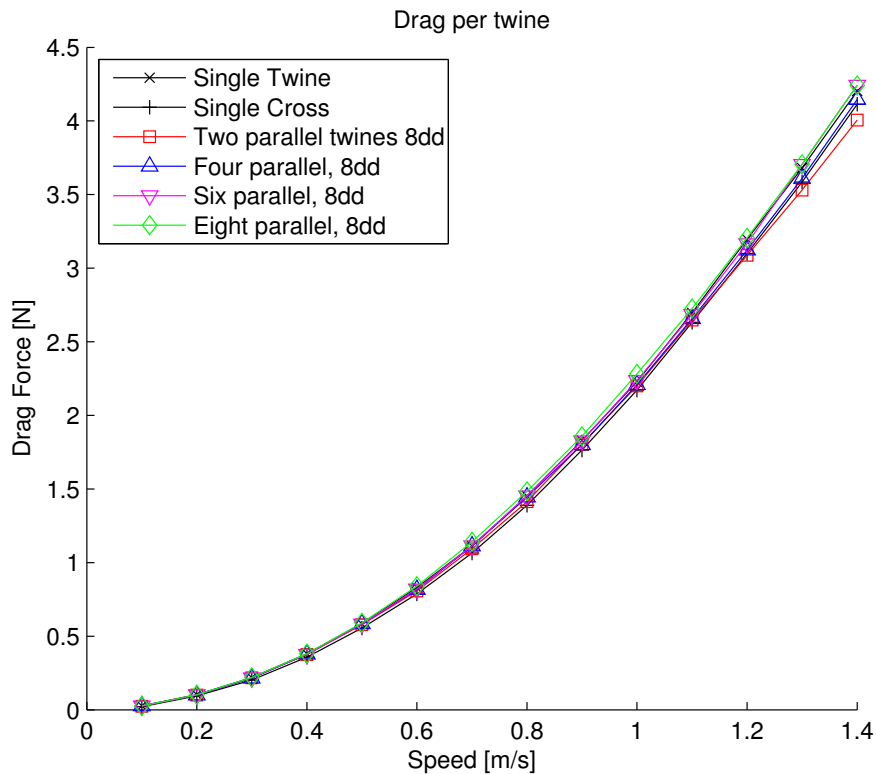


Figure 22: Drag force per twine for parallel twines with 24 mm spacing

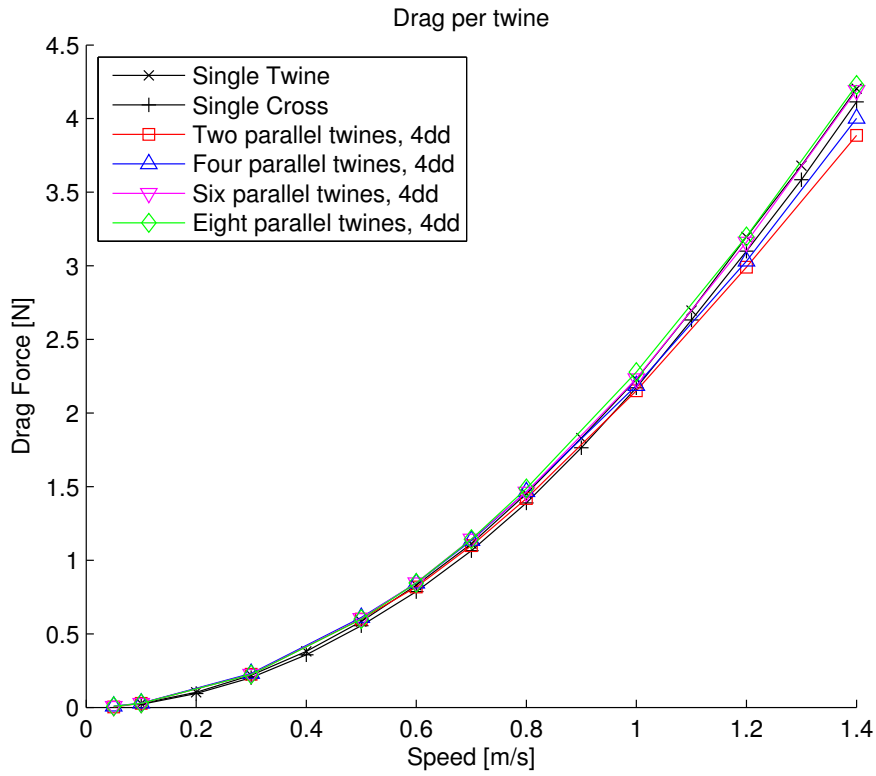


Figure 23: Drag force per twine for parallel twines with 12 mm spacing

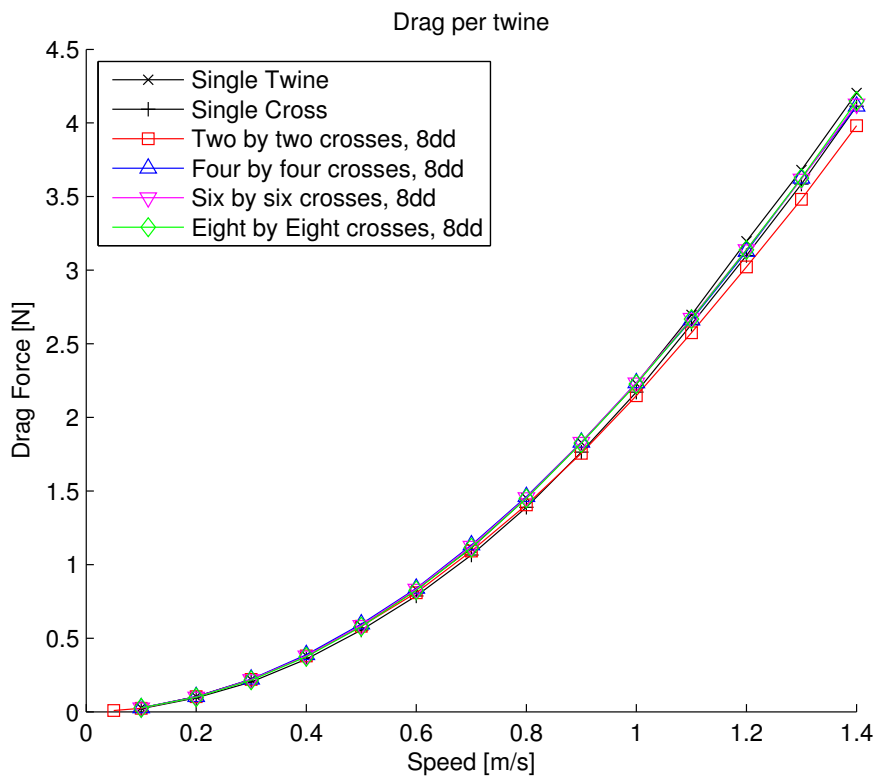


Figure 24: Drag force per twine for crossing twines with 24 mm spacing

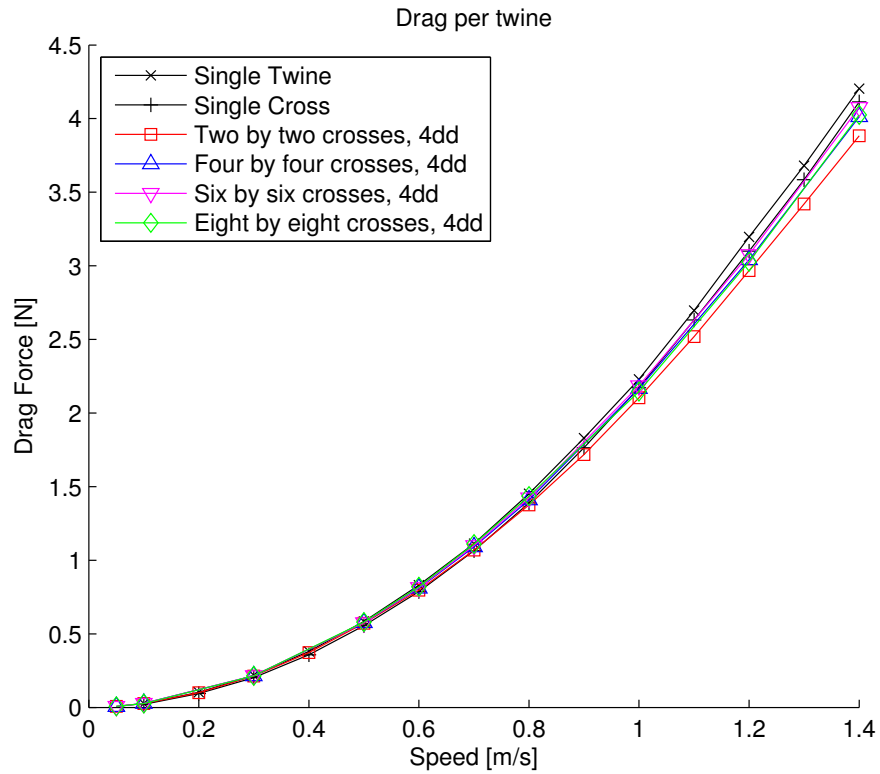


Figure 25: Drag force per twine for crossing twines with 12 mm spacing

5.2 Drag Coefficients

The next four figures gives the drag coefficients as a function of the Reynolds number. These drag coefficient were calculated based on the projected area of the twine core only, without the area of the artificial fouling. Figures 26 and 27 are for parallel twines with 24 mm spacing and 12 mm spacing respectively; and figures 28 and 29 are for the cruciform configurations. In the same way as in the previous figures, the single twine and single cross are included in all the figures.

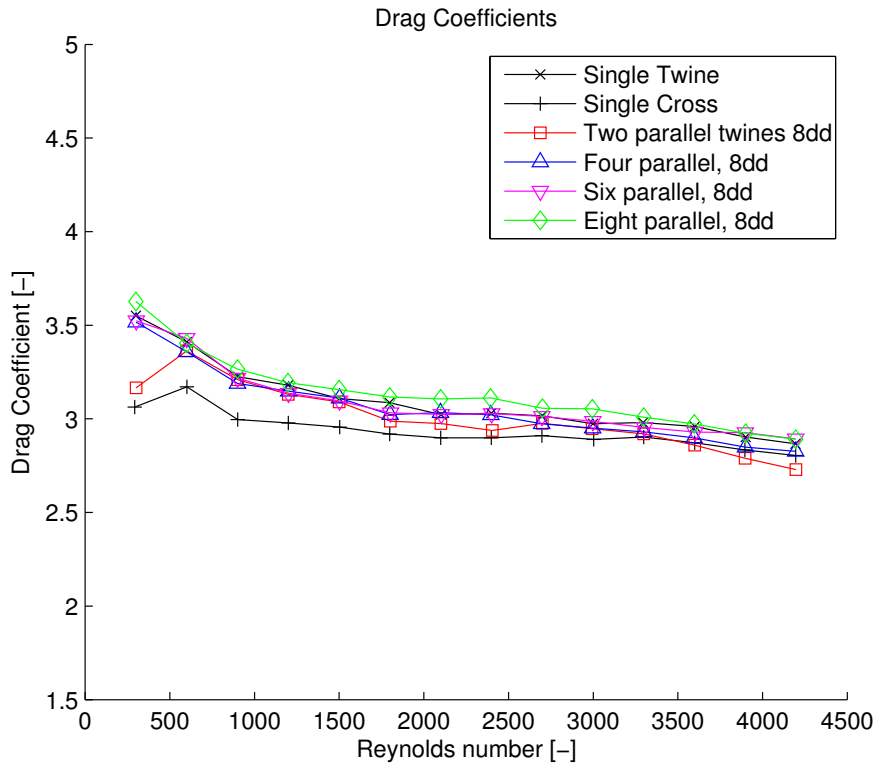


Figure 26: Drag coefficients for parallel twines with 24 mm spacing

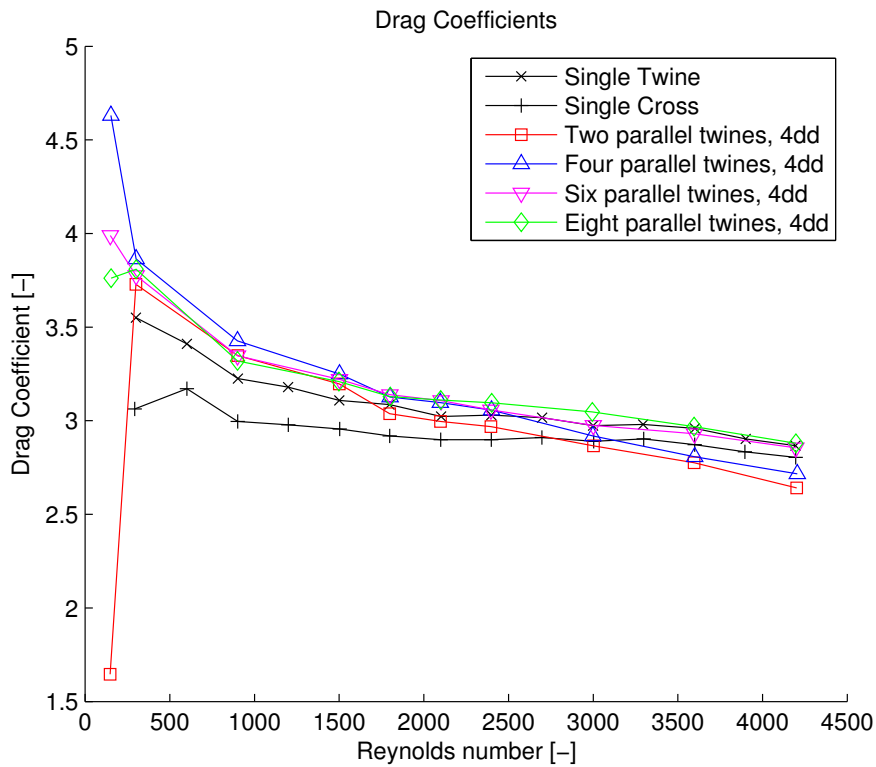


Figure 27: Drag coefficients for parallel twines with 12 mm spacing

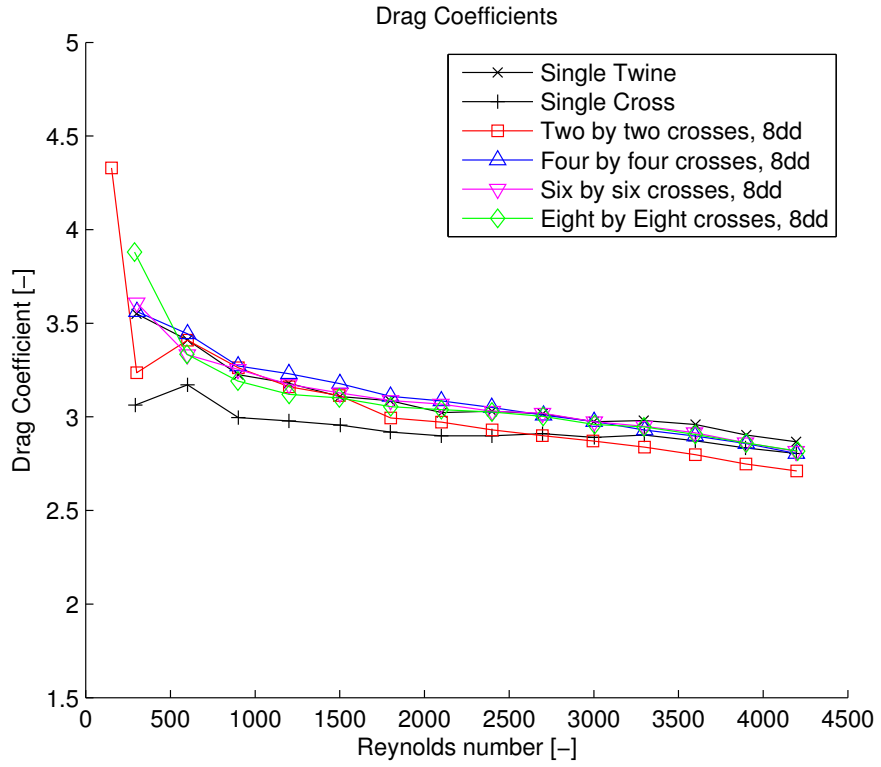


Figure 28: Drag coefficients for crossing twines with 24 mm spacing

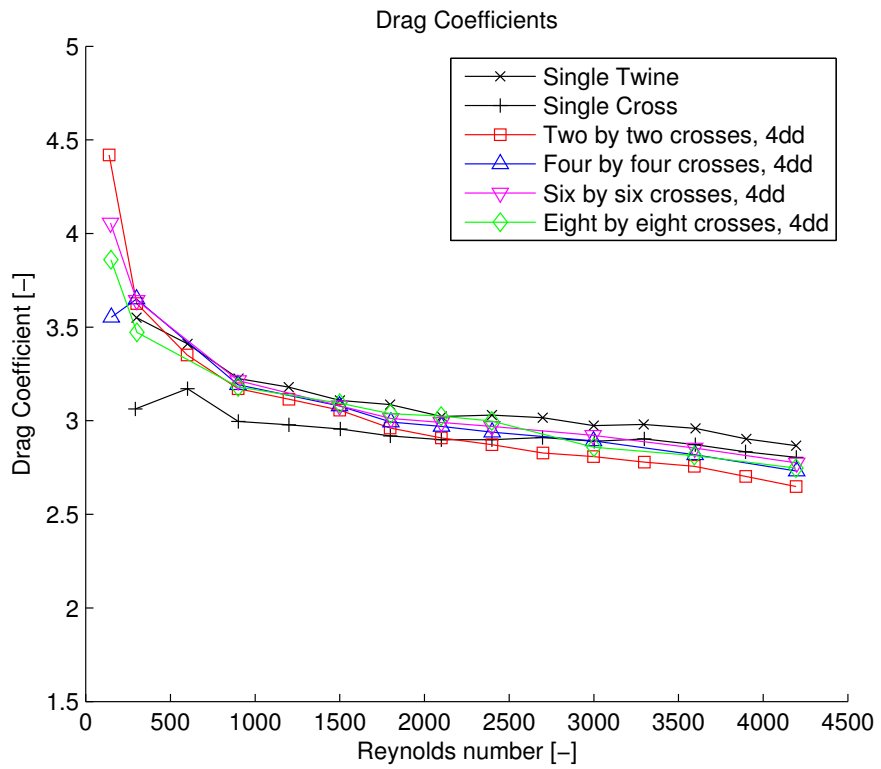


Figure 29: Drag coefficients for crossing twines with 12 mm spacing

5.3 Drag on Frame

Two test series were done measuring the drag on the frame without any models. Both of them contained all velocities from 0.1 m/s to 1.4 m/s with 0.1 m/s increments. In addition the first series included a measurement at 1.5 m/s, which was unused, while the second included a measurement at 0.05 m/s. In figure 30 both of them are plotted together with the average of the two. It was the average values that were used in the calculations. The plot also shows the standard deviation of each time series, to illustrate the magnitude of the noise and vibrations.

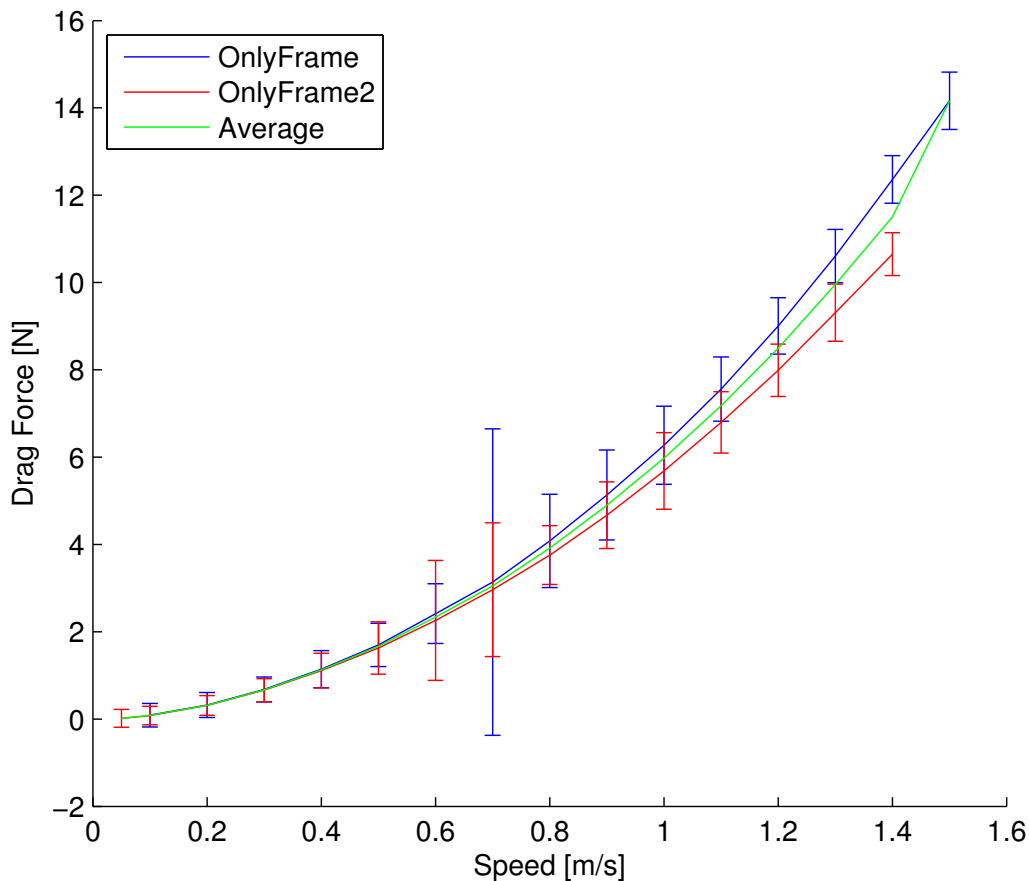


Figure 30: Drag force on the frame without any models

5.4 Accuracy and Reliability

Five of the test cases were repeated five times each, to make an estimate of the precision error of the results. This was done for the velocities 0.1 m/s, 0.8 m/s and 1.4 m/s, for the configuration with two parallel twines and 24 mm spacing, and for the velocities 0.4 m/s and 1.1 m/s, for the configuration with eight-by-eight crosses and 24 mm spacing. Figure 31 shows the drag force on one twine as a function of velocity, with error-bars illustrating the precision error at the data points where it was estimated. The error-bars are plotted with an X marking the average value of the five measurements at

that particular velocity. Only the precision error of the force measurements were included in the error estimation, while the other variables were assumed to be constant, since there were no information available about the error of these variables. It seems reasonable to assume that the precision error in the velocity, the projected area, the density of the water and the number of twines are all very small, and not significant. However, bias errors in any of these variables, or the force measurements, could be present; and they are not quantified in the error estimation. Figure 32 shows the drag coefficients as a function of Reynolds number, with the precision error plotted in the same way as in the previous figure (Fig. 31).

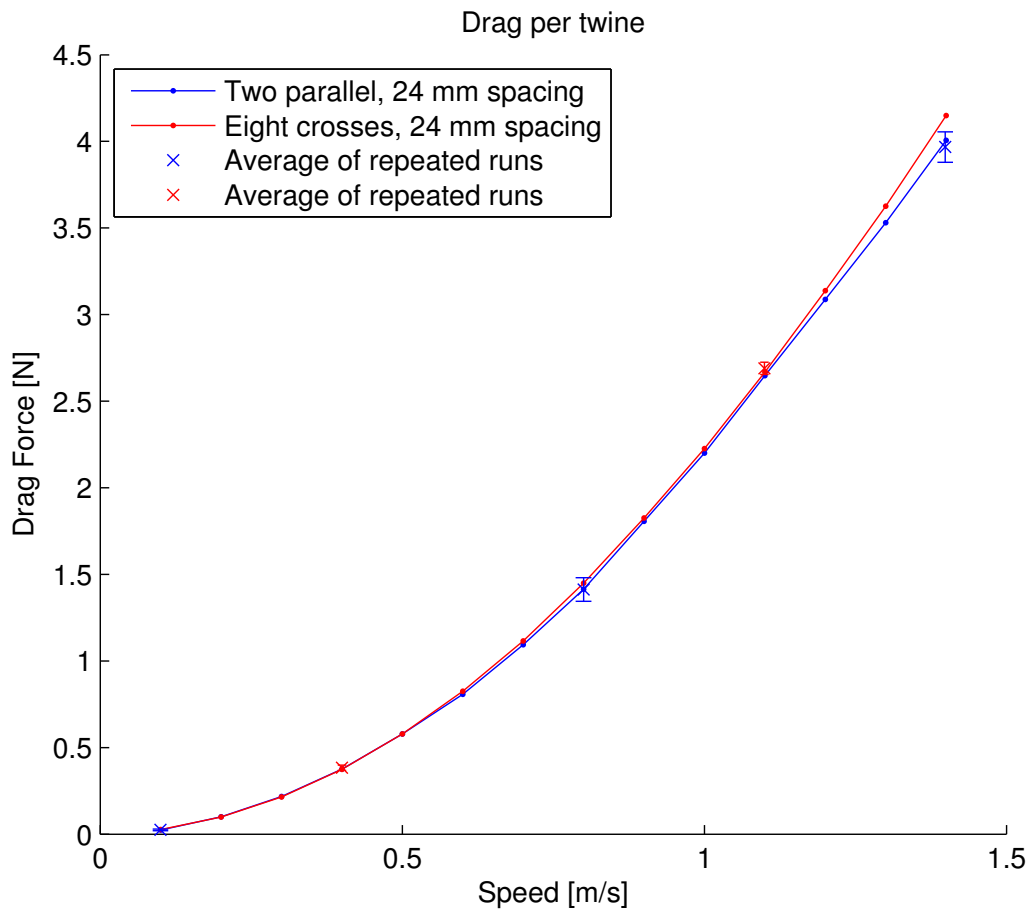


Figure 31: Drag on one twine, with precision error at the points where it was estimated.

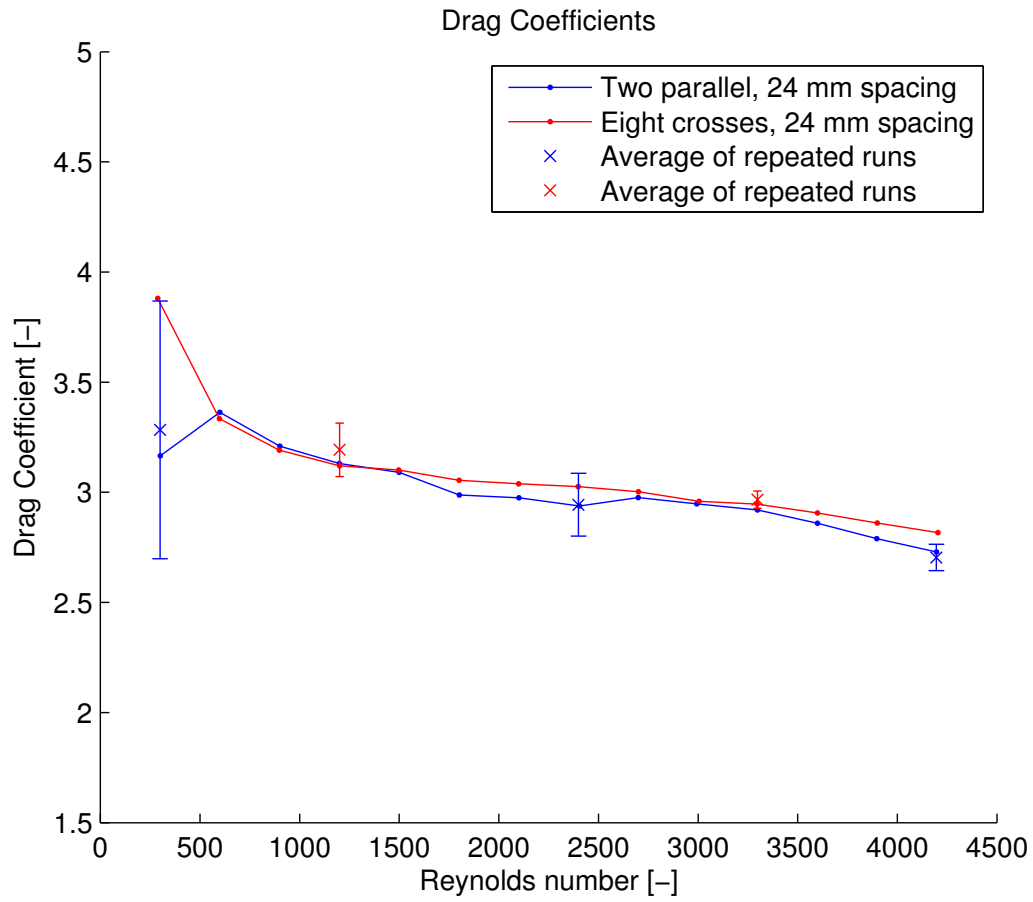


Figure 32: Drag coefficients, with precision error at the points where it was estimated.

6 Discussion

6.1 Velocity Dependency

The drag coefficient of the fouled twine models are clearly not constant within the velocity range of these experiments. In the figures 26, 27, 28 and 29 it is clear that the drag coefficient decreases with increasing velocity (Reynolds number) for all the configurations. The decrease is most significant for the lower half of the velocities. For a circular cylinder it is expected that the drag coefficient remains constant at about 1.0 in the velocity range from $Re = 1000$ to $Re = 4000$ (For the 3 mm twine core $Re(0.3m/s) = 900$ and $Re(1.4m/s) = 4200$) (Hoerner 1965). The core of the twine models is not a circular cylinder, but with the glue between the steel rods it is close to a rough cylinder, and Lader et al. (P. Lader et al. 2014) found that the core behaves similarly to a circular cylinder up to $Re = 2600$.

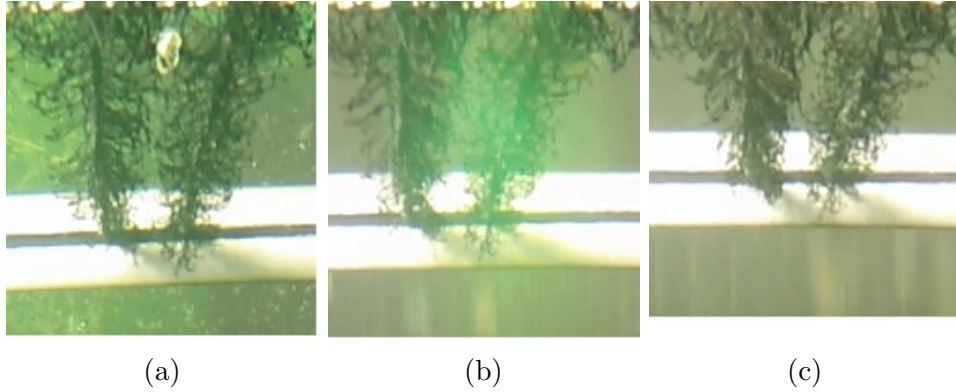


Figure 33: Image of hydroid deflection taken from videos. The image to the left (33a) is when the models are stationary, in the middle (33b) is at 0.8 m/s and to the right (33c) is at the maximum velocity of 1.4 m/s.

P. Lader et al. (2014) gives a possible explanation for the reduction in drag coefficient for higher velocities; because the hydroid models are flexible they deform at higher velocities, and the models with fouling becomes more streamlined, thus reducing the drag coefficient. The videos from the present tests show that the hydroid models deflect slightly at the higher velocities (Fig. 33), but the deflection does not seem to be large enough to make the models significantly more streamlined. Therefore, another possible explanation is suggested: The hydroid models are made of fishing line with a diameter of 0.32 mm; this smaller diameter means that if the stems of the hydroids are considered independently, they are in a Reynolds number range from $Re(0.1m/s) = 32$ to $Re(1.4m/s) = 448$, which is approximately a tenth of the Reynolds number for the twine core ($Re(0.1m/s) = 300$ to $Re(1.4m/s) = 4200$). In this lower Reynolds number range the drag coefficient for a circular cylinder is decreasing with increasing velocity (Hoerner 1965), in a similar way to the drag coefficient of the twine models ($C_D(Re = 32) \approx 1.8$ and $C_D(Re = 448) \approx 1.2$). Accordingly, the trend in

the drag coefficients for the fouled models might be caused by the contribution from the thin cylindrical hydroid stems, even if they don't deflect.

6.2 Comparison of Configurations

To make it easy to compare the drag coefficients for the different configurations, the drag coefficients were plotted as function of the number of parallel twines, like in figure 34. The plots are grouped with two figures for each velocity, one for parallel twines (Fig. 34a) and one for crosses (Fig. 34b). Only three of velocities which were representative for the general trends are included here; plots for all velocities can be found in appendix C.

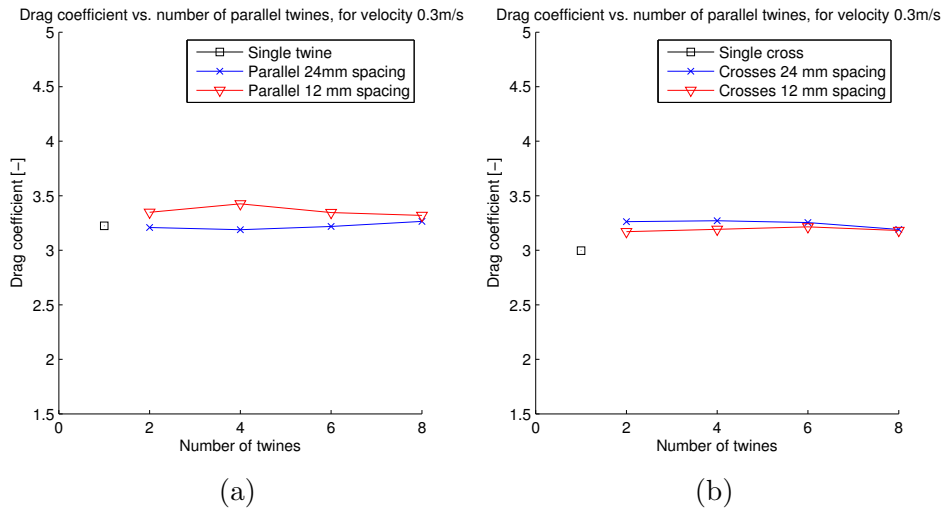


Figure 34: Drag coefficient as a function of number of twines, for current velocity 0.3 m/s. Parallel twines to the left (34a), and cruciform configurations to the right (34b).

In figure 34a one can see that the drag coefficients are larger for 12 mm spacing than for 24 mm spacing in the parallel configurations. This trend was consistent for the lower velocities, up to 0.7 m/s. For 0.8 m/s (Fig. 35a) and 1.0 m/s it seemed like the drag coefficient was independent of the spacing, while for the velocities above 1.0 m/s the drag coefficient was highest with 24 mm spacing (Fig. 36a). The differences are small compared to the uncertainty at lower velocities (Fig. 32), and could therefore be caused by precision errors. However, the fact the trend is consistent independently of the number of parallel twines, for several velocities, suggests that it is not an error. A higher drag coefficient when the twines are closer together corresponds well with other experiments for cylinders, which shows an increase in the drag coefficient when two parallel cylinders are located close to each other, perpendicular to the flow (Bearman and Wadcock 1973). This increase might be caused by the blockage effect of the twines, which gives a higher local velocity between the twines, but this does not explain why the effect only is present at lower velocities.

The figures 34b, 35b and 36b shows that for the configurations with crossing twines, the drag coefficients are highest for the 24 mm twine spacing. The differences are not significant in this case either, but the trend is consistent through all velocities from 0.3 m/s to 1.4 m/s.

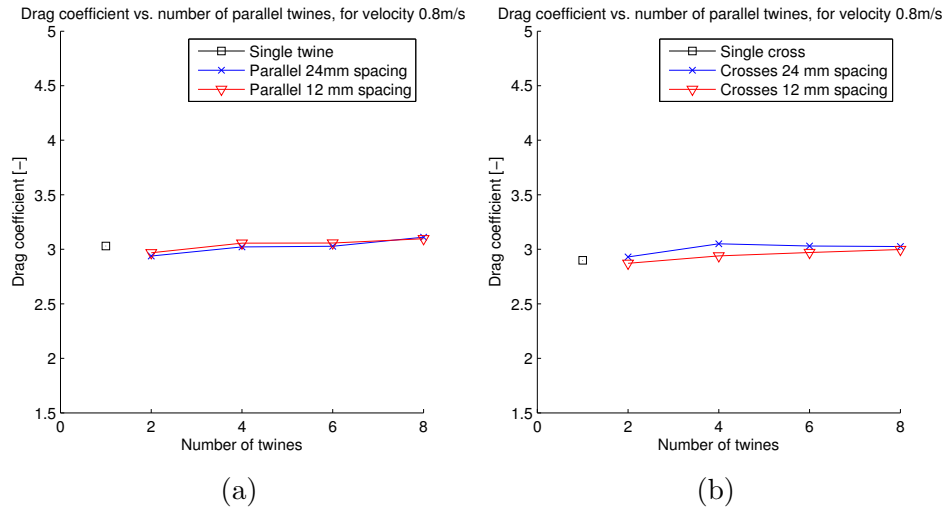


Figure 35: Drag coefficient as a function of number of twines, for current velocity 0.8 m/s. Parallel twines to the left (35a), and cruciform configurations to the right (35b).

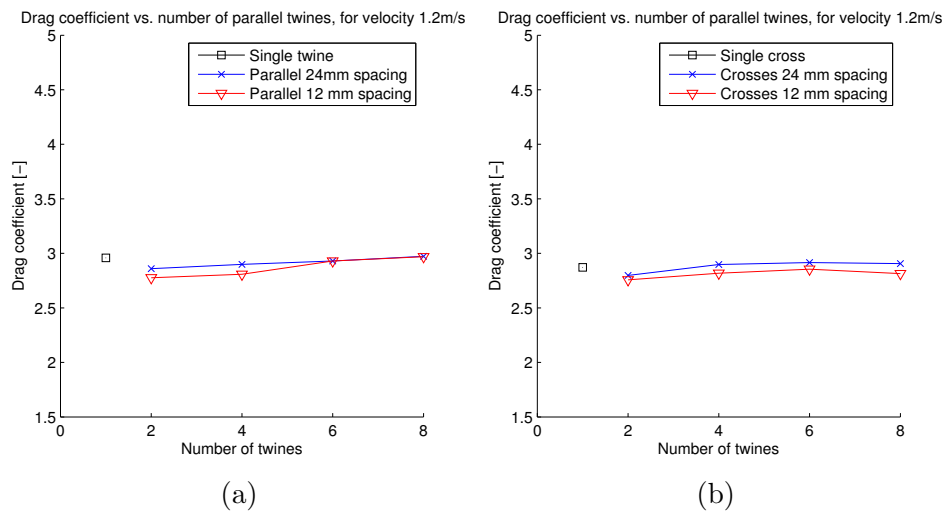


Figure 36: Drag coefficient as a function of number of twines, for current velocity 0.8 m/s. Parallel twines to the left (36a), and cruciform configurations to the right (36b).

The number of twines in the configuration have very little influence on the drag coefficient. Figure 34 shows no conclusive trend for the lower velocities, while from above 0.6 m/s there is a slight, but not at all significant, trend of increasing drag coefficient for increasing number of twines (Fig. 35). The exception from this is the single cross configuration, which have a lower drag

coefficient at low velocities, and a slightly higher drag coefficient at higher velocities. This can also be seen in the figures 28 and 29 where the drag coefficient for the single cross is almost constant, while the others have a decrease in drag coefficient with increasing velocity.

For the two lowest velocities, 0.05 m/s and 0.1 m/s, the drag coefficients is more fluctuating. This matches the high precision error found for 0.1 m/s (Fig. 32), and although some of the trends fit well with the higher velocities, one should be careful to draw conclusions based on the tests at the lowest velocities.

The differences when drag coefficients for parallel twines are compared with drag coefficients for the cruciform configurations are also small, and overall it seems like the configuration does not influence the drag on one twine much. This suggest that results from test on a small number of twines can be extrapolated to larger net panel applications, and hence the method of making models single twines with fouling can give results that are useful in real life applications.

6.3 Drag on Net Section

Figure 37 and 38 shows the drag coefficients that were estimated for the net section in the middle of the configurations with crosses. These drag coefficients are calculated based on the outline area of the net section, to make them comparable to other empirical data for nets.

For the net sections with 24 mm twine spacing (Fig. 37), the drag coefficients are converging towards a line with the increasing number of twines, and the lines for six twines and eight twines are almost identical. This convergence suggests that the drag coefficient for the net section would be similar also for larger number of twines, and hence the drag coefficient for the largest net section could be a good estimate for the drag coefficient of a net panel. Most of the drag coefficients for the 24 mm spacing nets seems consistent, but the fact that the single cross configuration have a negative drag coefficient for the three lowest current velocities, indicates that the effects of small errors are scaled up in the calculations. Therefore, the results might be unreliable, in particular for the lower velocities. The solidity of the fouled net section with 24 mm spacing was 0.34.

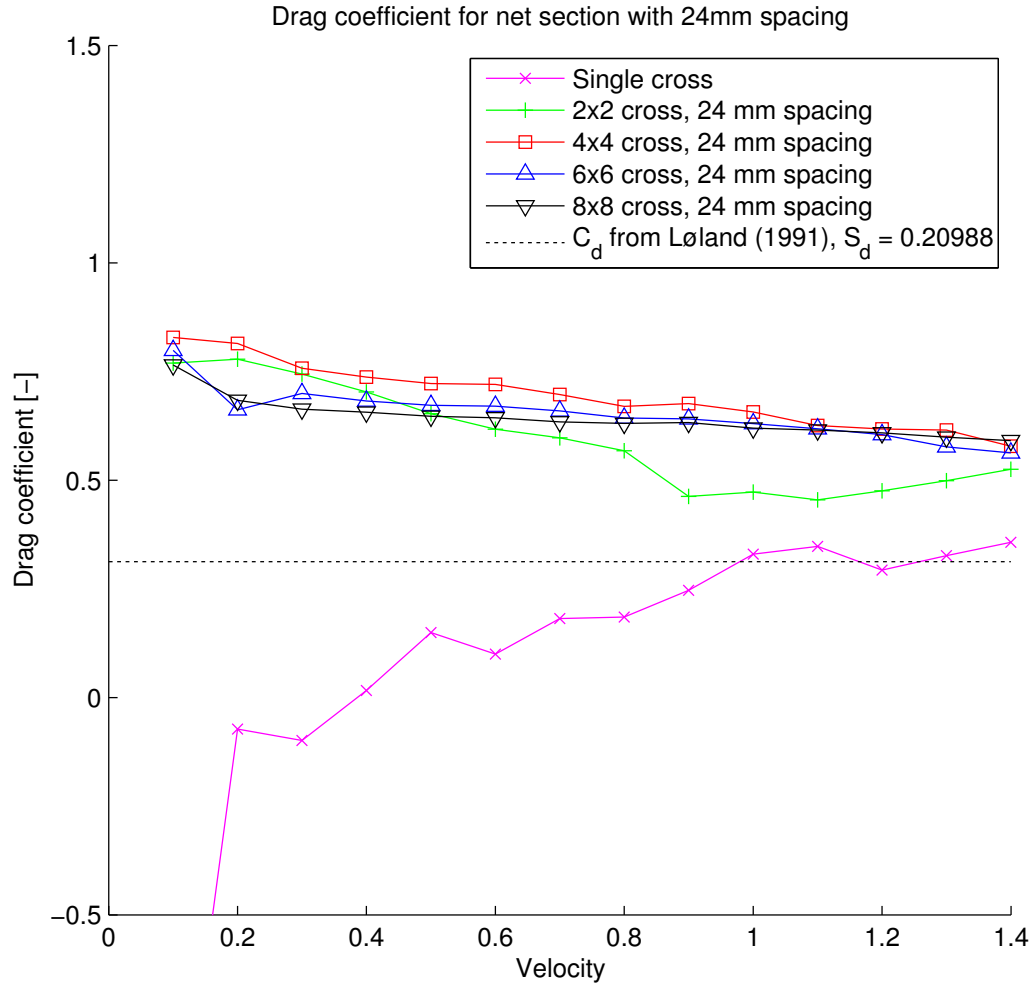


Figure 37

For the net sections with 12 mm twine spacing (Fig. 38) the trend of convergence is only clear at the highest current velocity. This is either because eight parallel twines is not enough to represent a net well at this twine spacing, or because the uncertainties are too large. Anyway, it is not likely that the drag coefficient on the largest net section is a good estimate for a larger net panel in this case, so test with a higher number of twines should be done. Some of the results for the lowest velocity (0.05 m/s) were clearly not realistic in this case as well, as they far exceeded the range of the plots. The solidity of the fouled net section with 12 mm spacing was 0.52.

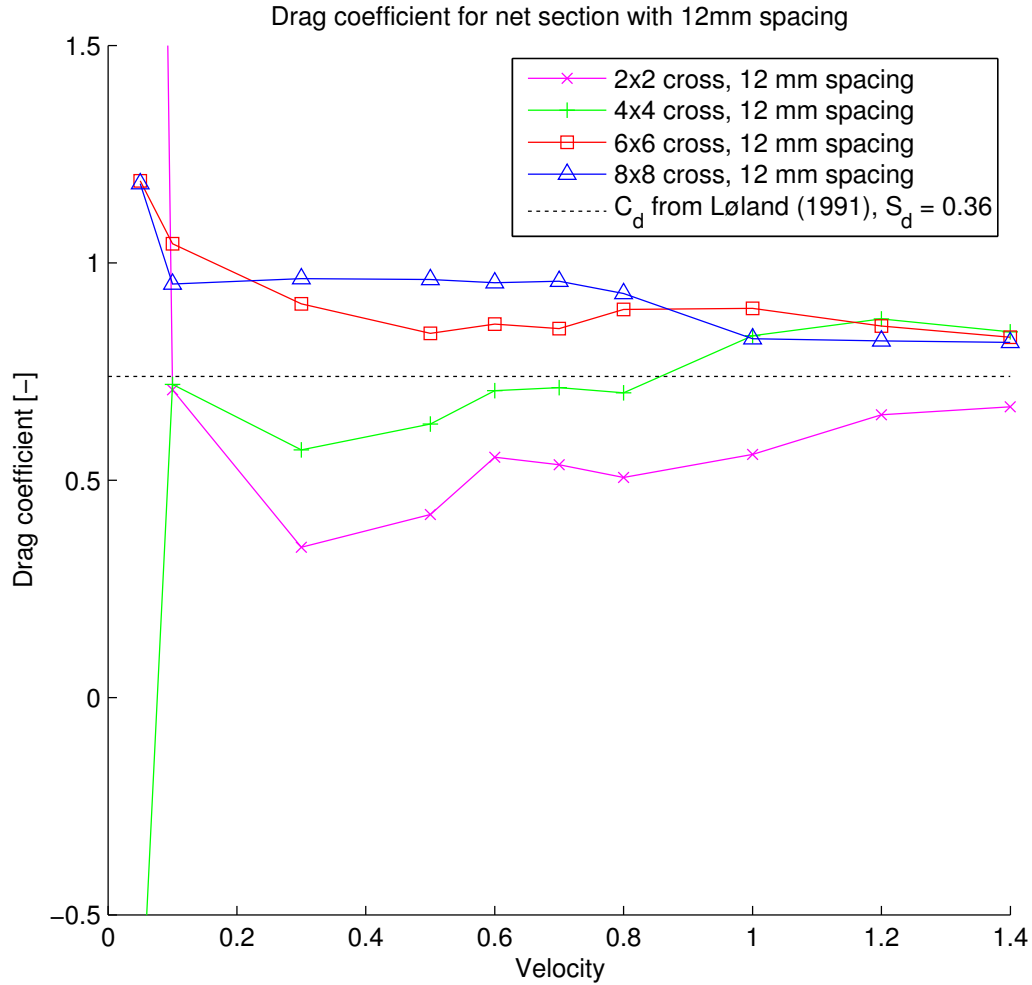


Figure 38

The figures also includes a line which shows the drag coefficient for an equivalent clean net. The solidities for clean nets with similar twine diameter and spacing would be 0.21 and 0.36 respectively for 24 mm and 12 mm twine spacing. The clean net drag coefficients are calculated based on these solidities, with the empirical formula given by Løland (1991) (eq. 3). For the 24 mm twine spacing the expected clean net drag coefficient is 0.31, while the measured drag coefficients varies between 0.65 and 0.59. This means that the drag is increased by about 100% because of the fouling.

For the 12 mm spacing the drag increase compared to the clean net data is smaller, and not significant, but in this case the drag coefficient estimate was not reliable. It should also be noted that according to Kristiansen and Faltinsen (2012) a solidity of 0.36 is above the validity range of the empirical formula for clean nets, and hence there could be a significant error.

6.4 Comparison with Similar Experiments

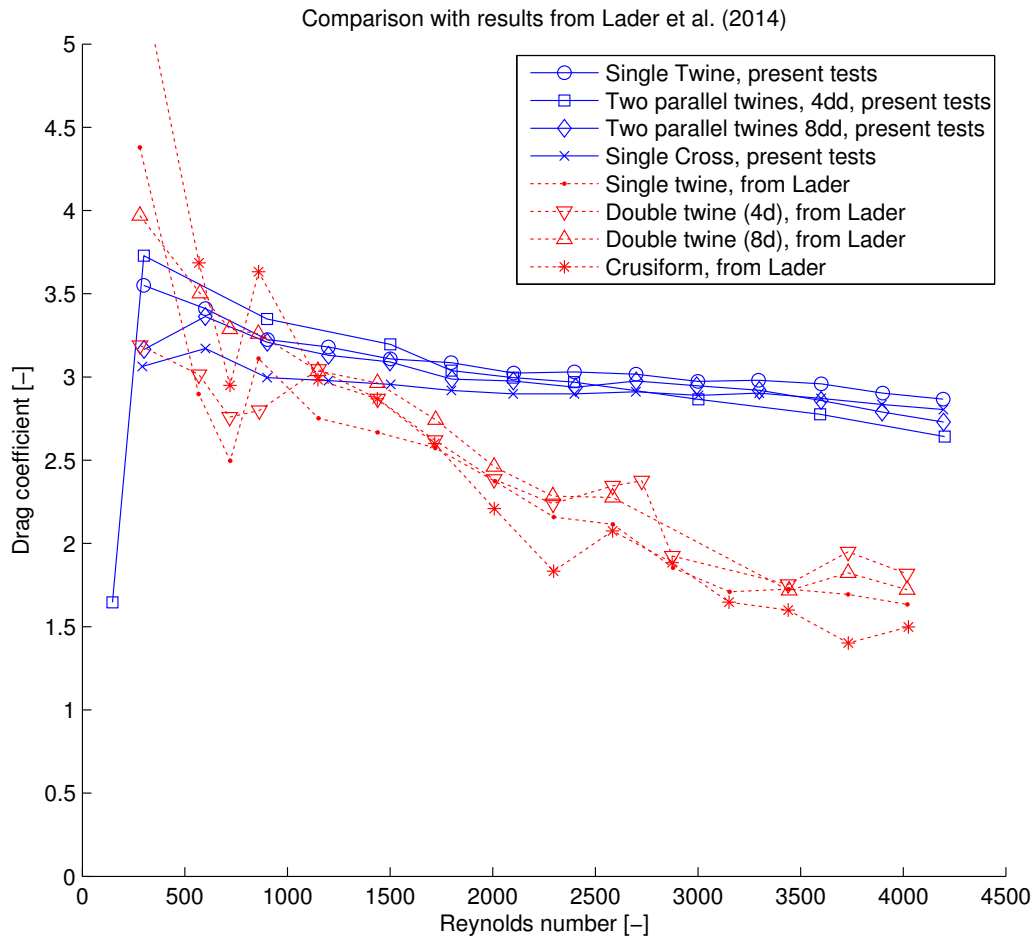


Figure 39: Plots of drag coefficients from P. Lader et al. (2014) (dotted red lines) and from the present study (blue line), for the configurations that were equivalent.

To assess the validity of the results, the drag coefficients from the configurations that were equivalent in the study by P. Lader et al. (2014) and the present study are plotted together in figure 39. At the low velocities, up to about $Re = 1200$ the results are in the same range, while from $Re = 1500$ and upwards the trend of decreasing drag coefficient with higher velocity are stronger for the first group of experiments, and at $Re \approx 4000$ the difference is significant. The drag coefficients from the present study are about 60% larger than the ones from the first study at the highest velocity. This might be caused by a systematic measurement error, but this is considered to be unlikely for two specific reasons. Firstly, the calibration was checked manually both before and after the experiments, and although the check was not very accurate, a 60% error would have been noticed in these tests. Secondly, there were only two twines in the configurations that are considered here, so the forces were relatively small, and if there was an error for larger forces, this would have been visible also for lower velocities for the configurations with

16 twines. Since the results were consistent between all the configurations, a force dependent error is unlikely.

Another possible explanation of the differences lies in the stiffness of the fishing line. P. Lader et al. (2014) describes that the hydroid models in their tests were bent almost directly downstream for the highest velocities, and this was not the case for the present experiments (Fig. 33). A difference in the stiffness would give similar drag forces for low velocities, when the deflections are small, and larger differences at higher velocities, when the deflections are larger. This corresponds well with the observations. The fishing lines used in the two studies should have the same specifications, and be from the same manufacturer, but the comparison of the results suggests that there must be some differences. This emphasises the importance of quantifying the stiffness of both real hydroids and the models

6.5 Some Limitations

In addition to the possible error sources and uncertainties that have been mentioned earlier, there is a couple of limitations regarding the applicability of the results from this study.

Firstly, all the drag tests have been done with the models orthogonal to the towing direction (current direction), and therefore one can not be sure that the results are valid for inflow from an angle. Most fish farm net pens are circular, and inflow from all angles are necessary to model circular net pen accurately.

Secondly, the bio fouling is normally not evenly distributed, and there will most likely also be other species than hydroids. The models that are used in this study are very simplified; and hence they are more suitable for studying the basics concepts of bio fouling induced drag, and less suitable for estimating the forces on a fouled real life net accurately.

7 Conclusions

There are several conclusions that can be drawn from the work with this thesis. The scope was to investigate how different twine configurations influence the drag on the models with artificial bio fouling, and based on this also study the drag increase on a net due to bio fouling. Overall the experiments went well, and they provided satisfactory results, although limited time for preparations before the experiments, and also limited time in the lab, caused some deviations from the original plan.

Most of the results are consistent, and they seem to be accurate. The exception from this is the results from the lower velocities, in particular 0.05 m/s and 0.1 m/s, where the drag coefficients are more scattered. For the repeated test at 0.1 m/s the precision error was also significant. The test series with the single cross configuration was also slightly different from the typical trend, with a lower drag coefficient below 0.7 m/s. It is not known if this was caused by some systematic error, or if it was a real physical effect. Comparison with the results from P. Lader et al. (2014) shows that the results are similar at lower velocities, while the drag forces in the present study are approximately 60% larger for the highest velocities. This might be caused by a difference in the stiffness of the hydroid models.

The trend of decreasing drag coefficient for higher Reynolds numbers, which was observed by P. Lader et al. (2014) with one or two twines, is consistent also with more than two parallel twines. This trend was present for all the configurations; and it is probably caused by either the deflection of the hydroid models, which make them more streamlined, or the fact that the hydroid stems are in a lower Reynolds number range, where the drag coefficient for a circular cylinder increases with lower velocity. It might also be a combination of both.

The drag coefficient for one twine varies little between the different configurations. There were some consistent trends connected with the spacing between the twines; for the cruciform configurations the drag was highest for the 24 mm spacing, while for the parallel configurations it was highest for the 24 mm spacing above 1.0 m/s and highest for the 12 mm spacing below 0.8 m/s. However, the differences were insignificant compared to the magnitude of the drag coefficients. The number of twines, and whether there were just parallel twines or also crossing twines, had no significant influence on the drag coefficients either. This means that the drag on one twine is almost independent of the surrounding twines, and hence it is likely that results from tests with a few twines can be extrapolated and used in real life applications.

When the drag on the net section in the middle of the cruciform configurations was extracted the drag coefficients for the net with 24 mm twine spacing were converging as the number of twines increased. The convergence means that any higher number of twines would not change the drag coefficients, so the values from the largest net section can be a good estimate for the drag coefficient of a larger net panel with similar properties. Based on this it was found that the drag coefficient for the fouled net was twice as

high as the empirical drag coefficient for a clean net with a similar clean-net-solidity. With 12 mm spacing the drag coefficients did not converge, so the results were inconclusive, and it is likely that a higher number of twines would be necessary to get an estimate of the drag on a fouled net.

7.1 Recommendations for Further Work

A couple of topics that could be interesting for further work were identified during the work with this thesis. The most obvious of these is to do more similar tests with the same kind of models. This would be beneficiary to verify if the results are correct, but it could also be interesting to try different hydroid lengths and densities, or other configurations.

Because the hydroids are flexible, and deform in high current velocities, it would also be interesting to measure the stiffness of the hydroid stem. No quantitative comparison of the stiffness of real hydroids versus the hydroid models (fishing line) have been made yet, but this would be useful when attempting to make equivalent replicas of real hydroid fouling. Since the force required to deform a hydroid is very small, this would probably be very difficult to do with normal bending tests, but it can maybe be done by measuring the deformation caused by a small known weight. Data describing the mechanical properties of the fouling organisms can also be utilised in numerical simulations of the local flow around a net with fouling.

It was suggested that the variation in drag coefficient for different Reynolds numbers might be caused by the low Reynolds number flow around the hydroid stems, and this could be investigated further. One approach to this is to do drag tests measuring the drag on only the fishing line, or if possible even on just one hydroid. Another approach is to make curve fit, and see if the drag force can be divided into two components; one with constant C_d being the contribution from the twine core, and another with C_d matching the line from Hoerner (1965, , p. 3 - 9) from $Re(0.1m/s) = 32$ to $Re(1.4m/s) = 448$, which would then be the contribution from the hydroids.

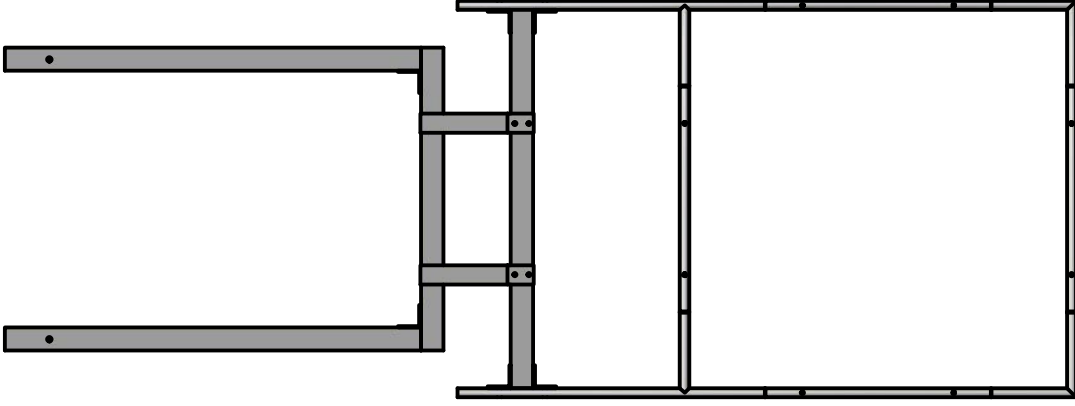
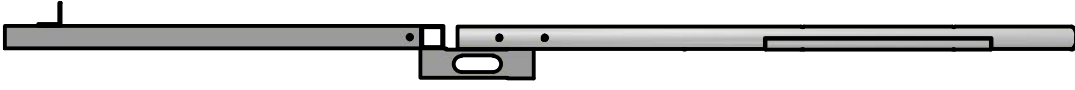
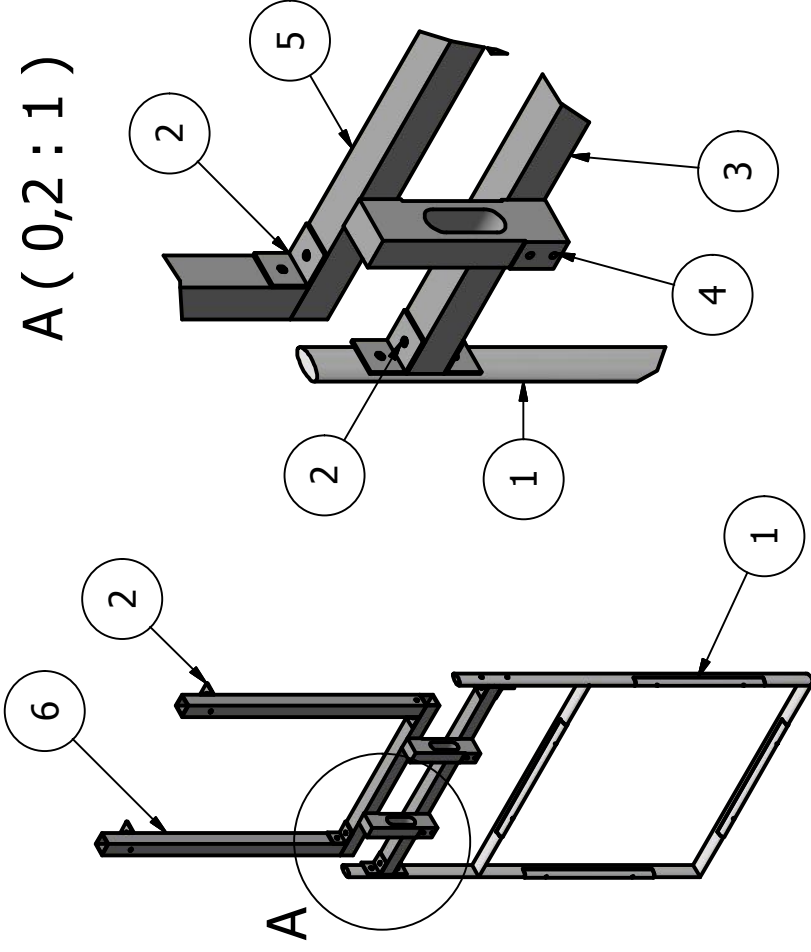
References

- Amplitude Estimation and Zero Padding* (2014). MathWorks, Inc. URL: <http://se.mathworks.com/help/signal/ug/amplitude-estimation-and-zero-padding.html>.
- Balash, Cheslav et al. (2009). “Aquaculture Net Drag Force and Added Mass”. In: *Aquacultural Engineering* 41.1, pp. 14–21.
- Bearman, P. W. and A. J. Wadcock (1973). “The interaction between a pair of circular cylinders normal to a stream”. In: *Journal of Fluid Mechanics* 61 (03), pp. 499–511.
- Faltinsen, Odd M. (1993). *Sea Loads on Ships and Offshore Structures*. Cambridge Ocean Technology Series. Cambridge University Press. ISBN: 9780521458702.
- Fitridge, Isla et al. (2012). “The impact and control of biofouling in marine aquaculture: a review”. In: *Biofouling* 28.7, pp. 649–669.
- Gansel, Lars et al. (2013). “Drag on clean and fouled net panels”. Draft received from Gansel, L. in meeting, 21-10-2013.
- Guenther, Jana, Ekrem Misimi, and Leif Magne Sunde (2010). “The development of biofouling, particularly the hydroid *Ectopleura larynx*, on commercial salmon cage nets in Mid-Norway”. In: *Aquaculture* 300.1–4, pp. 120–127.
- Hoerner, S.F. (1965). *Fluid-dynamic Drag: Practical Information on Aerodynamic Drag and Hydrodynamic Resistance*. Hoerner Fluid Dynamics.
- Kristiansen, Trygve and Odd M. Faltinsen (2012). “Modelling of current loads on aquaculture net cages”. In: *Journal of Fluids and Structures* 34, pp. 218–235.
- Lader, Pål F. and Arne Fredheim (2006). “Dynamic properties of a flexible net sheet in waves and current—A numerical approach”. In: *Aquacultural Engineering* 35.3, pp. 228–238.
- Lader, Pål et al. (2014). “Drag on hydroid fouled nets - an experimental approach”. Draft received from Gansel, L. August 2014.
- Løland, G. (1991). *Current Forces on and Flow Through Fish Farms*. Doktor ingeniøravhandling / Norges Tekniske Høgskole, Universitetet i Trondheim. Division of Marine Hydrodynamics, the Norwegian Institute of Technology. ISBN: 9788271192693.
- Marine Technology, Dep. of (2014). *Ship towing tanks*. NTNU. URL: www.ntnu.edu/imt/lab/towing.
- Milne, P.H. (1979). *Fish and Shellfish Farming in Coastal Waters*. Fishing News Books Limited. ISBN: 9780785569190.
- Steen, Sverre (2014). *TMR7 Experimental Methods in Marine Hydrodynamics*. Department of Marine Technology, NTNU. Lecture notes.
- Swift, M. Robinson et al. (2006). “Drag force acting on biofouled net panels”. In: *Aquacultural Engineering* 35.3, pp. 292–299.

A Drawings of Frame

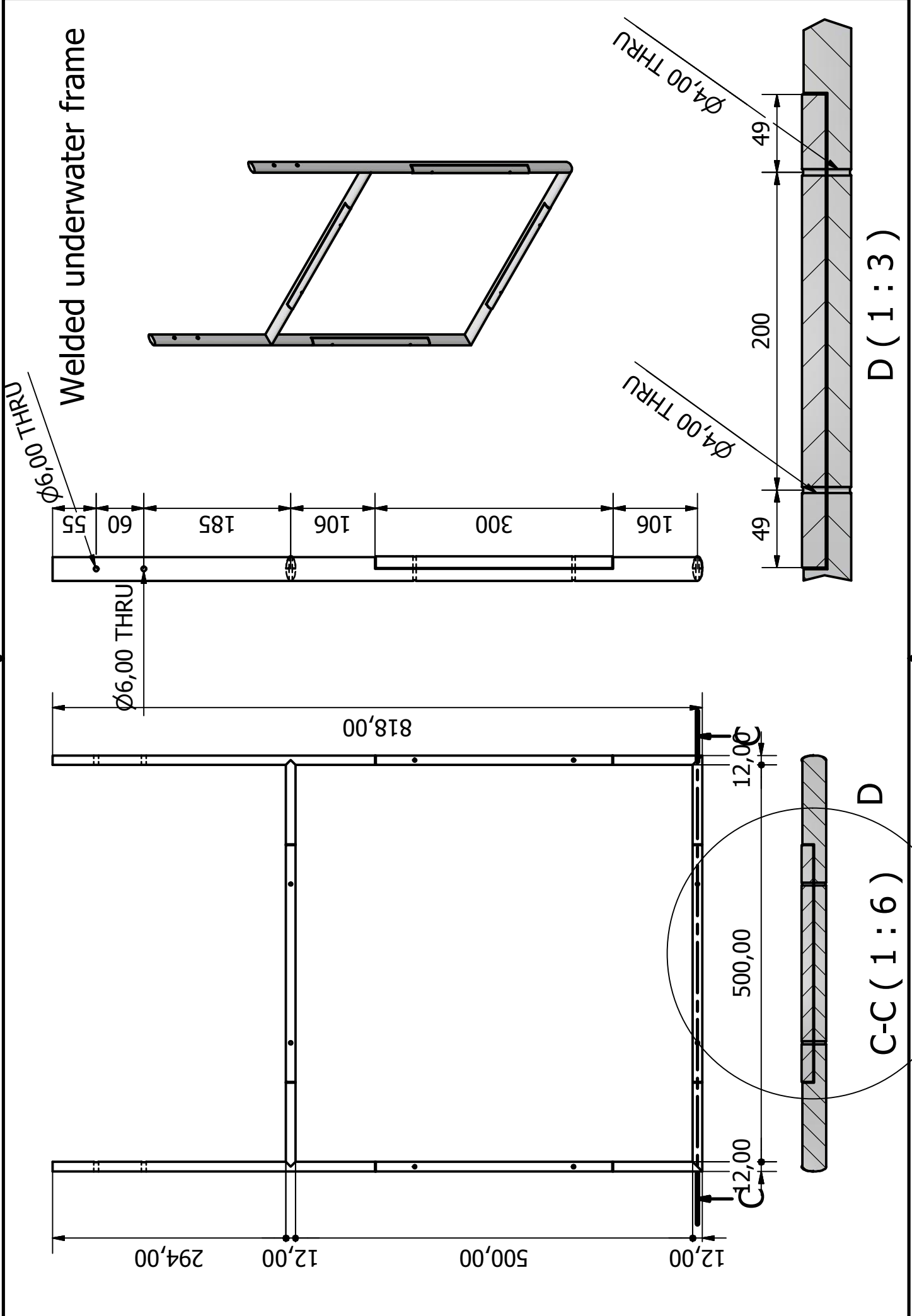
On the next four pages is the drawings of the set up that was made. The first page shows the whole assembly, and the next three pages are more detailed drawings of the parts.

A (0,2 : 1)

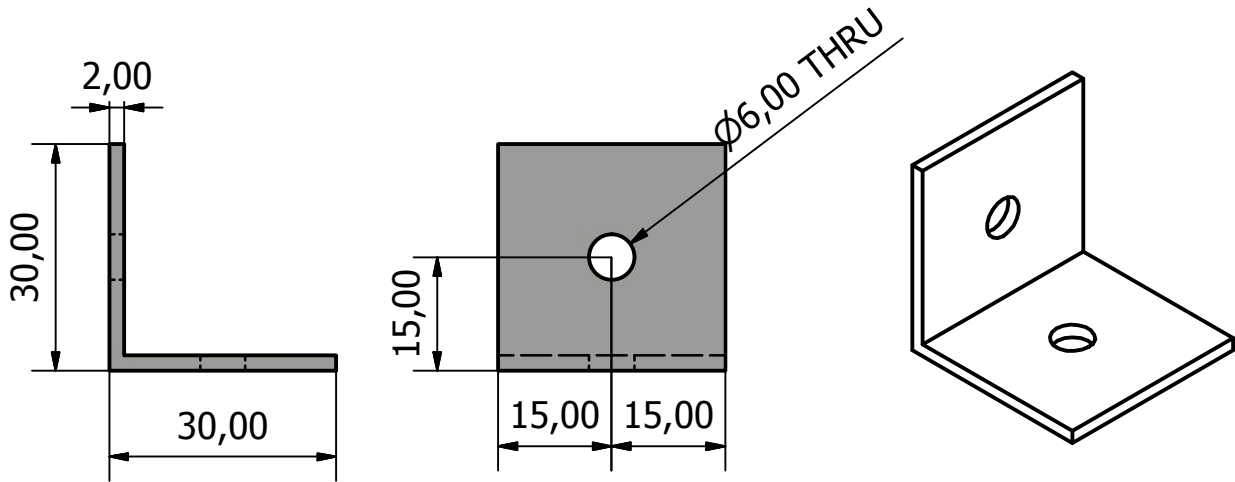


PARTS LIST

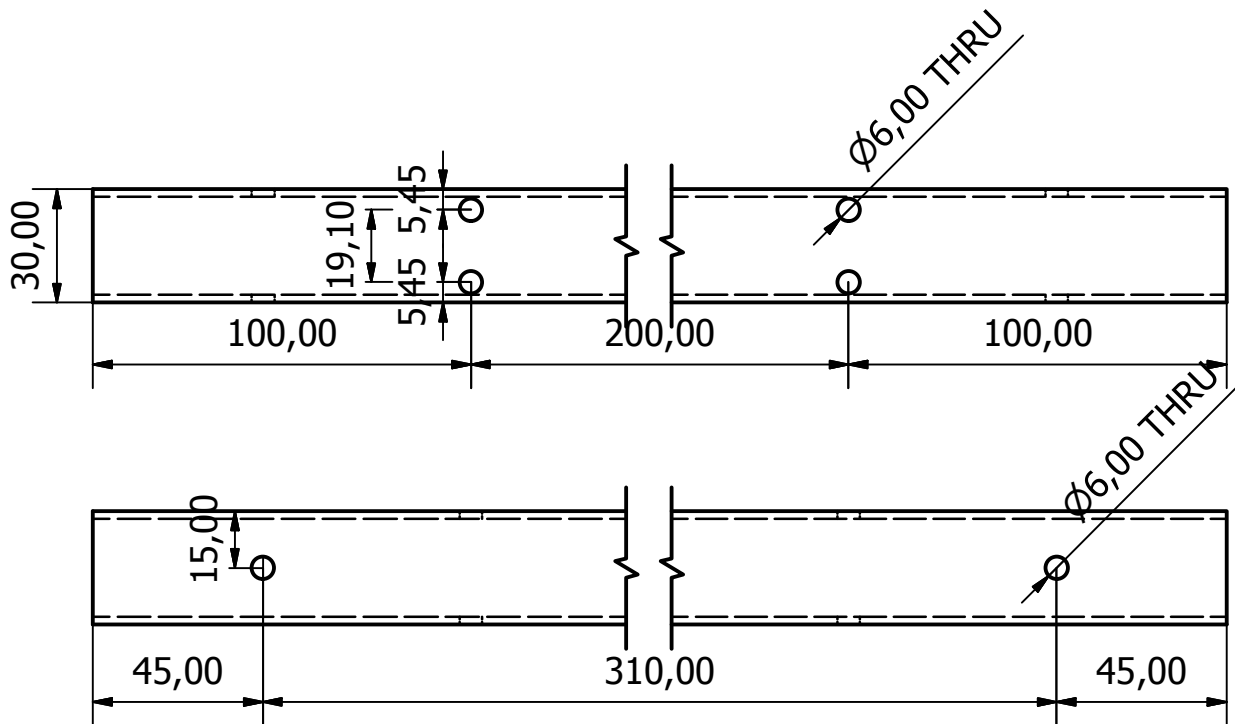
ITEM	QTY	PART NUMBER	DESCRIPTION
1	1	NewFrame	Welded frame 30x12mm elliptical profiles
2	8	30x30angle	
3	1	Square500mm	
4	2	LoadCellSP4M18kg	
5	1	Square400mm	
6	2	Square550mm	



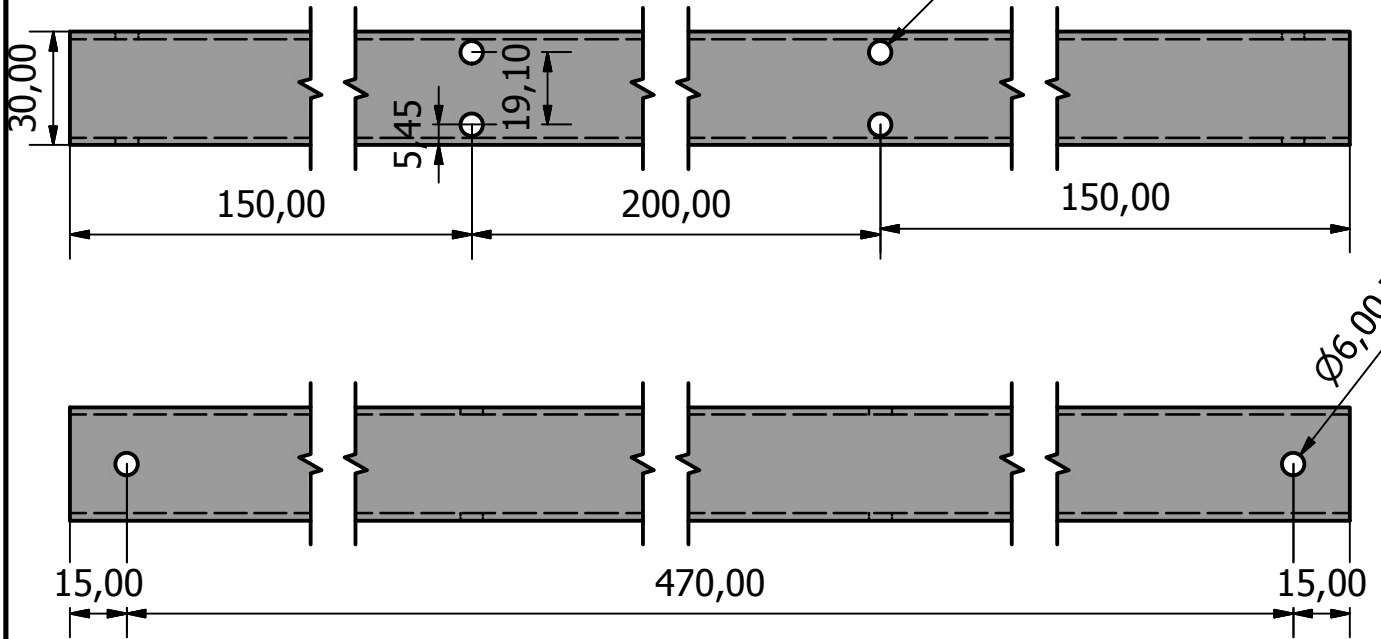
30x30angle



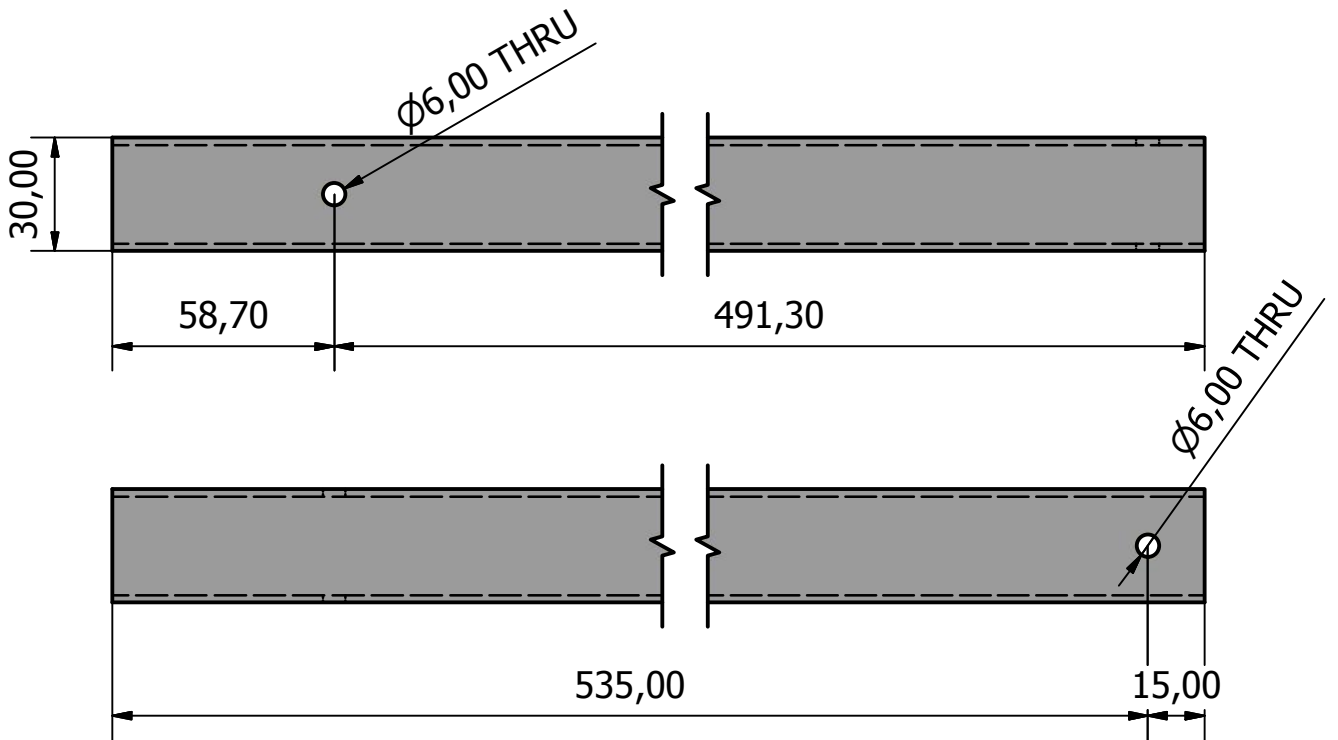
Square400mm



Square 500 mm



Square 550 mm



B Drag Forces and Coefficients for Each Test Series

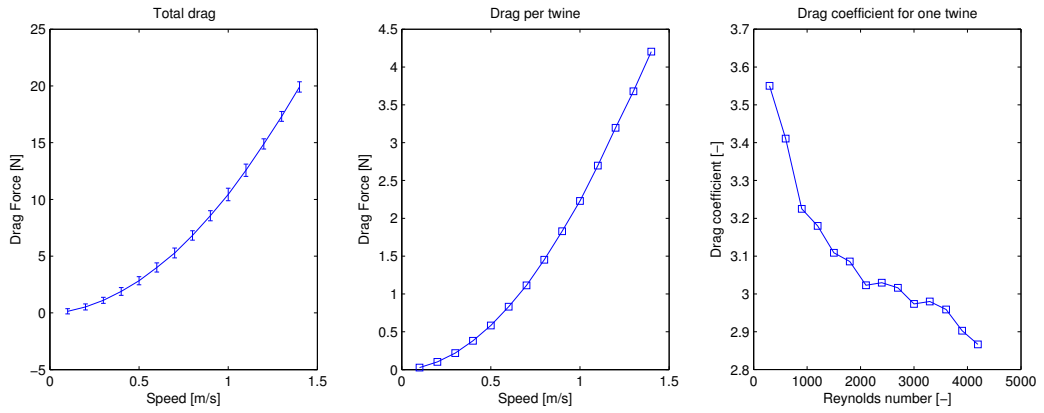


Figure 40: Single twine

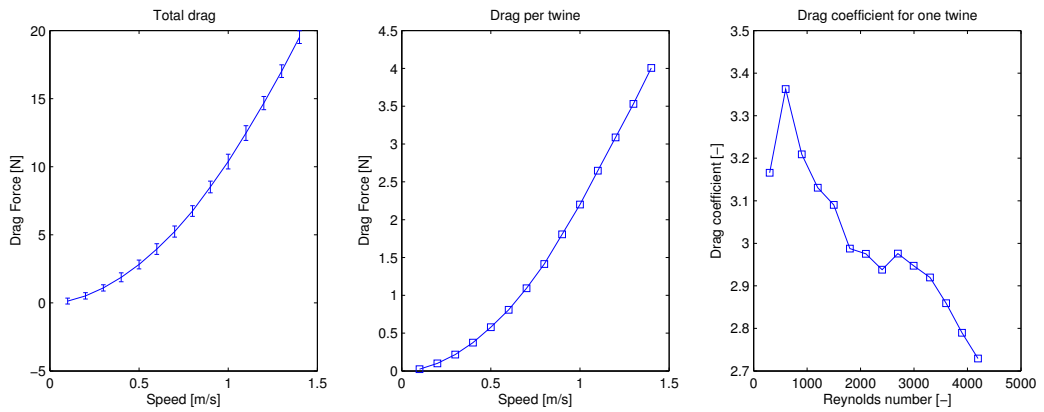


Figure 41: Two parallel twines, 24 mm spacing (2par8dd)

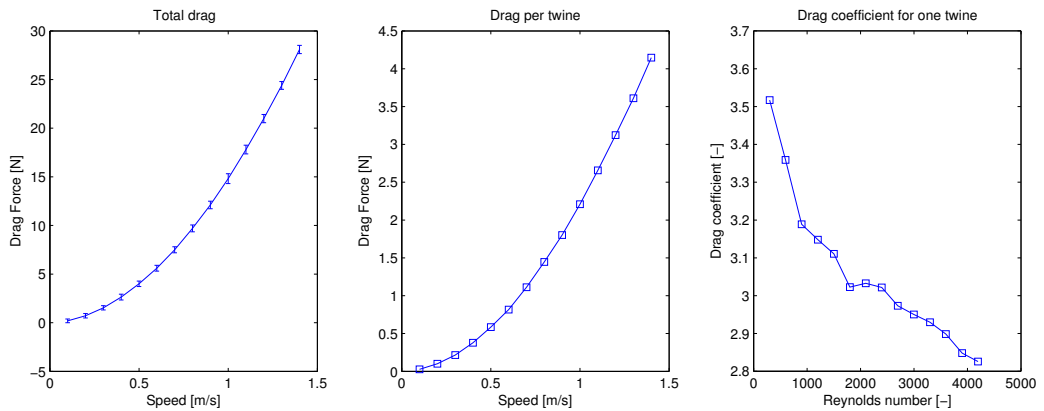


Figure 42: Four parallel twines, 24 mm spacing (4par8dd)

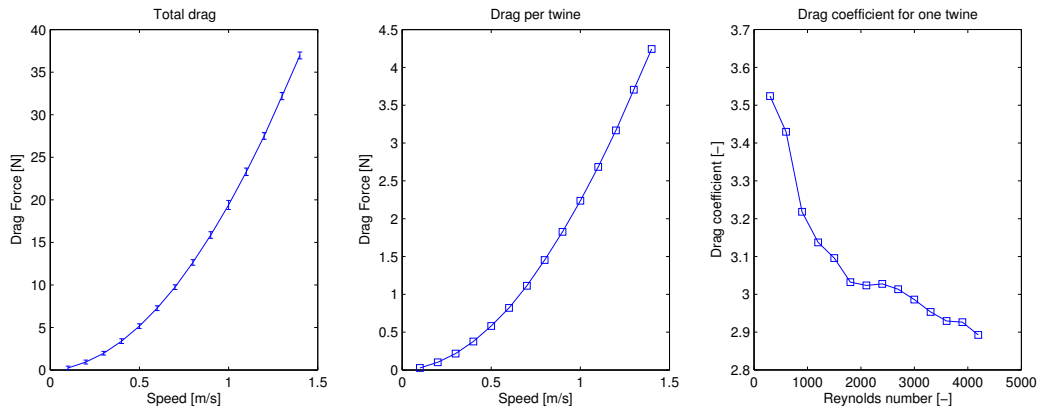


Figure 43: Six parallel twines, 24 mm spacing (6par8dd)

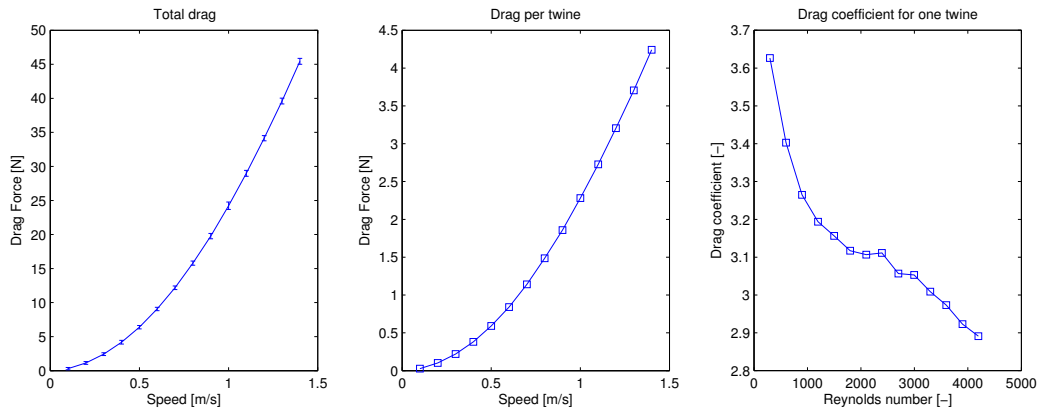


Figure 44: Eight parallel twines, 24 mm spacing (8par8dd)

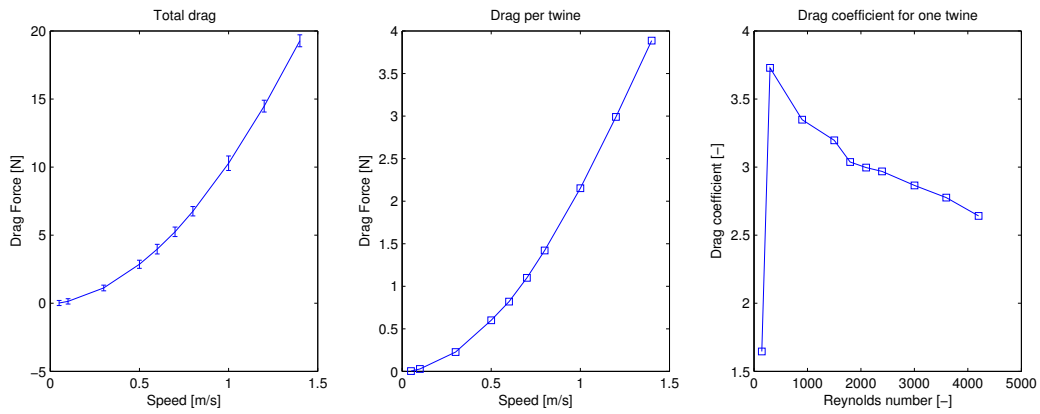


Figure 45: Two parallel twines, 12 mm spacing (2par4dd)

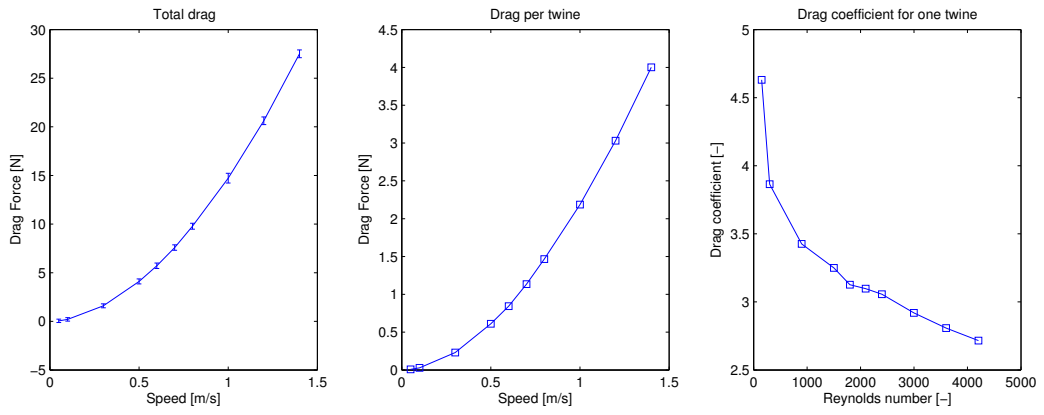


Figure 46: Four parallel twines, 12 mm spacing (4par4dd)

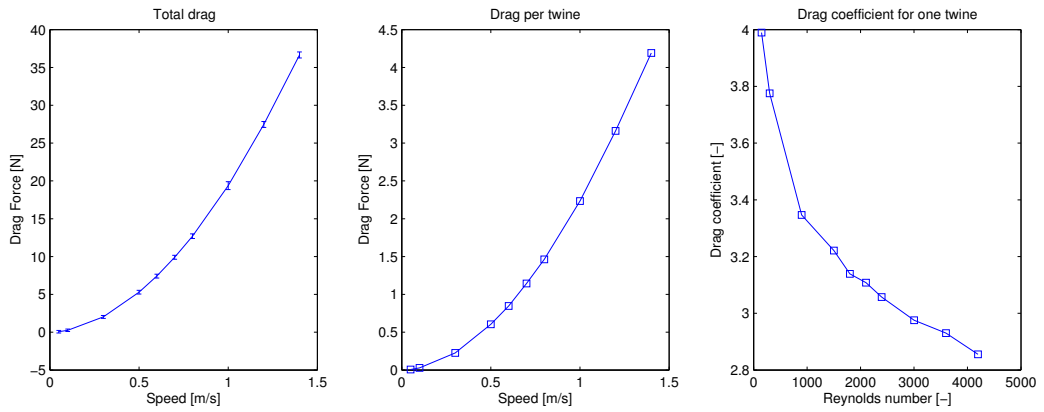


Figure 47: Six parallel twines, 12 mm spacing (6par4dd)

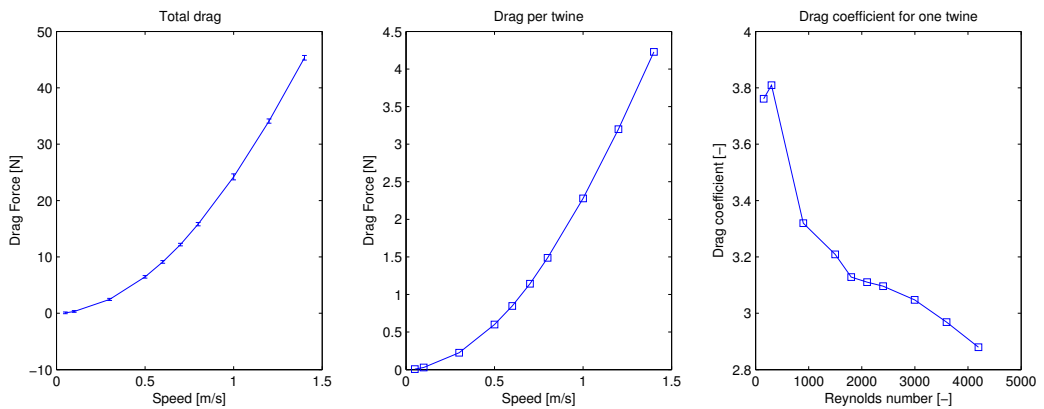


Figure 48: Eight parallel twines, 12 mm spacing (8par4dd)

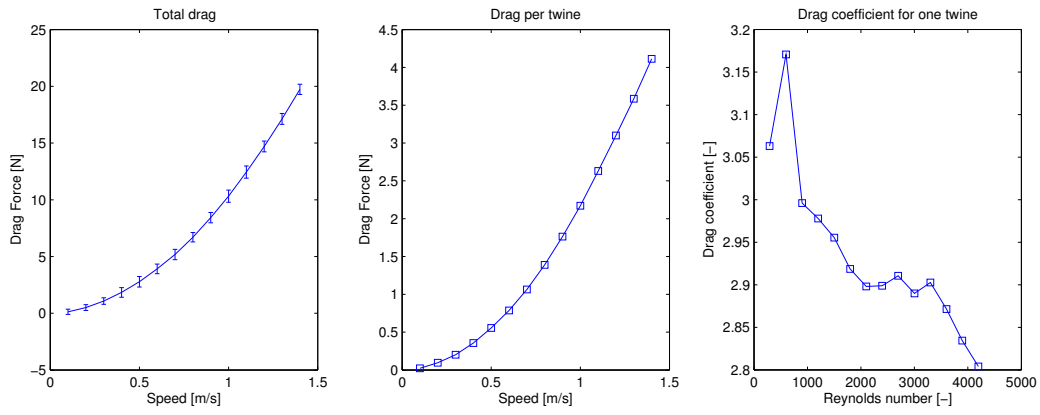


Figure 49: Single cross

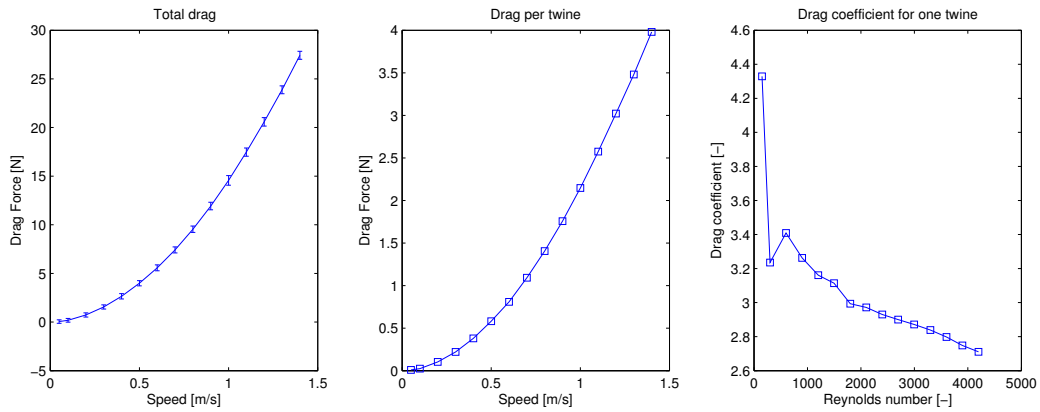


Figure 50: Two crossing twines, 24 mm spacing (2cross8dd)

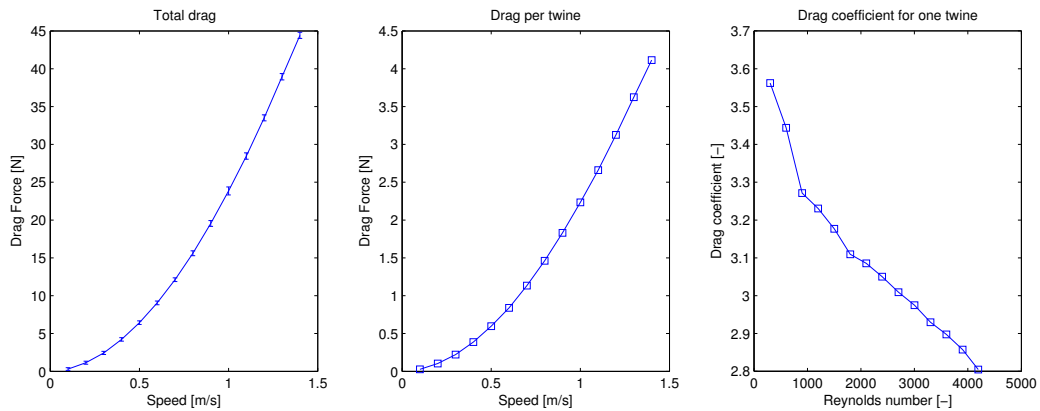


Figure 51: Four crossing twines, 24 mm spacing (4cross8dd)

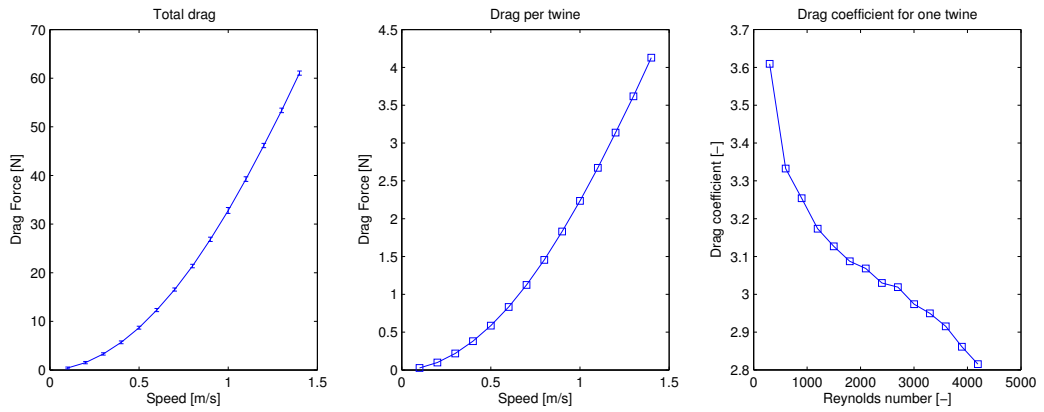


Figure 52: Six crossing twines, 24 mm spacing (6cross8dd)

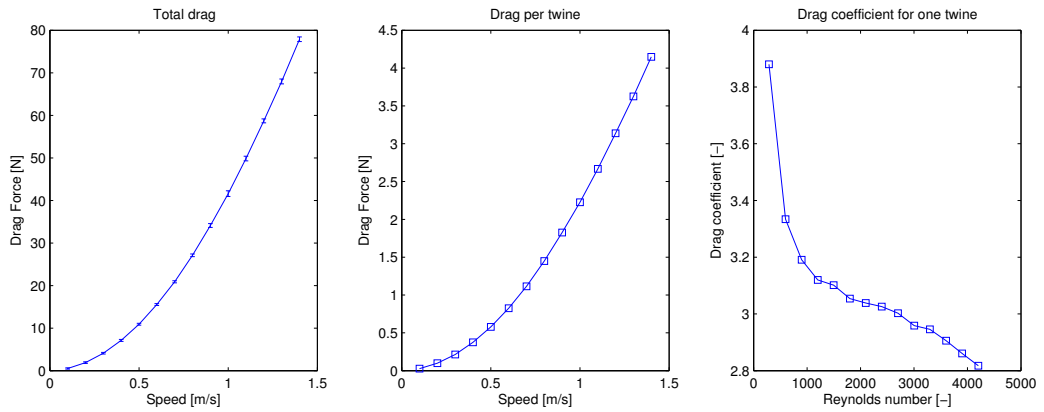


Figure 53: Eight crossing twines, 24 mm spacing (8cross8dd)

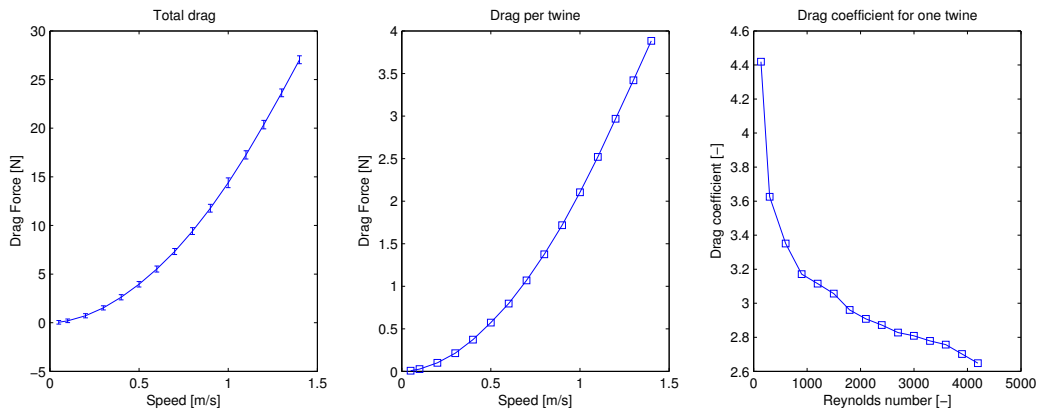


Figure 54: Two crossing twines, 12 mm spacing (2cross4dd)

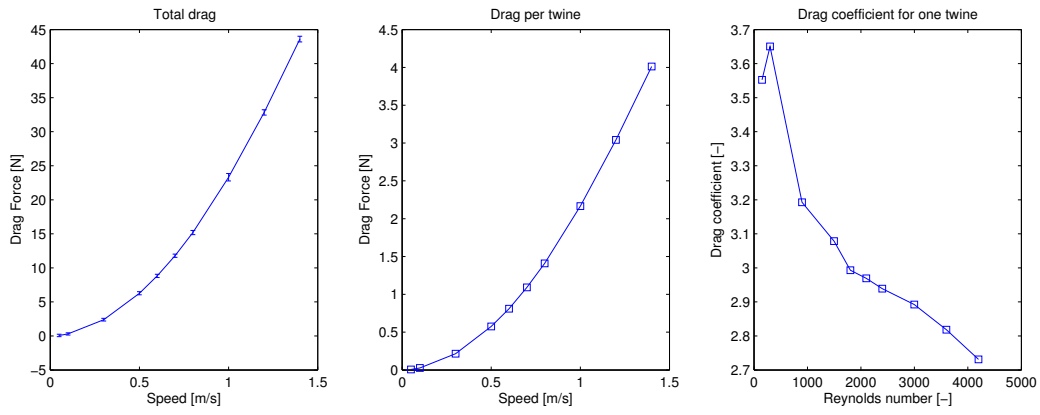


Figure 55: Four crossing twines, 12 mm spacing (4cross4dd)

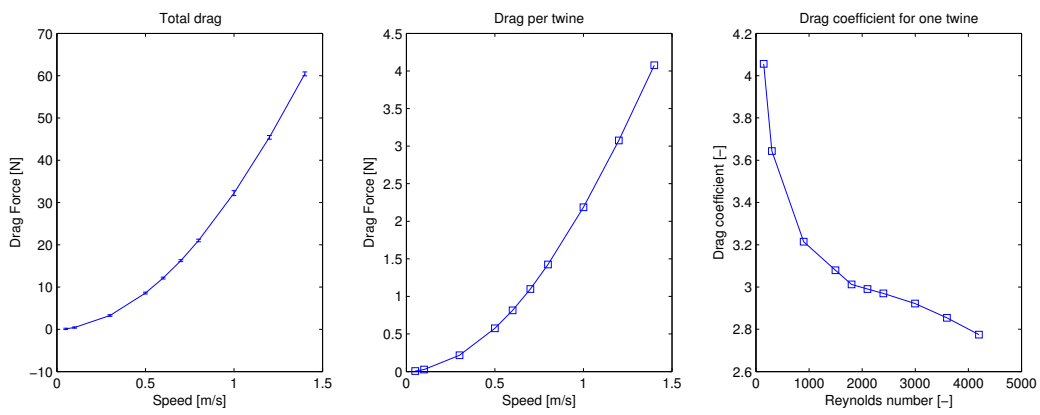


Figure 56: Six crossing twines, 12 mm spacing (6cross4dd)

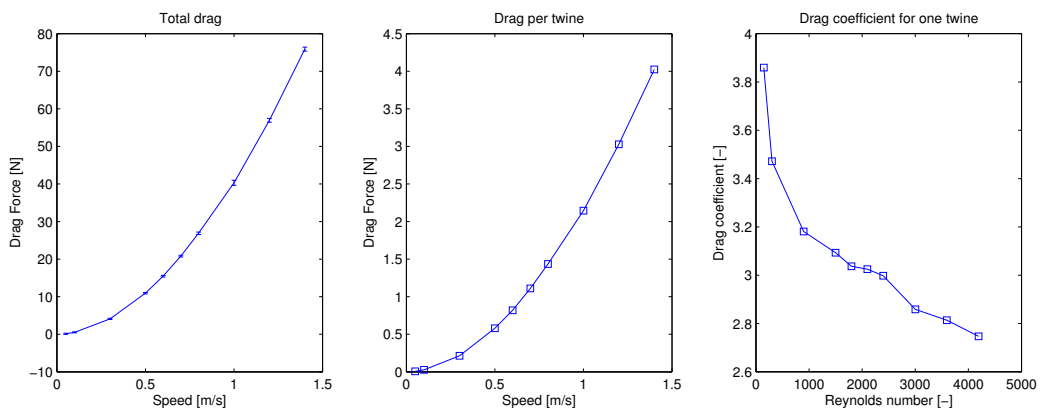


Figure 57: Eight crossing twines, 12 mm spacing (8cross4dd)

C Plots of Drag Coefficients vs. Number of Twines

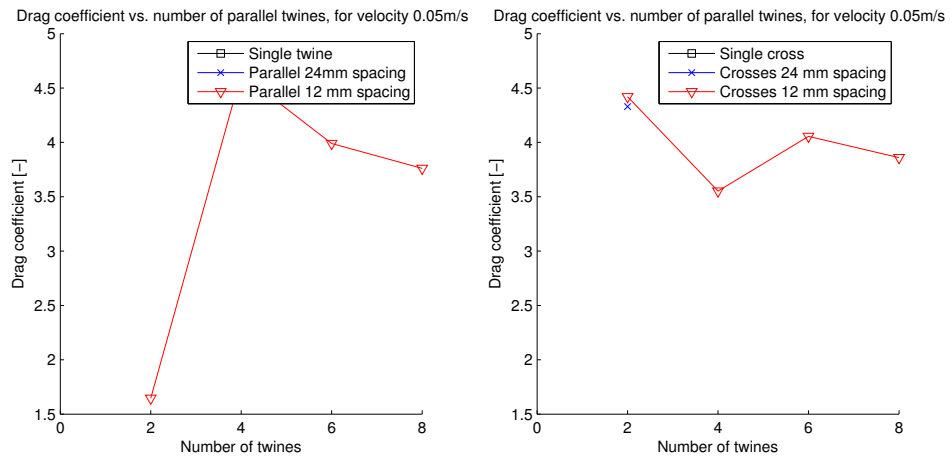


Figure 58: Drag coefficient vs. number of twines, 0.05 m/s

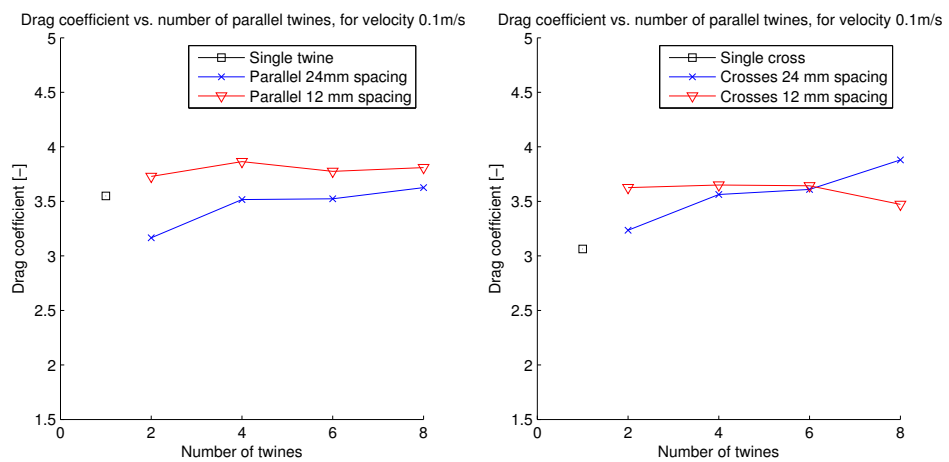


Figure 59: Drag coefficient vs. number of twines, 0.10 m/s

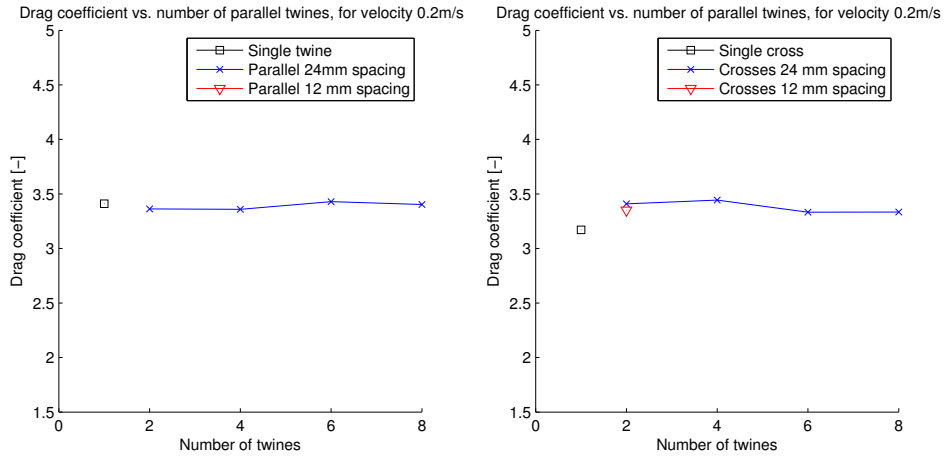


Figure 60: Drag coefficient vs. number of twines, 0.20 m/s

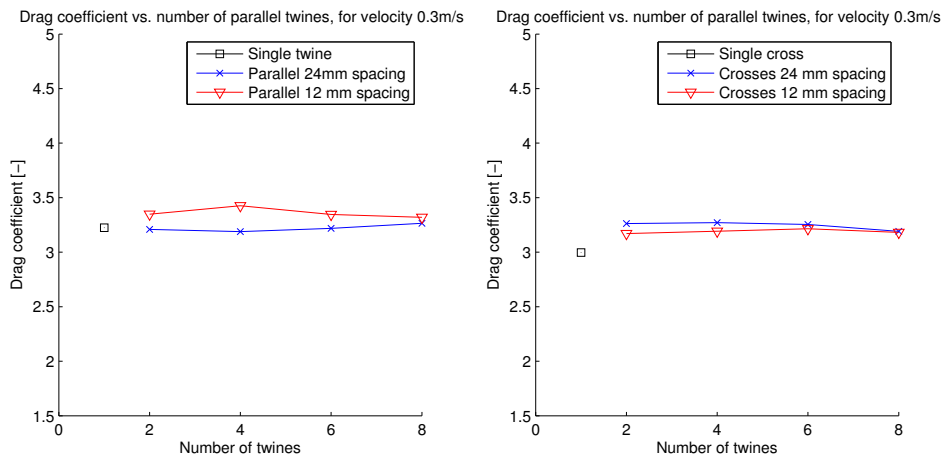


Figure 61: Drag coefficient vs. number of twines, 0.30 m/s

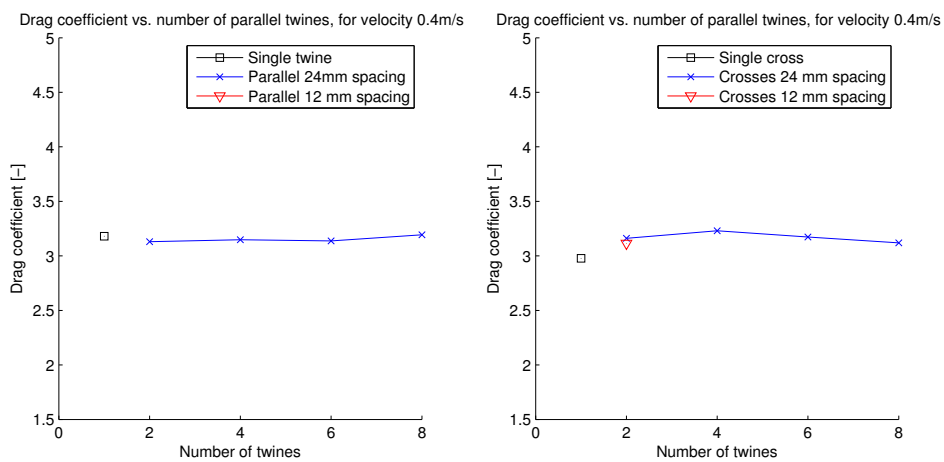


Figure 62: Drag coefficient vs. number of twines, 0.40 m/s

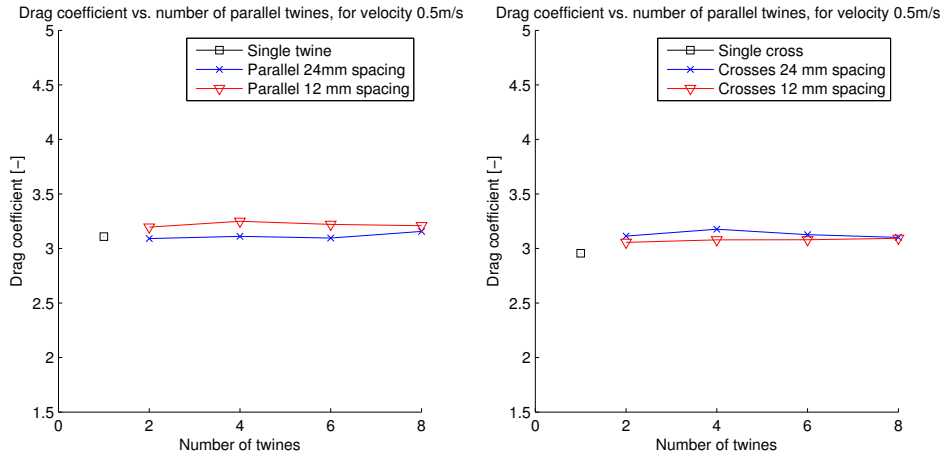


Figure 63: Drag coefficient vs. number of twines, 0.50 m/s

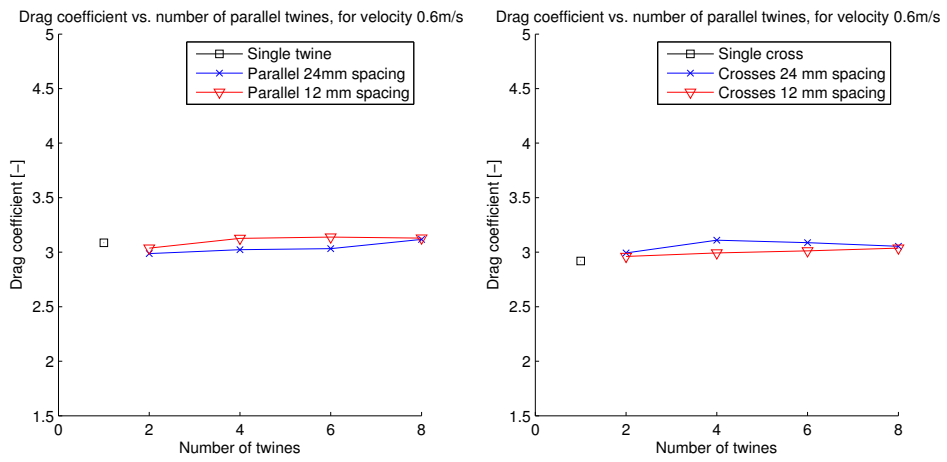


Figure 64: Drag coefficient vs. number of twines, 0.60 m/s

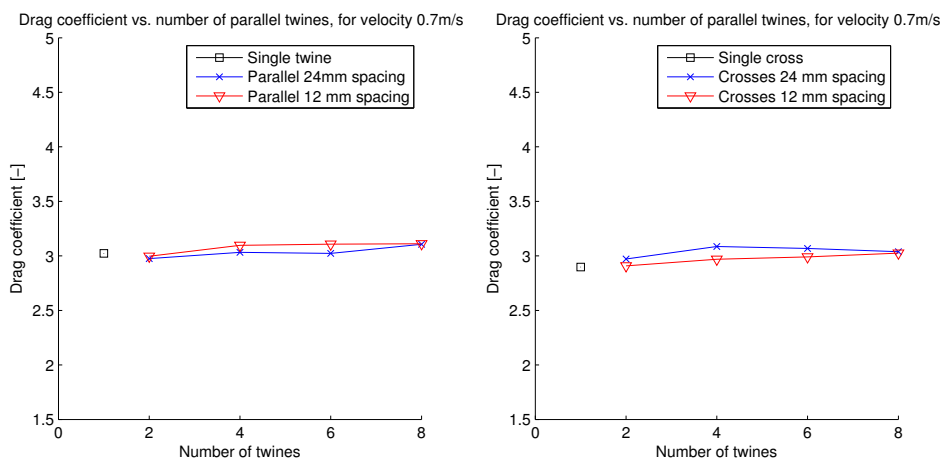


Figure 65: Drag coefficient vs. number of twines, 0.70 m/s

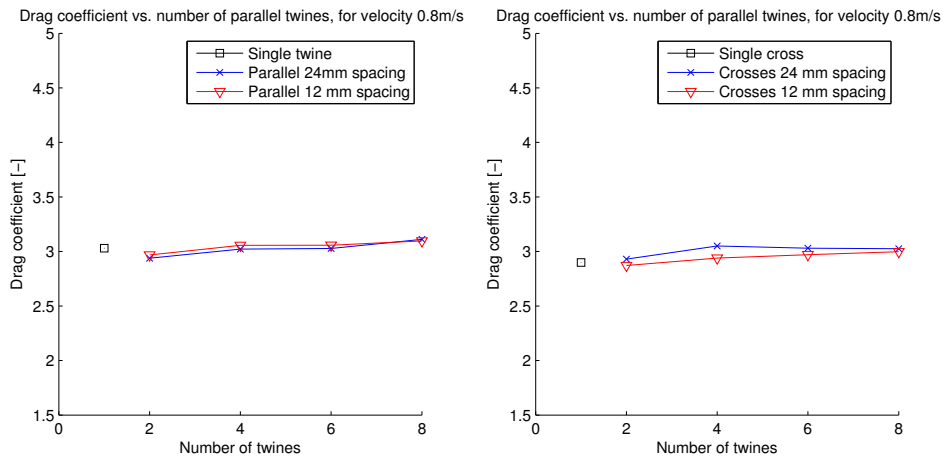


Figure 66: Drag coefficient vs. number of twines, 0.80 m/s

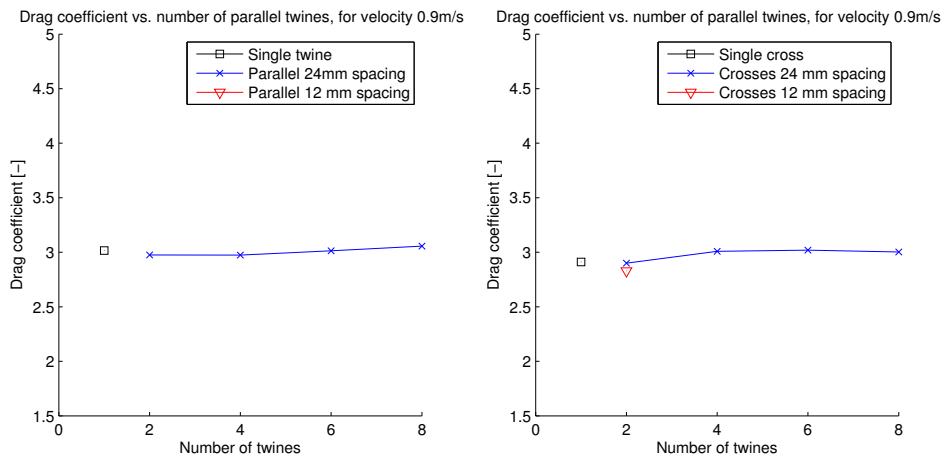


Figure 67: Drag coefficient vs. number of twines, 0.90 m/s

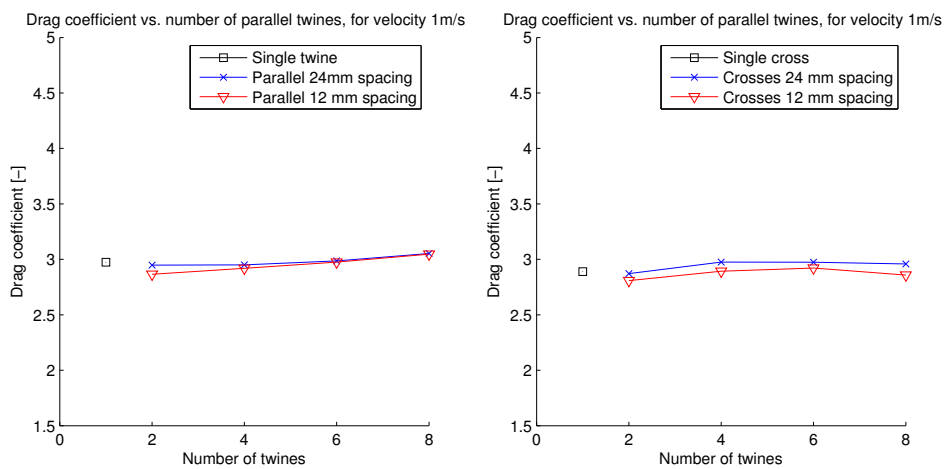


Figure 68: Drag coefficient vs. number of twines, 1.0 m/s

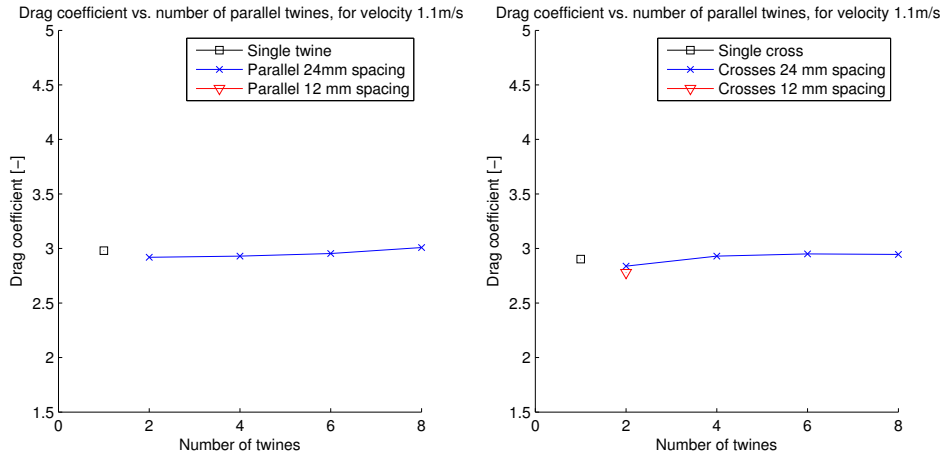


Figure 69: Drag coefficient vs. number of twines, 1.1 m/s

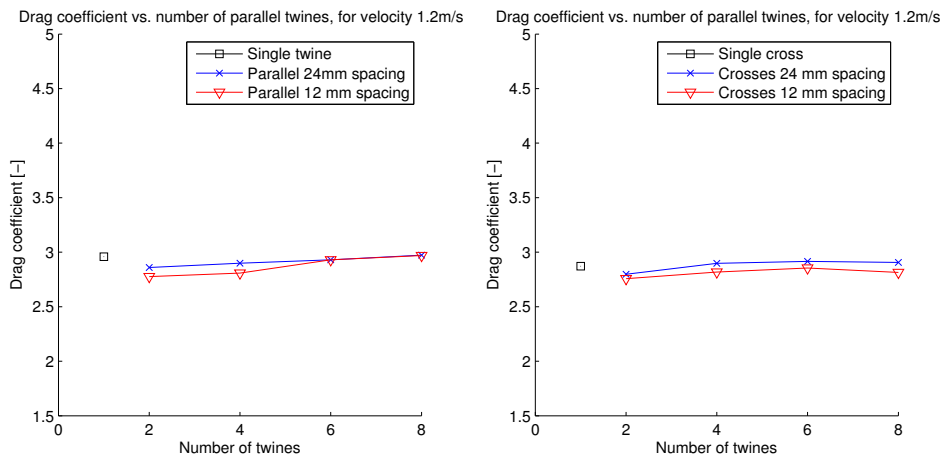


Figure 70: Drag coefficient vs. number of twines, 1.2 m/s

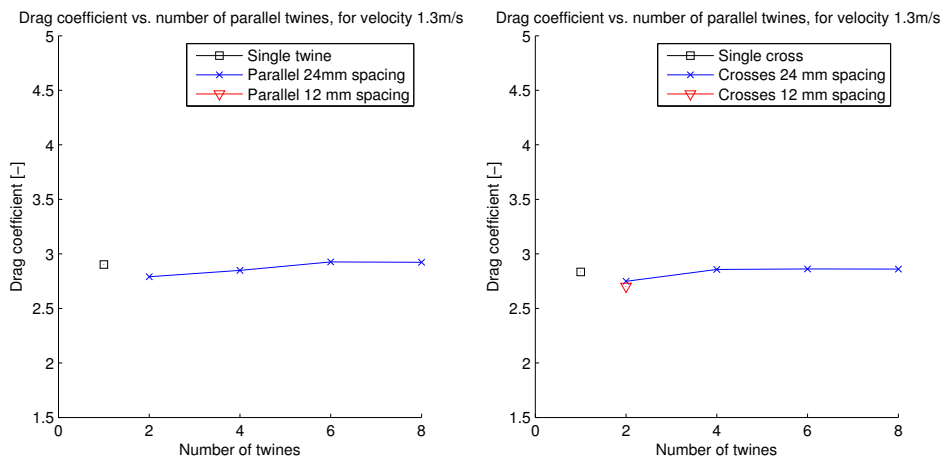


Figure 71: Drag coefficient vs. number of twines, 1.3 m/s

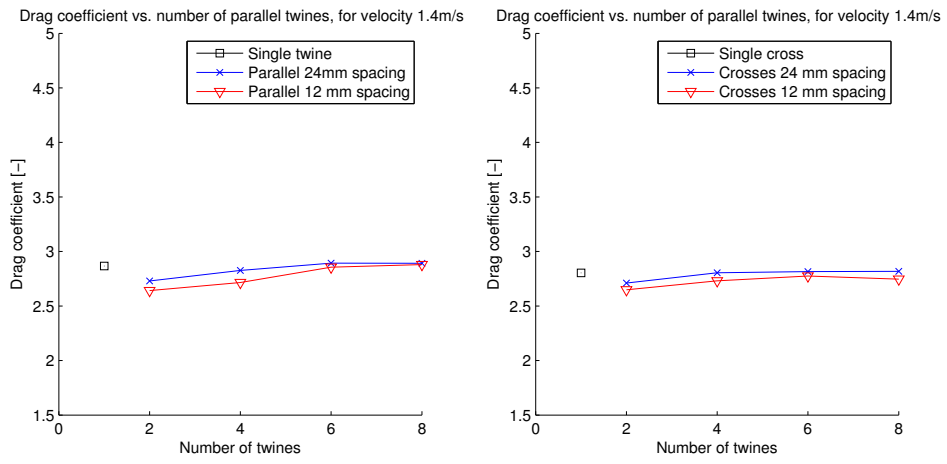


Figure 72: Drag coefficient vs. number of twines, 1.4 m/s

D Overview of MatLab Scripts

The code for analysing and plotting the data was divided into many scripts. To make it easier to understand, a brief overview of the files and folders in the **MatLab** folder are included here

Folders

./data/ All the data from the recording computer in the lab, one file for each run

./fig/ All plotted figures are stored here.

./results/ All the results from the analysis of the time series are stored here. Drag forces, drag coefficients, etc.

./images/ The raw images for the calculation of the projected area. (This folder was very large, and is therefore left out from the digital attachments.)

The folder **./altmany-export_fig-6c11f9f/** contains the function **export_fig.m** which was used to export the figures to pdf-format. The function was obtained from <http://www.mathworks.com/matlabcentral/fileexchange/23629-export-fig> on 11th January 2015.

Input-files

Hydroid_data.xlsx Data from P. Lader et al. (2014).

image2attempt.xls Input file relating images to configurations

Planforexperiments.xls Information about all configurations and runs. Notes from the Lab. Used as input to MatLab scripts.

repeattests.xls Input file for analysing repeated tests. Used to relate file-names to the right run.

Scripts

The scripts that are used for calculations and plotting are described shortly here. If some files are removed from the **./results/** folder the scripts should be run in the order they are listed.

DataAnalysisMasterRamme.m Calculates the forces on the frame. Run once for each test with only the frame. Depends on the functions:

- **catman_read_5r8.m**
- **readtimes.m**
- **steadyState.m**

- SingleRunStats.m, which uses spektrumdfft.m
- plotTSandSPEC.m

rammeComparison.m Compares the results from the test series with only the frame, and calculates the average for further use.

DataAnalysisMaster.m Calculates forces, drag coefficients, velocity, reynolds nr, etc. for all the runs. Run once for each configuration. Depends on the functions:

- catman_read_5r8.m
- readtimes.m
- steadyState.m
- SingleRunStats.m, which uses spektrumdfft.m
- sortbyfirst.m
- plotTSandSPEC.m

DecayAnalysisMaster.m Calculates frequency spectra for the decay tests. Depends on the functions:

- catman_read_5r8.m
- steadyState.m
- spektrumdfft.m

repeatabilityAnalysis.m Calculates forces, drag coefficients, velocity, reynolds nr, etc. for the repeated runs. Run once for each repeated configuration. Depends on the functions:

- catman_read_5r8.m
- readtimes.m
- steadyState.m
- SingleRunStats.m, which uses spektrumdfft.m

plottingMaster.m Plots the drag force per twine and drag coefficients as functions of velocity and Reynolds number respectively.

plottingMaster2.m Plots the drag coefficients as a function of number of twines.

plotUncertainty.m Plots the drag force per twine and drag coefficients as functions of velocity and Reynolds number respectively for the test series with repeated runs. The precision errors is plotted as error-bars.

projAreafromImgWhite.m Calculates projected area from images of the configurations (These images are not included). Depends on the function:

- `backgroundimage.m`

NetDragMaster.m Calculates drag coefficient and solidity for the net section in the middle of the cruciform configurations.

laderComparison.m Plot results from P. Lader et al. (2014) together with results from the present study for the test that are equivalent.

The function **catman_read_5r8.m** are used to load the binary files from the recording software. This function is not written by the author; it was obtained a couple of years ago when similar software was used in a lab report.

E List of Digital Attachments

In addition to these appendices some files are included in a .zip file that follows the report. These are:

- The folder `./videos/` which contains two short example videos from the configuration with two by two crosses and 24 mm spacing. The videos are cut to avoid large filesizes.

GoPro139 for 0.6 m/s

GoPro148 for 0.05 m/s

- The folder `./MatLab/` which contain all the MatLab code that was used (See appendix D), and the input and output data, including plots.
- The folder `./MatLab/fig/singleruns/` contains plots of timeseries and frequency-spectra for all the **drag tests**. This is to many images to include in the printed appendix.
- The folder `./MatLab/fig/decay/` contains plots of timeseries and frequency-spectra for all the **decay tests**.